

Y 3. At7

AEC

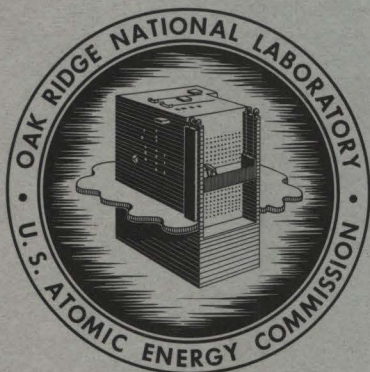
RESEARCH REPORTS

221 ORNL-3416

UNIVERSITY OF
ARIZONA LIBRARY
Documents Collection
APR 20 1963

ORNL-3416
UC-80 — Reactor Technology

MARITIME REACTOR PROGRAM
ANNUAL PROGRESS REPORT
FOR PERIOD ENDING NOVEMBER 30, 1962



OAK RIDGE NATIONAL LABORATORY

operated by

UNION CARBIDE CORPORATION

for the

U.S. ATOMIC ENERGY COMMISSION

metadc100416

Printed in USA. Price: \$2.50 Available from the
Office of Technical Services
U. S. Department of Commerce
Washington 25, D. C.

— LEGAL NOTICE —

This report was prepared as an account of Government sponsored work. Neither the United States, nor the Commission, nor any person acting on behalf of the Commission:

- A. Makes any warranty or representation, expressed or implied, with respect to the accuracy, completeness, or usefulness of the information contained in this report, or that the use of any information, apparatus, method, or process disclosed in this report may not infringe privately owned rights; or
- B. Assumes any liabilities with respect to the use of, or for damages resulting from the use of any information, apparatus, method, or process disclosed in this report.

As used in the above, "person acting on behalf of the Commission" includes any employee or contractor of the Commission, or employee of such contractor, to the extent that such employee or contractor of the Commission, or employee of such contractor prepares, disseminates, or provides access to, any information pursuant to his employment or contract with the Commission, or his employment with such contractor.

Contract No. W-7405-eng-26

MARITIME REACTOR PROGRAM ANNUAL PROGRESS REPORT
For Period Ending November 30, 1962

H. C. McCurdy
Program Coordinator

Date Issued

'APR - 4 1963

OAK RIDGE NATIONAL LABORATORY
Oak Ridge, Tennessee
operated by
UNION CARBIDE CORPORATION
for the
U.S. ATOMIC ENERGY COMMISSION

CONTENTS

	<u>Page</u>
SUMMARY.....	v
1. INTRODUCTION.....	1
2. N.S. SAVANNAH PROJECT — GENERAL SUPPORT.....	4
Shield Study.....	4
Equipment and Procedures.....	4
Results.....	6
Conclusions.....	8
Iodine Adsorption Studies.....	10
Laboratory Studies.....	10
Shipboard Tests.....	14
Environmental Monitoring.....	18
Bioassay Development Program.....	19
Urinalysis.....	19
Direct Gamma Counting.....	19
Safety Evaluations.....	20
Activity Release Studies.....	21
Port Survey Visits.....	37
Physics Calculations.....	39
Comparison of One- and Two-Zone Core Reactivity Lifetimes.....	39
Comparison of Axial Slab-Geometry Model with Experimental Analysis.....	41
3. PRESSURIZED-WATER IN-PILE LOOP.....	46
Loop Operation.....	46
Water Chemistry Studies.....	48
Observed Activity Behavior.....	49
Activity Transport Mechanism.....	55
Conclusions.....	64

4. ADVANCED CORE DEVELOPMENT.....	66
Physics Calculations.....	66
Comparison of Radial and "Window-Shade" Methods for Calculating N.S. SAVANNAH Core I Burnups.....	66
Window-Shade Burnup Results for 4.2 wt % Zircaloy Egg-Crate Core.....	72
Fuel Development.....	75
Preparation of Irradiation Test Specimens for ORR Loop.....	75
Manufacture of Test Bundles for Irradiation in the Vallecitos Boiling-Water Reactor (VBWR).....	78
Vibratory-Compaction Development.....	83
Fuel Irradiation Tests.....	86
Postirradiation Metallographic Examination of Fuel Specimens Irradiated in ORR Loop.....	95
Fuel Cladding.....	96
Fuel Columns.....	98
Conclusions.....	102
Evaluation of Nonsintered UO ₂ Fuel for an N.S. SAVANNAH Core.....	102
Thermal Performance.....	103
Waterlogging.....	105
Other Performance Considerations.....	112
Economics.....	113
Conclusions.....	114

SUMMARY

N.S. SAVANNAH Project — General Support

A survey of the N.S. SAVANNAH reactor shield was carried out during the period May 20 through May 25, 1962. Because of the low values specified for permissible radiation levels in passenger and crew areas, special instrumentation was necessary; the measurements were made with the reactor at full power. The survey was under the direction of the ORNL Neutron Physics Division and was conducted by a team of 41 people recruited from several project-affiliated organizations. Gamma-ray and neutron dose rates were measured at points on a 3-ft rectangular grid on the outer surface of the secondary shield and at a large number of additional points in passenger and crew areas. The results showed that the shield effectively met the design specifications.

An experimental program was undertaken to determine the iodine-removal efficiency that may be expected of the activated charcoal unit in the emergency ventilation system of the N.S. SAVANNAH reactor compartment and to develop a method for measuring the efficiency of shipboard installations. A number of small-scale laboratory experiments were carried out to obtain information on the behavior of several types of charcoal and to measure the iodine-removal efficiency of prototype charcoal units. Tests at 90 to 100°C with air 80 to 90% saturated with water vapor showed the efficiency of the prototype charcoal unit to be $99.86 \pm 0.07\%$ at the 95% confidence level.

Two procedures were developed and applied to the in-place testing of the iodine adsorption units installed aboard the N.S. SAVANNAH. One procedure calls for the injection of iodine vapor labeled with the radioactive isotope I^{131} . Samples of the air stream are taken upstream and downstream of the iodine filter and analyzed by counting the radioactive constituent. The other procedure uses nonradioactive iodine, and the samples are analyzed by the neutron-activation method. Both procedures were used for in-place tests of the SAVANNAH installations. The results were in good agreement and showed that the charcoal adsorber units, as installed, were capable of the iodine-removal efficiency observed in laboratory tests.

The I^{131} procedure is presently considered to be the more reliable, primarily because there is more experience with this procedure and because it appears to be less susceptible to contamination errors.

Experiments directed toward developing a shipboard bioassay program for the N.S. SAVANNAH Medical Department were completed. Simplified procedures were devised for using equipment available aboard the ship to screen personnel suspected of having a body burden of radioactive corrosion products or fission products.

Activity release from the N.S. SAVANNAH in the maximum credible accident was studied to determine the effect of power history, delay in release and transport of activity through the containment system, and radioactive decay of fission products on the rate of activity release and the resultant exposures. The combined effect of these factors, when treated in a conservative manner, is to reduce the calculated exposures by approximately an order of magnitude for situations of interest. This reduction may be important in assessing the feasibility of evacuating personnel from the immediate vicinity following an accident and of moving the stricken ship to a remote anchorage without excessive exposures to the people involved.

During the interim operating period, U.S. ports to be visited by the N.S. SAVANNAH are first visited by a port survey team, which evaluates the port area from a nuclear safety standpoint and makes operational arrangements for the forthcoming visit. The Laboratory provided nuclear engineering assistance for these surveys.

The effect on reactivity lifetime of replacing the actual two-zone fuel loading of core I by a single-zone loading with the inner-zone enrichment was investigated analytically. The two-zone core was found to increase the reactivity lifetime by only about one month. A single-zone core treatment should, therefore, be suitable for many kinds of studies. The two-zone core has a slightly smaller peak-to-average radial power ratio than the uniformly loaded core, but the flatter radial-power distribution of the two-zone loading is vitiated with burnup.

The inventories of fissionable materials in core I were computed as a function of operating time. The burnup of U^{235} was found to be fairly

linear, with a slope of about 25 kg per full-power year. The buildup of Pu^{239} occurs at a rate of about 8 kg per full-power year during the first full-power year and at a rate of about 6 kg per full-power year during the second year of full-power operation. The buildup of Pu^{241} is quadratic in nature. At the end of core life (~ 1.7 full-power years), the plutonium isotopes contribute about 10% of the power production, U^{238} contributes about 9%, and U^{235} provides the remainder.

Pressurized-Water In-Pile Loop

The ORR pressurized-water in-pile loop continued to operate in a satisfactory and essentially trouble-free manner. In July 1962, upon completion of the irradiation phase of the currently planned tests of nonsintered fuel, this facility was transferred from the Maritime Reactor Program to the Army Reactors Program.

Water chemistry studies were continued to investigate long-lived water-borne activity and the transport and deposition of corrosion products ("crud"). Samples of fuel-rod crud deposits were analyzed and found to have specific activities comparable to the dissolved and particulate fractions of water-borne activity. A simple activity transport mechanism is postulated in which the dissolved ionic material, which is present at very low concentrations, is responsible for appreciable transport of activity from in-flux to out-of-flux crud deposits. This hypothesis is discussed in terms of data obtained from the loop.

The possibility that nonradioactive magnetite would be an effective high-temperature filter and ion exchange medium for accumulating activity in neutral-pH pressurized-water reactor systems was explored in preliminary tests. A high-temperature filter unit was added to the sample station as a side stream to the loop and is being used in the magnetite experiments.

Advanced Core Development

A previously reported comparison of reactivity lifetimes of Zircaloy and stainless steel egg-crate cores containing a uniform loading of 4.2 wt % U^{235} was based on a radial burnup calculation. Because of the striking

effect of the Zircaloy egg crate on core reactivity lifetime, this comparison was repeated by the more realistic one-dimensional window-shade method, which allows simulation of axial rod-bank control. The control-rod programming scheme was based on withdrawal of rod banks from the outer regions of the core first.

Core lifetimes calculated by the window-shade method were in good agreement with but slightly longer than the lifetimes estimated by the radial burnup calculations. The slightly greater core life is attributed to the more uniform fuel depletion produced by the rod-programming scheme employed in the window-shade calculations. The comparison again predicts that replacement of stainless steel by Zircaloy in the fuel-element container structure will essentially double the reactivity lifetime of core I fuel elements. Axial power distributions obtained from the window-shade calculations were combined with radial distributions obtained from two-dimensional PDQ calculations in the horizontal plane to give some information on three-dimensional power distributions within the cores. The most severe power peaking was higher for the Zircaloy egg-crate core than for the stainless steel egg-crate core but was below the core I design value of 3.75.

In fabricating test specimens for the ORR loop the bulk density obtainable with vibratory-compacted sintered-and-ground UO_2 was slightly lower than could be attained with fused-and-ground oxide under similar conditions. This difference results from the fact that the individual particles of the sintered material are less dense. Some problems were encountered during fabrication of fuel rods containing fused-and-ground oxide because of breakup of UO_2 particles during the compaction process. These problems were circumvented by using previbrated UO_2 for the coarse particle fractions of the ternary mixture and ball milling the fine fraction. A series of difficulties was encountered in the manufacture of a test bundle for irradiation in the Vallecitos Boiling Water Reactor. The difficulties may be attributed broadly to deficiencies in the UO_2 material procured for this purpose. Completion of the test bundle awaits procurement of additional UO_2 .

Vibratory-compaction studies performed with depleted, fused UO_2 indicate that it is reasonable to expect a bulk density of 90% of theoretical

in a reactor core loading. Binary mixtures of particle sizes appear to yield bulk densities equal to those obtainable with ternary mixtures. A correlation was found to exist between the bulk density and an apparent Stokes diameter. The densities of compacted distributions seem to increase with decreasing particle size down to an apparent Stokes diameter of approximately $15\ \mu$. If the size is less than this, the density appears to decrease.

Irradiation tests of nonpelletized UO_2 fuel were conducted in the ORR pressurized-water loop to aid in the determination of the suitability of such fuel for use in a replacement core for the N.S. SAVANNAH reactor. Twenty-seven nonpelletized fuel rods were irradiated at peak heat ratings ranging from 95 to 540 w per centimeter of fuel length and to peak burnups ranging from about 1,000 to over 10,000 Mwd/T. Eighteen of these rods have been destructively examined at the Vallecitos Laboratory of the General Electric Company and the remainder are awaiting destructive examinations to be performed at ORNL.

Metallographic examination of the irradiated specimens revealed structural changes ranging from little or no sintering in specimens which had operated at low heat ratings to extensive sintering in the specimens tested at higher heat ratings. The highest rated rod examined (400 w/cm) contained a central void approximately 0.040 in. in diameter. There was no evidence of sintering near the cladding or of central melting of the UO_2 in any of the fuel rods. The highest fission-gas release observed was 23.4% in the specimen which developed a central void. There was no evidence of corrosion at the outer surfaces of the type 304 stainless steel cladding, but a lamellar and intergranular precipitate was observed at the inner cladding surface of some rods that extended to a maximum depth of 0.005 in. This precipitate was apparently dependent upon the nitrogen impurity level of the UO_2 .

Based on information available from ORNL and other programs, an overall evaluation was made to assess nonsintered fuel for application in the N.S. SAVANNAH reactor. It was concluded that nonsintered UO_2 fuel could be applied with confidence in all aspects of performance, with one important exception. The susceptibility of this fuel to waterlogging failures

and the consequences of such failures are at present uncertain. It appears, therefore, that more experience is necessary before sufficient confidence has been established for use of nonsintered UO_2 in the N.S. SAVANNAH reactor.

1. INTRODUCTION

The purpose of the ORNL Maritime Reactors Program is to provide technical assistance to the AEC Division of Reactor Development (Maritime Reactors) in the development of nuclear-powered merchant ships. Since September 1957 when this assistance program was initiated, the bulk of the ORNL effort has been associated with the N.S. SAVANNAH project. The nature and extent of assistance activities have gradually changed as the project progressed through design, construction, test, and operation stages.

The N.S. SAVANNAH, which is the first nuclear-powered merchant ship, was built by the New York Shipbuilding Corporation of Camden, New Jersey; the pressurized-water reactor and the propulsion equipment were supplied by the Babcock & Wilcox Company of Lynchburg, Virginia; and the ship is being operated by States Marine Lines, Inc., as an agent for the Maritime Administration. Over-all program direction is exercised for the government by the Atomic Energy Commission-Maritime Administration Joint Group.

Initial criticality of the N.S. SAVANNAH reactor was achieved on December 21, 1961. In the period from December 21, 1961 to January 18, 1962 a series of low-power tests was conducted at the Camden, New Jersey, yard of the New York Shipbuilding Corporation, culminating with tests at approximately 10% of full power (about 6.9 Mw thermal). The ship was moved from Camden under auxiliary steam power on January 31, 1962 and arrived at the U.S. Coast Guard Reserve Training Center in Yorktown, Virginia, on February 2, 1962. Following additional dockside testing at power levels up to 40% of full power, the initial sea run was made March 23-26, 1962, during which 80% of full power was attained. The first operation at full power occurred during the Builder's Trial April 3-6, 1962. The Acceptance Trial (primarily ship tests) was conducted April 24-26, 1962. The ship was delivered to the Maritime Administration on May 1, 1962, and operations were transferred from the New York Shipbuilding Corporation to the operating agent, States Marine Lines, Inc.

Following additional dockside and sea operations, the Atomic Energy Commission on August 3, 1962 authorized a period of interim sea and port operations, including the first group of port visits, with these operations to be conducted under special interim restrictions. The first port visitation was to Savannah, Georgia, August 22-28, 1962. Subsequently, during the current report period, the N.S. SAVANNAH visited Norfolk, Virginia (August 30-September 13, 1962), traversed the Panama Canal (September 18), and visited Seattle, Washington (October 1-November 16, 1962), San Francisco, California (November 17-26, 1962), and Long Beach, California (arriving November 27, 1962). It is planned that the ship will visit several additional ports and then enter the Todd Shipyard at Galveston, Texas, early in 1963 for an extended reactor and ship outage to evaluate the condition and performance of the ship and power plant and to incorporate a number of planned modifications.

As the N.S. SAVANNAH project progressed, several ORNL assistance tasks associated with the preoperational and testing phases were completed. These included a comprehensive radiation survey of the reactor shield, development of a shipboard bioassay program, additional safety evaluations, and inspection-engineering assistance during fabrication of replacement control rod drives.

A further reduction in the ORNL program resulted from the AEC decision during the current report period to curtail development work on future cores for the N.S. SAVANNAH reactor. Operation of the pressurized-water in-pile loop in the Oak Ridge Research Reactor and the associated water-chemistry studies for the Maritime Reactors Program were discontinued, and the facility was transferred to another program. Postirradiation examination of fuel specimens irradiated in the loop is being completed. Fuel fabrication development was terminated, except for manufacture of a nonsintered fuel test bundle for irradiation in the Vallecitos boiling-water reactor. The core design, fuel cycle, and core physics studies which were under way have been largely brought to completion.

Activities which are continuing into the operational phase of the N.S. SAVANNAH include shipboard testing of iodine and particulate filters, iodine adsorption studies to further validate and to improve in-place

testing procedures, assistance in port surveys, and review and consultation on proposed plant modifications.

2. N.S. SAVANNAH PROJECT — GENERAL SUPPORT

Shield Study

E. P. Blizzard T. V. Blosser
R. M. Freestone, Jr.

The design requirements for the shielding on the N.S. SAVANNAH were chosen to ensure that the passengers would receive no more radiation than is allowed the general public, even if they lived permanently on board ship with the reactor constantly at full power. The design rate for passenger areas was therefore 0.5 rem/yr.

The requirements were also that the crew of the vessel receive no more radiation than workers in atomic energy installations, even if they remained on board ship all the time with the reactor constantly at full power. Thus, the design rate for crew areas was 5.0 rem/yr.

Finally, it was required that the stevedores handling cargo receive no more radiation than is allowed the general public, even if they continuously worked in the cargo spaces with the reactor at one-fifth full power. The design rate for cargo spaces was therefore 0.5 rem/yr at one-fifth full power.

In order to determine whether these design specifications had been met, a survey of the radiation from the N.S. SAVANNAH shield was made during the period May 20 through May 25, 1962. The survey was made with the reactor at its full power of 69 Mw during a cruise of 2821 miles in the Atlantic Ocean out of Yorktown, Virginia.

Equipment and Procedures

A complete set of special instrumentation housed in a light Ford Vanette, the ORNL Mobile Shielding Laboratory No. 1, was developed for the N.S. SAVANNAH study. Its operation was thoroughly tested during a series of studies of land-based reactor shields¹ during the months

¹These studies were made under the sponsorship of the Division of Compliance, Atomic Energy Commission, and are individually reported in USAEC Reports ORNL TM-178, -290, and -332, Oak Ridge National Laboratory, 1962.

preceding the present study, as well as by calibrations performed at the ORNL Bulk Shielding Facility.²

The Vanette and its equipment were described previously.²⁻⁴ Gamma-ray dose rates were measured with the anthracene scintillation dosimeter, and thermal-neutron dose rates were measured with the modified long counter.

Preliminary estimates of the magnitude of the SAVANNAH survey indicated that a round-the-clock operation was desirable in order to minimize the time the ship would be at sea. A total of 41 people participated in the survey. Twenty-three of these people came from various Oak Ridge Installations (ORNL, ORGDP, and Y-12), and the remaining 18 were from the Martin-Marietta Corporation, Todd Shipyards Corporation, Babcock & Wilcox Company, and the U.S. Maritime Administration. The group was divided into three watches of 12 persons each, comprising five two-men detector-counter teams plus a watch captain and his assistant. Normally, two gamma-ray detectors and two thermal-neutron detectors were in continuous operation, and a fifth team was busy making various special measurements.

Prior to the start of the survey the secondary shield was marked* with a rectangular, 3-ft grid, which served to control and locate all measurements. The general procedure for the survey consisted of taking a 1- or 1/2-min count (depending on counting statistics) in the center of each grid with both the gamma-ray and the thermal-neutron dosimeters. After the count, the area within the grid was slowly swept with the detector to find any area of unusual leakage. Fast-neutron dose rates were measured at carefully chosen locations over the shield to provide data

*Ernest Resner, States Marine Lines health physicist, supervised the marking of the secondary shield.

²T. V. Blosser, Shield Survey, p. 7, "Maritime Reactor Project Ann. Prog. Rep. Nov. 30, 1961," USAEC Report ORNL-3238, Oak Ridge National Laboratory.

³T. V. Blosser, Shield Survey, p. 5, "Maritime Reactor Project Ann. Prog. Rep. Nov. 30, 1960," USAEC Report ORNL-3046, Oak Ridge National Laboratory.

⁴E. P. Blizard, T. V. Blosser, and R. M. Freestone, Jr., "The Radiation Leakage Study of the Shield of the Nuclear Ship Savannah," USAEC Report ORNL-3336, Oak Ridge National Laboratory, Aug. 15, 1962.

for a good evaluation of the ratio of fast neutrons to thermal neutrons at locations typical of the several different shield configurations.

Measurements were also made at a number of special points for comparison with the predicted dose rates of the shield design.⁵ At these points a complete set of gamma-ray, fast-neutron, and thermal-neutron dose rates was measured.

A final experiment in the survey consisted of a measurement of the dose rates fore, aft, and amidship of the reactor shield as the water was pumped from the inner-bottom shield tanks under the containment shell.

Results

Since a detailed report of the survey has already been published,⁴ only some typical results are presented here. The detailed coverage of the shield is evident in Fig. 2.1, which shows the gamma-ray data from the forward and port sides of the shield. Typical special-point data are presented in Table 2.1, the points noted being graphically located in

⁵W. R. Smith and M. R. Turner, "Nuclear Merchant Ship Reactor Shield Design Summary Report," p. 46, USAEC Report BAW-1144-1, Babcock & Wilcox Company, Aug. 1, 1959.

Table 2.1. Comparison of Measured Dose Rates with Calculated Dose Rates at Special Points on Promenade Deck

Point No.	Observed Dose Rate				Calculated Dose Rate (ref. 5)		
	Fast-Neutron (mrem/hr)	Thermal-Neutron (mrem/hr)	Gamma Ray (mr/hr)	Total (mrem/hr)	Neutron (mrem/hr)	Gamma Ray (mrem/hr)	Total (mrem/hr)
	$\times 10^{-3}$	$\times 10^{-4}$	$\times 10^{-2}$	$\times 10^{-2}$	$\times 10^{-2}$	$\times 10^{-2}$	$\times 10^{-1}$
44	1.50	1.31	0.925	2.23	1.0	41.9	4.29
45	0.988	1.16	1.42	2.28	0	9.5	0.95
46	0.976	0.771	0.569	1.42	0.7	17.9	1.86
47	1.65	1.52	1.14	2.58			
48	1.51	0.412	1.09	2.39	1.0	11.0	1.20
49	1.92	0.581	1.16	2.82			
50	1.43	0.422	1.36	2.59			
52	0.923	0.242	0.669	1.46			
53	1.29	3.21	1.80	2.94			
54	1.40	0.570	1.53	2.75	2.4	8.4	1.08
56	0.897	2.09	0.624	1.42	1.6	11.0	1.26
57	0.845	0.369	0.360	1.10			
71	1.09	0.232	0.823	1.76	4.3	8.4	1.27
72	1.43	0.318	0.68	1.91	4.6	8.4	1.30
80	1.72	1.87	1.16	2.57			
81	1.73	1.26	1.60	3.10			
82	2.17	2.54	3.46	5.36			
85	1.39	0.635	0.579	1.79			
86	1.37	1.09	1.27	2.46			

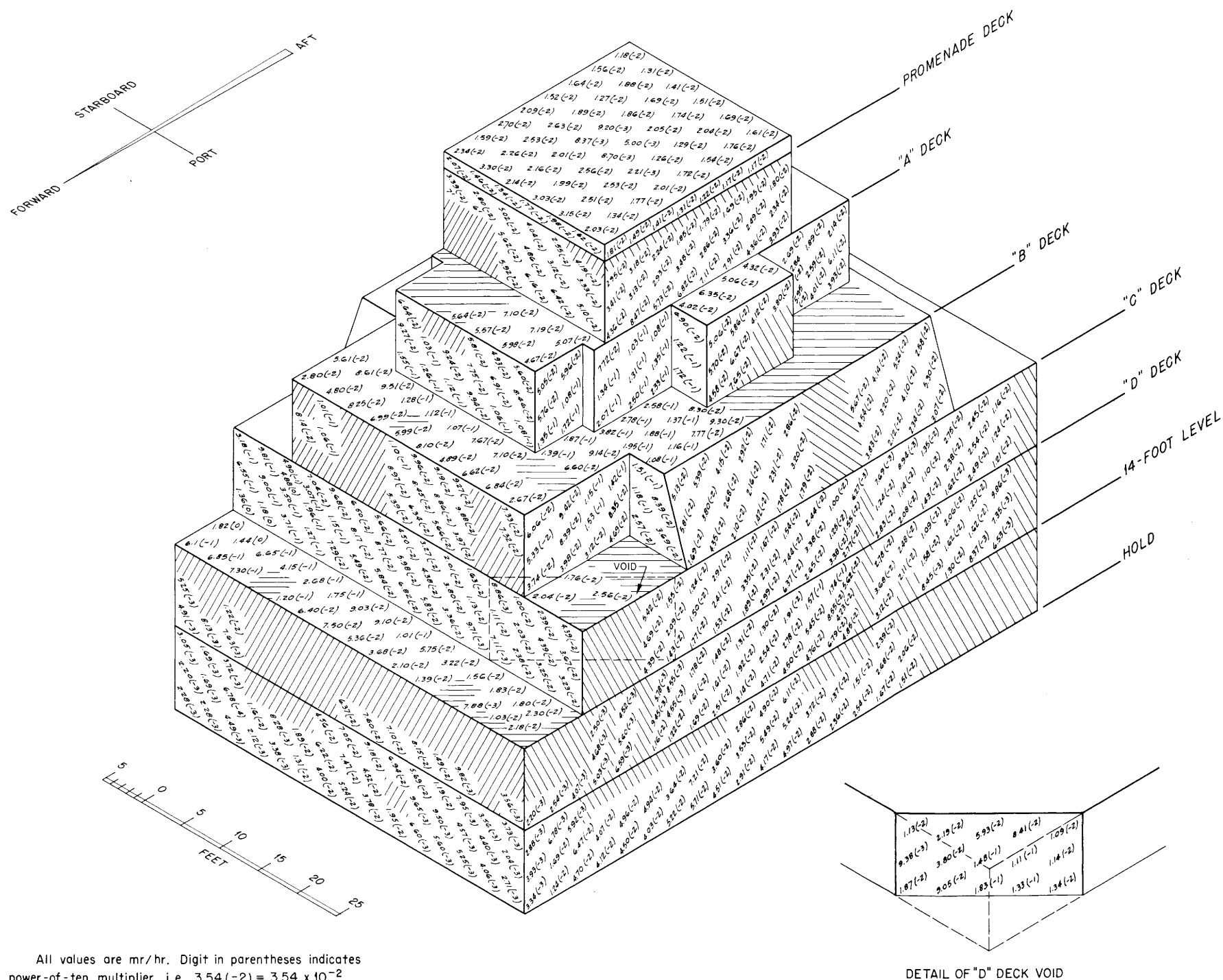


Fig. 2.1. Gamma-Ray Dose Rates on Forward and Port Surfaces of the N.S. SAVANNAH Shield.

Fig. 2.2. The effects of emptying the inner-bottom shield tanks are shown in Fig. 2.3.

Conclusions

The results of the survey show that the dose rates do not exceed the design levels in any areas to which passengers are permitted access. In the crew-access areas the design dose rate is exceeded in only a small area, that is, in the water-sampling room against the forward bulkhead. Entry to this area can easily be controlled. The results of the tank

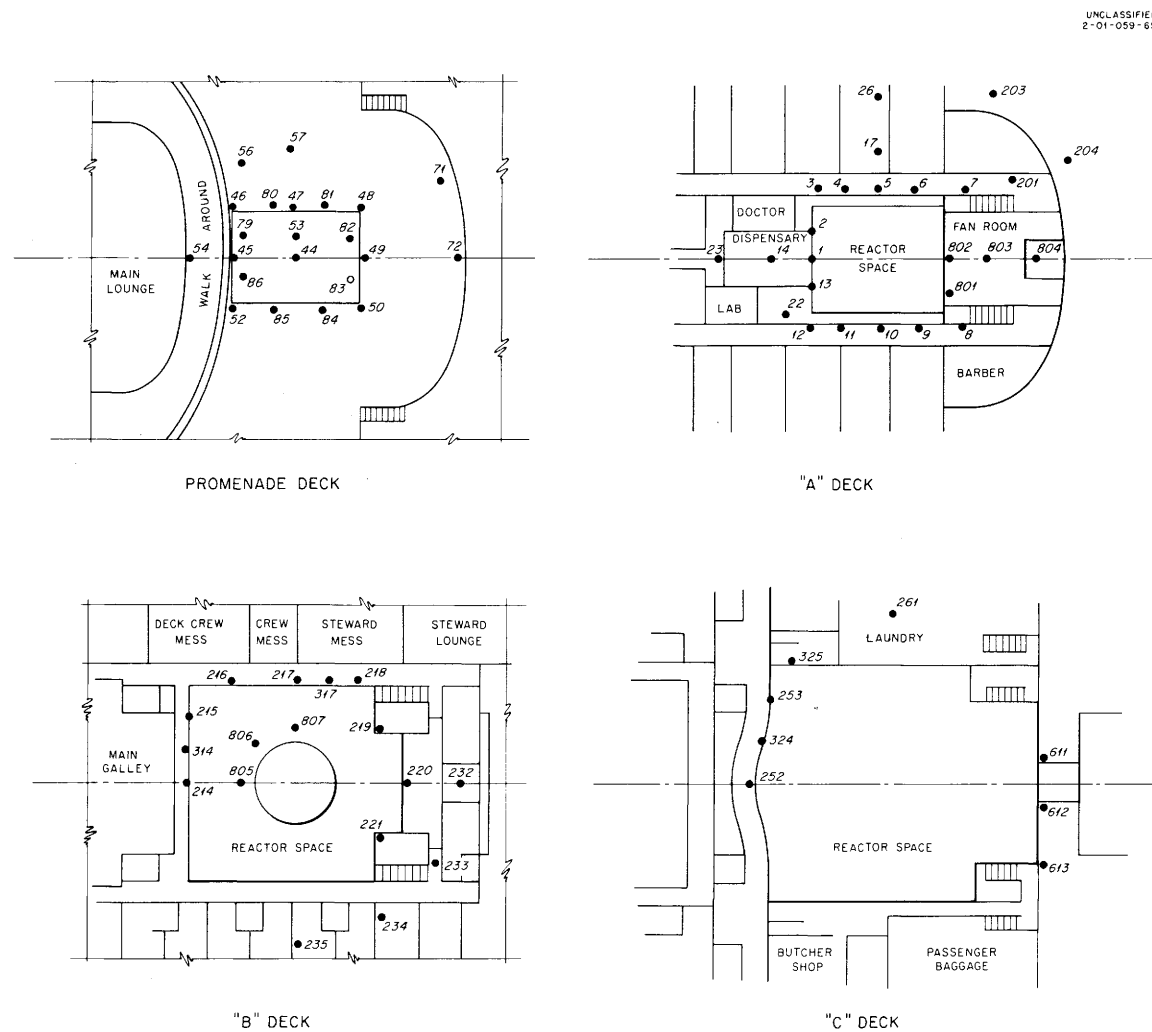


Fig. 2.2. Special-Point Locations on Promenade, "A," "B," and "C" Decks of N.S. SAVANNAH.

pump-down show that even with total loss of water a safe condition exists only a few feet from the shield. In short, the results prove that the shield effectively meets the stringent design specifications.

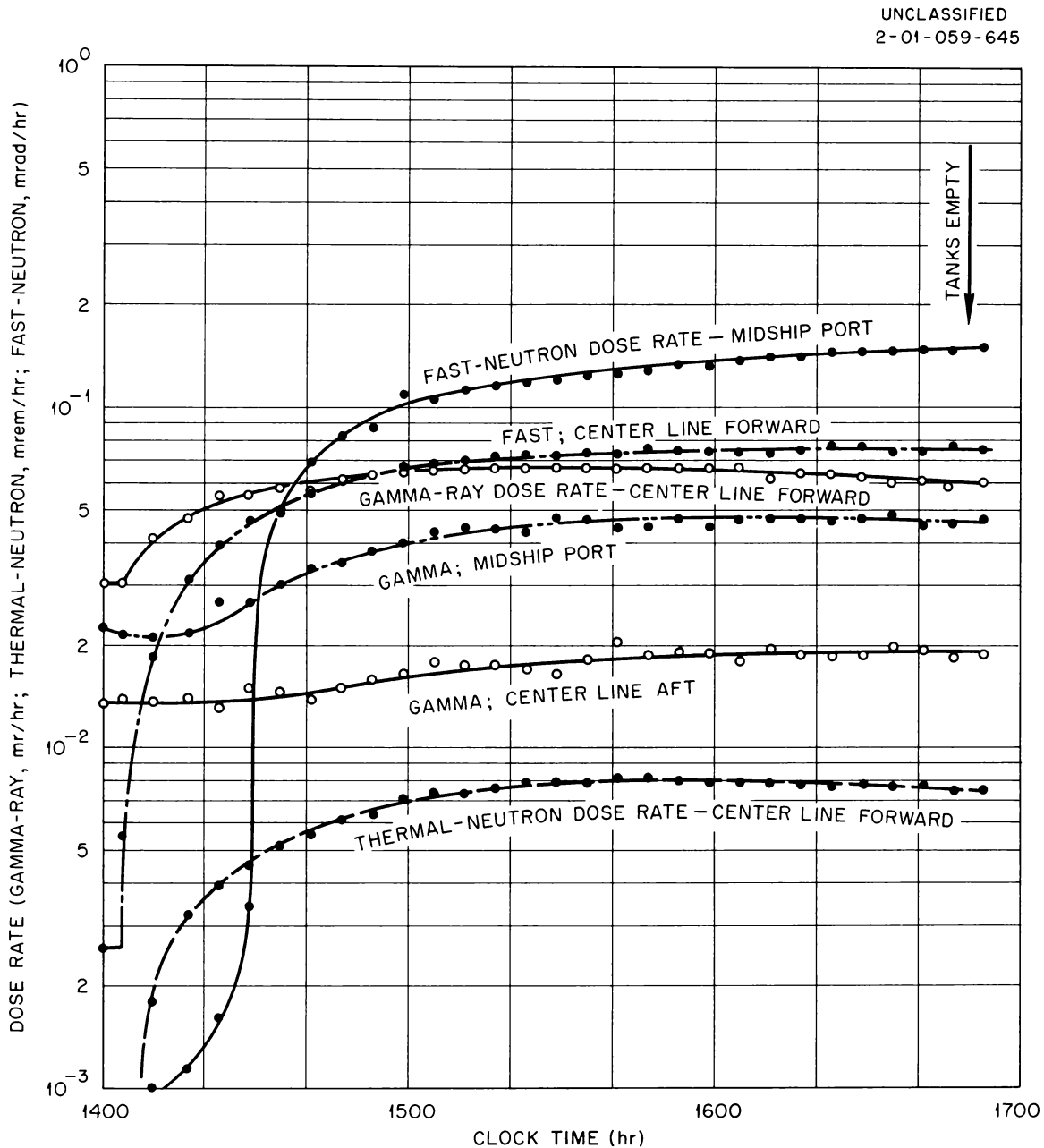


Fig. 2.3. Gamma-Ray, Thermal-Neutron, and Fast-Neutron Dose Rates at Three Locations During Emptying of N.S. SAVANNAH Subreactor Shield Tanks. All detectors were at tank-top level and against the reactor shield.

Iodine Adsorption Studies

R. E. Adams W. E. Browning, Jr.

The ventilation gases from the reactor compartment of the N.S. SAVANNAH are processed through particulate filters and iodine sorption units to provide for control of radioactive iodine vapor and particulate material. Two systems for ventilating the compartment are provided. The normal ventilation system is of 4000-cfm capacity, with provisions for processing the gases through three cleaning stages: (1) roughing filters and (2) high-efficiency filters for control of particulate material and (3) silver-plated copper-mesh units for iodine control. An auxiliary or emergency system of 200-cfm capacity is provided with five stages of gas cleaning. The ventilation gases are passed through (1) a prefilter, (2) a high-efficiency filter, (3) a silver-plated copper-mesh bed, (4) an activated-charcoal unit, and (5) a second silver-plated copper-mesh bed. Air leaving the filter unit is combined with approximately 1800 cfm of diluent air taken from outside the compartment before being exhausted to the atmosphere. The emergency system serves as a backup to the normal system and does not operate continuously.

While the information available at the time these systems were designed was sufficient to demonstrate the feasibility of using activated charcoal for the removal of iodine vapor from moist air at elevated temperatures, it was not sufficient to ensure that the full-scale units designed for the N.S. SAVANNAH would provide the required iodine-decontamination efficiency under conditions postulated to occur following a reactor accident involving fission-product release. Accordingly, an experimental program was undertaken to determine the iodine efficiency that could be expected of the activated-charcoal unit installed aboard the N.S. SAVANNAH.

Laboratory Studies

The laboratory studies were undertaken in two parts. Small-scale tests are being conducted on 10-g samples of activated charcoal to determine the iodine-adsorption efficiency under stated operating conditions. This phase of the study is intended to provide quantitative or

semiquantitative information as to the behavior of various types of charcoal at design and off-design conditions. To date, 50 tests have been completed on four types of charcoal (including the Pittsburgh BPL charcoal used in the full-scale units) under various combinations of temperature and humidity. These tests have indicated both normal and abnormal penetration of iodine through the activated charcoal mass under study. Variations in the environmental conditions of the laboratory, conditions of operation of the experiments, materials used in construction of the experimental apparatus, and the iodine vapor sources may, either singly or in combination, be responsible for this behavior. These possible causes of this rather unpredictable penetration of iodine are under experimental study.

The second part of the laboratory study involves the testing of iodine adsorption units, 11 in. square and 1.125 in. thick, produced by Flanders Filters, Inc. These units, containing Pittsburgh BPL charcoal, were manufactured by using the same materials and techniques as those used in producing the full-scale iodine-adsorption units installed aboard the ship. The experimental apparatus for these tests is illustrated in Figs. 2.4 and 2.5. The system is constructed of 4-in.-diam glass pipe with metal pieces making the transition to accommodate the 11-in.-square filter unit. The system is heated, externally, by flexible heating tapes to prevent premature condensation of the steam by the walls of the system. This heated zone terminates at point "B" of Fig. 2.4. From this point efforts are made to condense the steam for recovery of iodine.

A typical test involves the following operations. Iodine vapor (I^{127} containing radioactive I^{131}) is introduced continuously into the air-steam mixture passing into the system. Iodine vapor escaping from the iodine-adsorption unit under test is collected downstream on the walls of the apparatus, in the condensate drained periodically from the system, on the small rings comprising the steam condenser column packing, or in the two room-temperature charcoal adsorbers. During operation a small portion of the steam-air-iodine vapor mixture is passed through samplers located upstream and downstream from the test unit. After completion of a 12-hr test the system is cooled, completely drained,

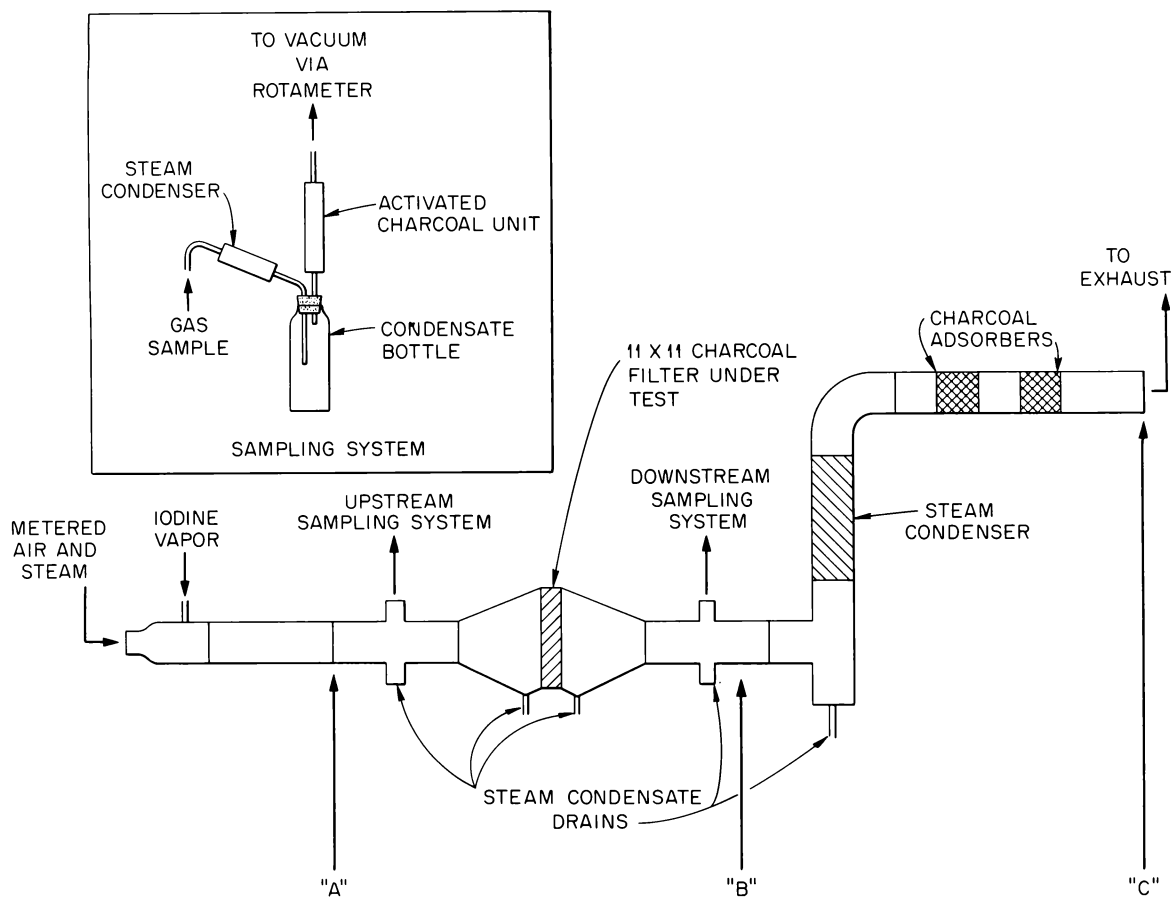


Fig. 2.4. Iodine-Adsorption Testing System for 11-in.-Square Charcoal Units.

and disassembled. The iodine-adsorption efficiency of the unit under test is then determined by radiochemical assay of the system from the point "A" to the point "C" indicated on Fig. 2.4. By comparing the amount of iodine residing in the test adsorption unit with the total amount found in (1) the test unit, (2) all downstream components, and (3) condensates, an iodine-adsorption efficiency is obtained. In addition, an iodine-adsorption efficiency is calculated from the data obtained by the two analytical samplers. Allowances for the observed deposition of iodine on the walls of the system are made in calculating this efficiency. Details and results of 14 tests on the 11-in.-square iodine filter units are presented in Table 2.2. These tests, conducted with continuous

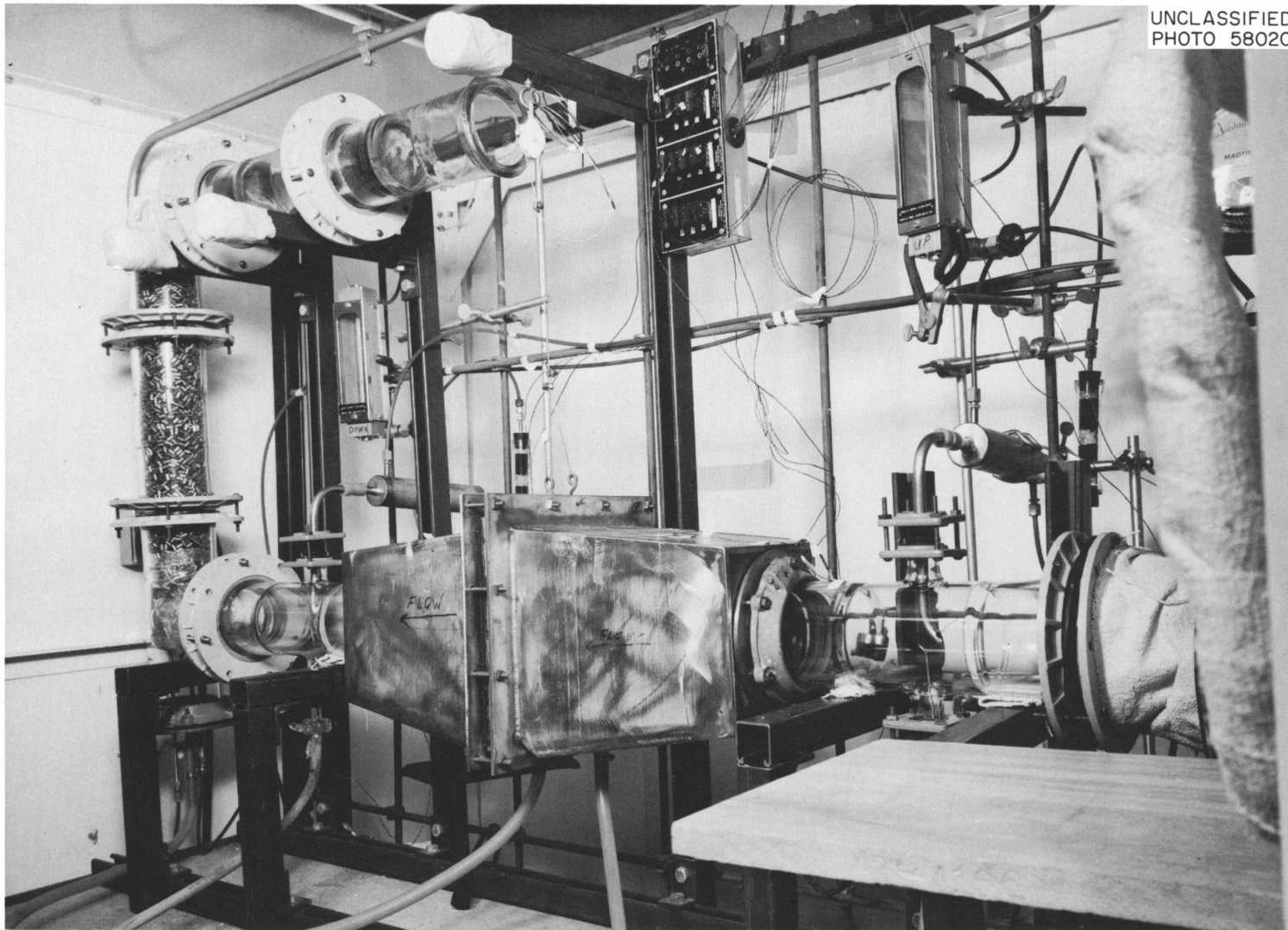


Fig. 2.5. Iodine Adsorption Testing System Before Installation of Heaters and Insulation.

Table 2.2. Conditions and Results of Iodine-Removal Efficiency Tests on 11-in.-Square Charcoal Adsorbers

Run No.	Temperature (°C)	Face Velocity (ft/min)	Steam Saturation (%)	Iodine-Removal Efficiency (%)	
				Inventory	Sampling
1	96	4.6	91.3	99.84	99.93
2	100	4.3	80.7	99.63	98.95
3	26	4.8		99.98	99.86
4	99	4.5	83.8	99.95	98.57
5	100	4.4	82.1	99.73	
6	98	4.8	88.9	99.67	99.50
7	99	4.5	85.2	99.95	99.12
8	99	4.8	86.3	99.95	97.38
9	98	4.8	89.0	99.86	98.04
10	99	4.7	86.1	99.90	97.84
11 ^a	100	4.7	83.4	99.90	99.43
12	98	5.0	89.6	99.83	99.38
13 ^a	98	4.9	88.6	99.95	99.56
14 ^a	98	4.9	89.3	99.72	95.00
Mean				99.86 ± 0.07%	98.66 ± 0.82%

^a24-hr tests; all other tests were of 12 hr duration.

iodine injection at 96 to 100°C and with 80 to 90% saturated steam in air, have shown the efficiency of the charcoal unit alone to be $99.86 \pm 0.07\%$ at the 95% confidence level. Eleven of the tests were of 12 hr duration, and three were continued for 24 hr. No significant effect of test duration was noted.

Shipboard Tests

First Series. In-place tests of the reactor-compartment main and emergency ventilation systems were conducted on board the ship to determine whether the installation of the adsorber units was such that the predicted efficiency of the adsorber medium could actually be realized. The charcoal adsorbers had been installed in the emergency ventilation system on December 14, 1961 and had been operated only intermittently for testing and system adjustment up to May 27, 1962, the time of the first in-place tests. Prior to installation they had been subjected to

two Freon penetration tests at the Edgewood Army Chemical Center and a stable iodine penetration test at Armour Research Foundation. In the latter test, 200 g of iodine was adsorbed.

In the in-place tests, 1 to 2 mg of elemental iodine labeled with I^{131} tracer was injected into the duct leading from the reactor compartment to the filter-adsorber assembly. Samples of the air were taken before and after this assembly and were radioassayed. The iodine was injected over a 15-min period, and the test was continued for 2 hr at the ambient temperature of the reactor compartment. Earlier laboratory tests had shown that at room temperature in air no movement of iodine in the system is observed after the initial injection. No radioiodine was found downstream from the adsorber within the limits of detection. Two tests were conducted using different amounts of tracer (5 and 15 millicuries of I^{131}). The limits of sensitivities were such that 1/1400 and 1/15,000, respectively, of the iodine collected upstream could have been detected in the downstream collector. Therefore the efficiencies were >99.93 and >99.99%. These tests indicated that the charcoal-absorber assembly, as installed, was capable of the iodine-removal efficiency observed in laboratory tests.

The in-place efficiency test conducted on the main reactor-compartment ventilation system was similar. The silver-plated copper-mesh iodine adsorber had been installed on December 14, 1961 and had been operated almost continuously up to the time of the in-place test. In this test 10 mg of elemental iodine containing 15 millicuries of I^{131} was injected. Two downstream iodine collectors were used, one immediately following the air-cleaning assembly, and the other on the deck of the ship at the base of the stack. Approximately the same amounts of iodine were found in the two downstream collectors. Comparison of this amount with that found in the upstream collector yielded an efficiency of 95%. This result is consistent with results of laboratory tests on silver-plated copper mesh in air at room temperature.

Second Series. A second series of in-place tests was conducted on August 15-16, 1962, and the test procedures and equipment used were identical to those in the initial tests. Iodine samples were analyzed using the RCL-128 gamma spectrometer on board the ship. The emergency system

tests employed 2 mg of elemental iodine containing 15 millicuries of I^{131} . Based upon the quantity of I^{131} found in the samplers, the iodine efficiency of the emergency ventilation system was 99.7%. The distribution of iodine radioactivity on the components of the downstream sampler suggested strongly that the iodine was predominantly associated with particulate matter. The distribution of activity in the upstream sampler was indicative of iodine in the vapor state. This behavior is contrary to that observed during the initial in-place tests of May 1962. Strict comparison of these efficiency values may be subject to question, however, because the emergency system was modified in the interval between tests. The modification included the installation of a metal transition piece between the original system intake duct and the particulate-filter housing upstream of the charcoal unit. The purpose of this modification was to provide multiple intakes for this ventilation system. The opening for this transition piece was cut into the top of the metal filter housing while the filter was in place, and the filter sealing flange and filter frame were damaged. In order to repair the damage, it was necessary to remove the charcoal unit from the housing. Upon replacement of the particulate filter, the charcoal unit was reinstalled. This was the condition of the emergency ventilation system during the second series of in-place tests.

In the second series of tests of the main reactor compartment ventilation system, the efficiency was found to be between 90 and 95%, based on the I^{131} radioactivity found in the two downstream samplers. This is consistent with the 95% efficiency determined in the initial in-place test and with results obtained in laboratory tests on silver-plated copper mesh in air at room temperature.

Third Series. The third series of in-place tests was conducted on September 12-13, 1962, and the test procedures and equipment were similar to those of the previous tests. Duplicate tests were made on the emergency system. Based on the amounts of I^{131} found in the samplers, the iodine efficiency of the emergency ventilation system was at least 99.99% for conditions prevailing at the time of the test. The distribution of activity in the upstream samplers was indicative of iodine in the vapor state. It was not possible to characterize the state of the iodine in

the downstream samplers because the amount of activity was not sufficiently different from background. The over-all behavior in these tests was identical with that of the initial tests conducted in May 1962. No tests were conducted on the main ventilation system during this series of tests.

Normal Iodine Tests. Since an in-place method for determining the efficiency of an iodine-removal system using normal iodine would be of considerable interest for application to the ventilation systems on the N.S. SAVANNAH, tests with normal iodine were also performed. Normal iodine is preferred over I^{131} tracer for in-place tests because its use would eliminate the risk of contamination of the ship. Tests with I^{131} have had to be performed while the ship is in a relatively unpopulated harbor or at sea, and these tests have interfered with the operating schedule of the ship. Tests using normal iodine could be performed while the ship is in any harbor or while carrying passengers without risk.

Two in-place efficiency tests with normal iodine and one background test in which no iodine was injected were conducted on the emergency system on September 11, 1962. Approximately 1 g of nonradioactive elemental iodine vapor was injected into the in-take duct leading from the compartment into the five-stage filter unit. Samples of the air stream before and after the filter unit were taken during the 2-hr test. Similar samples had been taken for a 2-hr period prior to injection of the iodine vapor. The samples from these tests were analyzed for iodine content by activation analysis. Each of the samplers from the background test contained approximately 0.5 μg of iodine. This amount agrees with the amount of iodine found in samples of the charcoal which had not been exposed to the air in the ship. The analyses of samples taken in the two tests where normal iodine was injected into the ventilation system indicated iodine-removal efficiencies of 99.996+ and 99.991+%, respectively. Pertinent details of the normal iodine tests are presented in Table 2.3. These results are in good agreement with the results obtained in the two tests conducted with I^{131} on September 12-13, 1962, at which time efficiencies of 99.99+ and 99.99% were obtained.

These results indicate that a satisfactory testing procedure can be developed by making use of normal iodine and activation analysis. Caution should be exercised in interpreting these results, however, because

Table 2.3. Conditions and Results of In-Place I^{127} Tests of
N.S. SAVANNAH Emergency Ventilation System

	Background Test	I^{127} Injection Tests	
		Test 1	Test 2
System flow rate, ^a cfm	200	200	200
Duration of test, hr	2	2	2
I^{127} injected, mg	0	1600	1200
I^{127} in upstream sampler, mg	6×10^{-4}	15.5	10.7
I^{127} in downstream sampler, mg	5×10^{-4}	5×10^{-4}	9×10^{-4}
Iodine-removal efficiency, %		>99.996	>99.991

^aSystem under emergency mode of operation with maximum offgas dilution.

the tests were conducted under only one set of conditions. Additional experience must be obtained to determine whether there is a significant variation in the iodine background with time or location of the ship. Further development of testing procedures is necessary to improve the efficiency of the testing operation and to reduce the dependence upon operator skill and experience.

Environmental Monitoring

Environmental monitoring for the presence of radioiodine in the various compartments of the ship is accomplished by passing a measured volume of air through an activated charcoal cartridge. Iodine radioactivity in the cartridge is then determined by one of several types of radiation-detection instruments. High-volume air flow and small sample size are necessary operational features; therefore, high linear gas velocities exist in the charcoal mass. Twelve experimental tests were conducted under conditions of low mass concentration of iodine in the air and high linear gas velocity. Under linear gas velocities of 295 fpm and iodine concentrations of the order of $1 \mu\text{g}/\text{m}^3$, efficiencies consistently greater than 90% were obtained from Pittsburgh PCB charcoal, 6/16 mesh, 1.75 in. deep, for a 45-min test period. The average efficiency was 97.4% under these conditions. Efficiencies in this range are considered adequate for environmental monitoring.

Bioassay Development Program

B. R. Fish G. W. Royster, Jr.

Experiments directed toward developing a comprehensive bioassay program for the N.S. SAVANNAH Medical Department were completed in June 1962. In recognition of the limitations in space and equipment aboard ship, all procedures were simplified and designed to entail a minimum of processing.

Urinalysis

The initial approach to providing a procedure for shipboard use was to count raw urine directly with a NaI(Tl) crystal and to determine efficiency factors and lower limits of detectability for the major corrosion and fission products. Indications are that the most likely internal exposure incidents aboard the N.S. SAVANNAH would involve radioactive corrosion products. Data from the SM-1 reactor show that soon after startup the predominant corrosion product is Co^{58} and that there is about seven times as much Co^{58} as Co^{60} . The other major corrosion products, Cr^{51} , Fe^{59} , and Mn^{54} , are present in the same order of concentration as Co^{60} . Thus, if Co^{58} is eliminated in the urine, it may be assumed that exposure to a gross mixture of corrosion products has occurred. By the same token, if Cs^{137} is eliminated in the urine, a fission-product exposure may be suspected. This development work was done with the N.S. SAVANNAH counting equipment, that is, a 128-channel analyzer and a 2-in. by 2-in. well-type NaI(Tl) crystal. A 3-in. by 3-in. solid NaI(Tl) crystal was later obtained to provide greater sensitivity.

The urinalysis program was designed primarily as a screening procedure with which significant cases of internal exposure could be recognized. Once the serious cases were identified, a more intensive effort could be applied to obtain estimates of internal dose.

Direct Gamma Counting

If an incident involved the inhalation of Co^{58} and Co^{60} , the most precise procedure for estimating body burdens of these gamma emitting

nuclides would be to measure the gamma radiation penetrating to the outside of the body from internal deposits. By using a collimated crystal the location and extent of internal deposits could be estimated. After inhalation of an insoluble mixture, such as corrosion-product Co^{58} and Co^{60} , urinary excretion would be a poor indicator of the actual lung deposit.

Equipment and Procedure. The 128-channel analyzer and 3-in. by 3-in. NaI(Tl) crystal would be utilized for external measurements. The crystal is mounted in an iron shield that has a removable top. When the top is removed, gamma radiation originating directly over the crystal is detected, and the walls of the shield effectively discriminate against gamma radiation originating elsewhere. A person lying on a cot placed over the shield could be scanned for gamma-emitting deposits by moving the cot so as to place any selected area of the body directly over the crystal.

Efficiency Factors. Sources were placed inside a pressed-wood phantom and counted in order to simulate conditions of shielding and geometry for the human body. Efficiency factors were established for the four major corrosion products and for Cs^{137} by using each nuclide individually. The gamma spectrum obtained by placing five different radionuclides in the pressed-wood phantom and counting for 13.1 min at 13.3 kev/channel is shown in Fig. 2.6. Each nuclide was contained in four vials of equal concentration and 20 vials were distributed in the phantom so as to simulate distribution in the lungs. The amounts of each nuclide calculated by analysis of the gross spectrum compare well with the actual amounts present in the phantom.

Safety Evaluations

During the late spring and summer of 1962 an intensive effort was made by government and contractor personnel to evaluate the safety of operation of the N.S. SAVANNAH in port areas. On the basis of this effort, tentative criteria were developed and were accepted by the regulatory authorities as a basis for authorizing operation of the N.S. SAVANNAH during an interim period. Among the investigations carried out in the

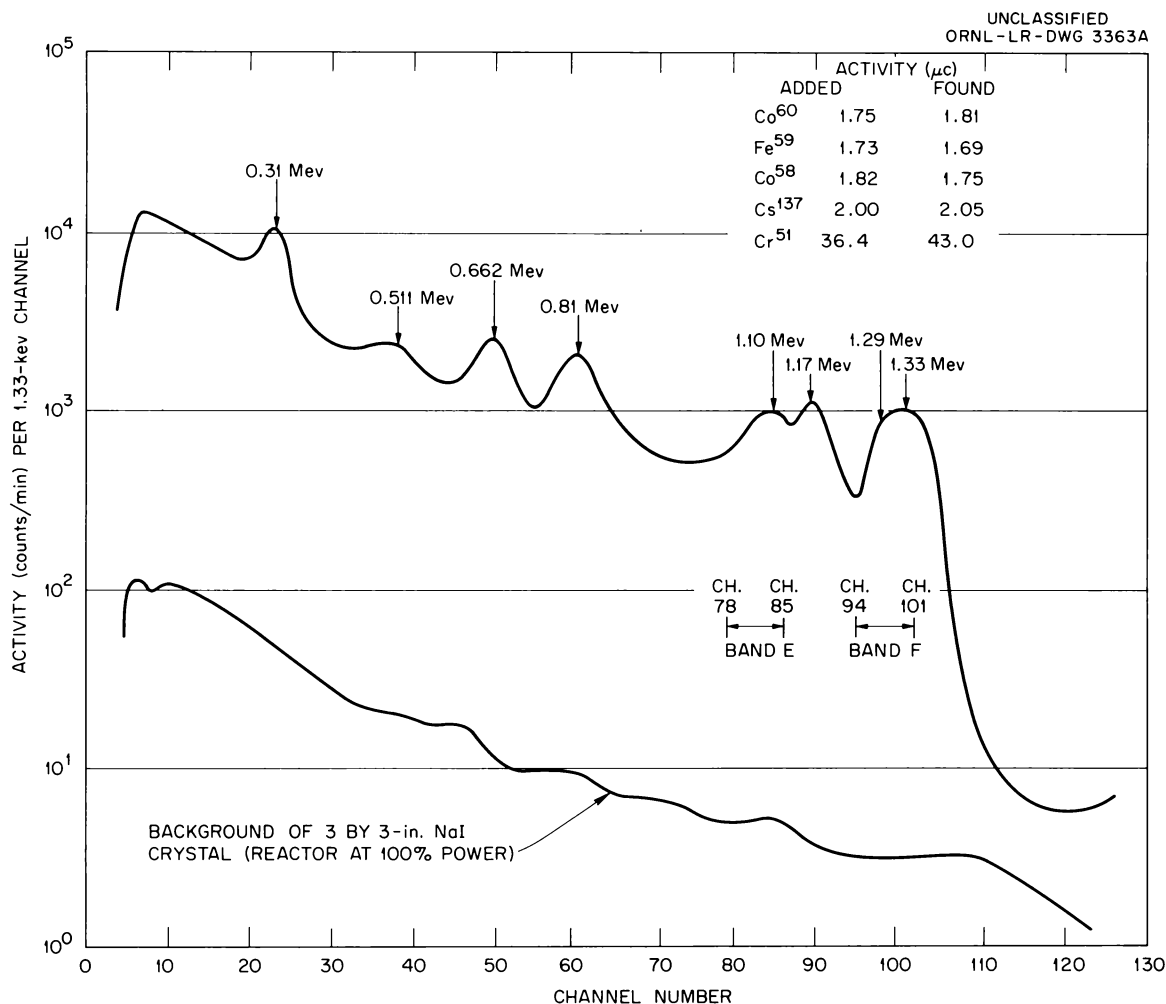


Fig. 2.6. Composite Spectrum from a Chest Phantom Containing a Corrosion-Product Mixture Plus Cs¹³⁷.

course of developing the port criteria was a re-evaluation of several factors affecting activity release in the event of the maximum credible accident.

Activity Release Studies (T. D. Anderson, J. Buchanan, W. B. Cottrell, M. Fontana, O. H. Klepper)

The maximum credible accident of the N.S. SAVANNAH reactor was identified⁶ as a large rupture of the primary coolant system. In previous

⁶"Nuclear Merchant Ship Reactor Final Safeguards Report," Vol. I, USAEC Report BAW-1164, Babcock & Wilcox Company, 1961.

analyses^{7,8} of the consequences of this accident, the following assumptions were made: (1) the accident occurred after long-term operation of the reactor at maximum power; (2) all fuel elements failed at the onset of the accident, and all releasable activity was immediately dispersed throughout the containment vessel; (3) released activity leaked from the containment vessel at the specified maximum leakage rate and passed to the environment with no further time delay; and (4) the activities were not depleted by radioactive decay. Assumptions similar to these are commonly employed in analyses of stationary power plants, where a lesser degree of conservatism is either difficult to justify or there is little incentive for doing so.

In the case of the SAVANNAH, however, there is incentive for a more realistic treatment of release mechanisms, particularly those which influence the rate of activity release during the period immediately following the accident. This is the period in which it would be advantageous to use the inherent mobility of the ship as a means for reducing the consequences of an accident after it occurred. Studies⁹ have indicated that with proper planning and preparation it would be physically feasible to evacuate unnecessary personnel from the ship and to move it from a dock position to an isolated anchorage within a period of 24 hr and probably within 2 hr after a reactor accident. The actual feasibility of carrying out such a move would, however, be dependent upon assurance that the radiation exposures to tug crews, essential ship personnel, and the general public could be held to acceptable levels.

A study¹⁰ was carried out to investigate the effect on exposure of power history, time delay in release and transport of activity through

⁷W. B. Cottrell et al., "Exposure Analyses of the N.S. SAVANNAH Operation at Camden," USAEC Report ORNL-2867 (rev.), Oak Ridge National Laboratory, Jan. 1, 1961.

⁸Site Report: York River, Virginia, Maritime Administration and U.S. Atomic Energy Commission, May 1960.

⁹Port Operation in the Matter of the N.S. SAVANNAH, AEC-MARAD Joint Group, 970/5053, Revised August 1, 1962.

¹⁰T. D. Anderson et al., "Activity Release from the N.S. SAVANNAH in the Maximum Credible Accident," USAEC Report ORNL-3361, Oak Ridge National Laboratory (in preparation).

the containment system, and radioactive decay of fission products. The rate of release of noble gases and of iodine isotopes as a function of time after the maximum credible accident was determined for two cases of power history and for alternate reactor compartment ventilation systems for comparison with a "reference release rate" determined by the previous simplified treatment. To illustrate the effect of the more detailed treatment of factors influencing release, exposures were determined for four cases of power history and compared with exposures for the reference case. Two of these cases will be discussed here.

Power Requirements in Harbor. Upon approaching the confined waters of a port area, the speed and therefore the power of an ocean-going vessel must be reduced. The operating procedure during this period usually precludes a sustained output of above 60% of the full-power rating. After docking, the power is further reduced to satisfy the hotel load of about 15% of full power. The power requirements during a typical port entry are indicated in Fig. 2.7.

Effect of Operating History on Time for Fuel-Element Failure. For comparison, two separate power histories were assumed: (1) continuous operation at 69 Mw prior to the accident, this being representative of the very conservative assumption made in the past, and (2) continuous full-power operation followed by 5 hr of operation at 50% of full power up to the time of the accident. The fission-product inventory for power history (2) is expected to approach the actual condition following an average port entry.

The time available between the occurrence of the accident and fuel-element failure depends, among other things, on the reactor power at the time of the mca and on the reactor operating history. Since detailed information on the probable temperature and pressure distribution within the core during the accident are not well known, it is difficult to predict the actual time required for the fuel to fail. If the fuel-element failure is assumed, however, to be a function of fuel temperature, as appears likely, a meaningful comparison of relative time to failure as a function of power history is possible. If it is further assumed (1) that shortly after the accident the outer surface of the claddings is thermally

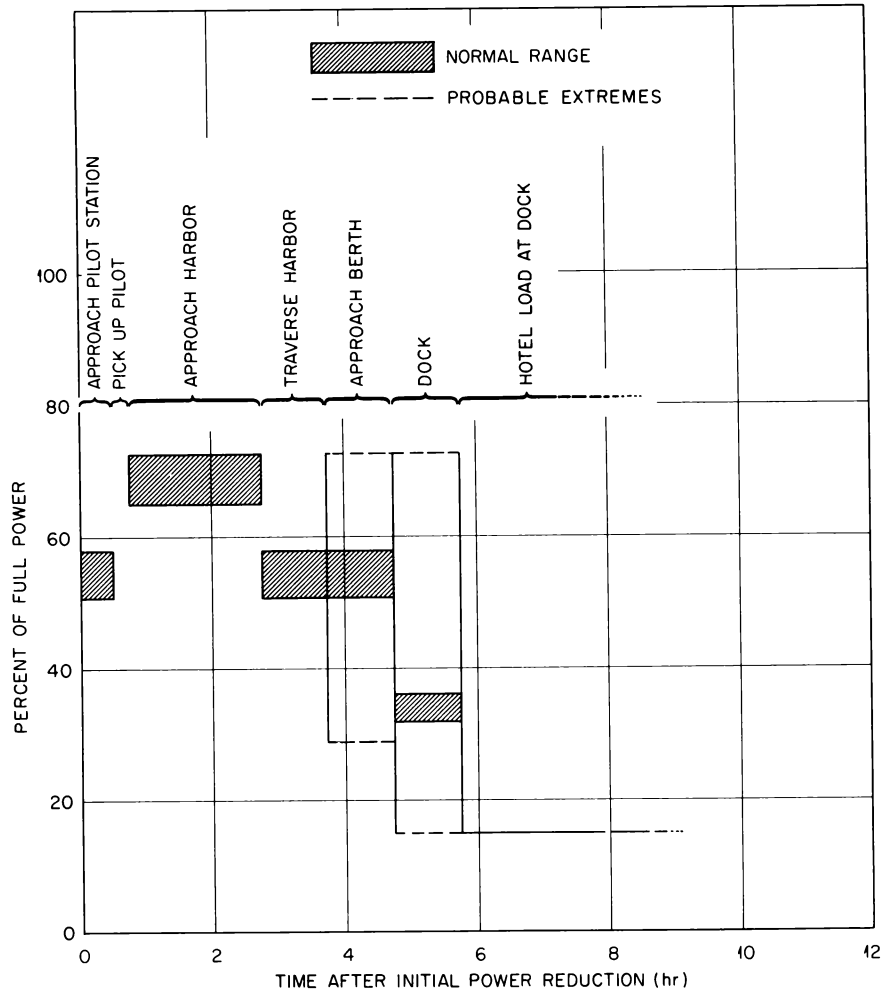
UNCLASSIFIED
ORNL-LR-DWG 69937

Fig. 2.7. Typical Reactor Operation While Entering a Port.

insulated, (2) that the cladding and UO_2 temperatures are the same at all times following the accident, (3) that the fuel cladding fails upon reaching a temperature of 2550°F , and (4) that all fuel in the rod that fails becomes exposed instantly, the fraction of fissioned fuel exposed by cladding failure can be computed as a function of time. The results of such computations are presented in Fig. 2.8 for Cases 1 and 2. The greatest difference between the cladding failure rates of Cases 1 and 2 exists within short times after the accident. For example, in Case 1, over half of the core fuel will have become exposed at 1100 sec after the accident, the time when cladding failure just begins in Case 2. In either case more than three-quarters of the fuel is exposed after 1 hr.

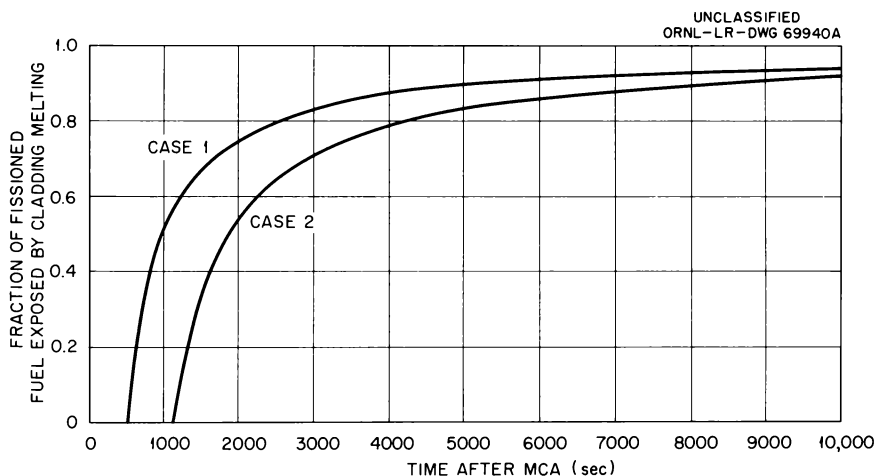


Fig. 2.8. Fraction of Fissioned Fuel Exposed by Failure of Cladding by Melting.

Fission-Product Decay. Previous studies⁷ showed that halogens and noble gases would be the main contributors to public exposure following the accident. Since some of the important isotopes have relatively short half-lives, their inventory will depend on the operating history shortly prior to the accident and the time elapsed after the accident. The fission-product inventory was computed by considering the fission yield of the isotope of interest and of one controlling precursor. Depletion by decay and neutron capture were also considered. Table 2.4 lists the results of calculations of the noble gas activity at the time of the accident, and Fig. 2.9 shows the diminishing gamma-energy release rate following the accident. As may be seen, the activity release rate is decreased to about one-half of the initial rate within 4 hr. The iodine activity to be expected following the accident is shown in Figs. 2.10 and 2.11. It is to be noted that the activity of the most important isotopes, I^{131} and I^{133} , decreases only slightly with increasing time.

Containment System Holdup. The primary containment vessel of the N.S. SAVANNAH is surrounded by a reactor compartment that is maintained at a slightly subatmospheric pressure by the ventilation system. Any leakage from the containment vessel flows first into the reactor compartment, where it remains until it is swept out by the air flow. The exhausted air is passed through particulate and halogen filters before being released to the environment.

Table 2.4. Krypton, Xenon, and Iodine Activity in Reactor Core at Time of Accident

Nuclide	Half-Life	Average Gamma Energy (Mev)	Total Core Inventory at Time of Accident (curies)	
			Case 1	Case 2
Kr ^{85m}	4.36 h	0.181	8.67×10^5	6.31×10^5
Kr ⁸⁷	78 m	0.56	1.53×10^6	8.19×10^5
Kr ⁸⁸	2.77 h	2.07	2.13×10^6	1.38×10^6
Xe ^{133m}	2.3 d	0.233	9.02×10^4	7.00×10^4
Xe ¹³³	5.27 d	0.081	3.67×10^6	3.66×10^6
Xe ^{135m}	15.6 m	0.52	1.02×10^6	8.28×10^5
Xe ¹³⁵	9.13 h	0.268	1.75×10^6	1.88×10^6
I ¹³¹	8.05 d	(a)	1.67×10^6	1.65×10^6
I ¹³²	2.4 h	(a)	2.54×10^6	2.52×10^6
I ¹³³	20.8 h	(a)	3.98×10^6	3.74×10^6
I ¹³⁵	6.68 h	(a)	3.41×10^6	2.72×10^6

^aThyroid dose is the important factor.

Two ventilation systems are provided. The one normally in operation draws 4000 cfm from the reactor compartment; and thus provides a complete air change every 7 1/2 min. The emergency ventilation system, which would be used after an accident, is capable of drawing 200 cfm from the reactor compartment and diluting this with 1800 cfm drawn from the atmosphere. Two and one-half hours is required for this system to complete an air change of the reactor compartment. The actual residence time in the reactor compartment of air-borne activity leaking from the containment vessel is difficult to predict, since it would depend on the location of the leak relative to the air flow, and leakage is expected to emanate from a number of points in the event of an accident. As an approximation, it was assumed that only one-half of the reactor compartment volume would be exhausted by the ventilation system and that instantaneous mixing of all leaked activity would take place in the reduced volume. It was further assumed that all precursor isotopes would move through the system in the same manner as the isotopes of interest. This assumption should overestimate the integrated exposures to fission gases, since some of the isotopes of interest have nonvolatile or filterable precursors.

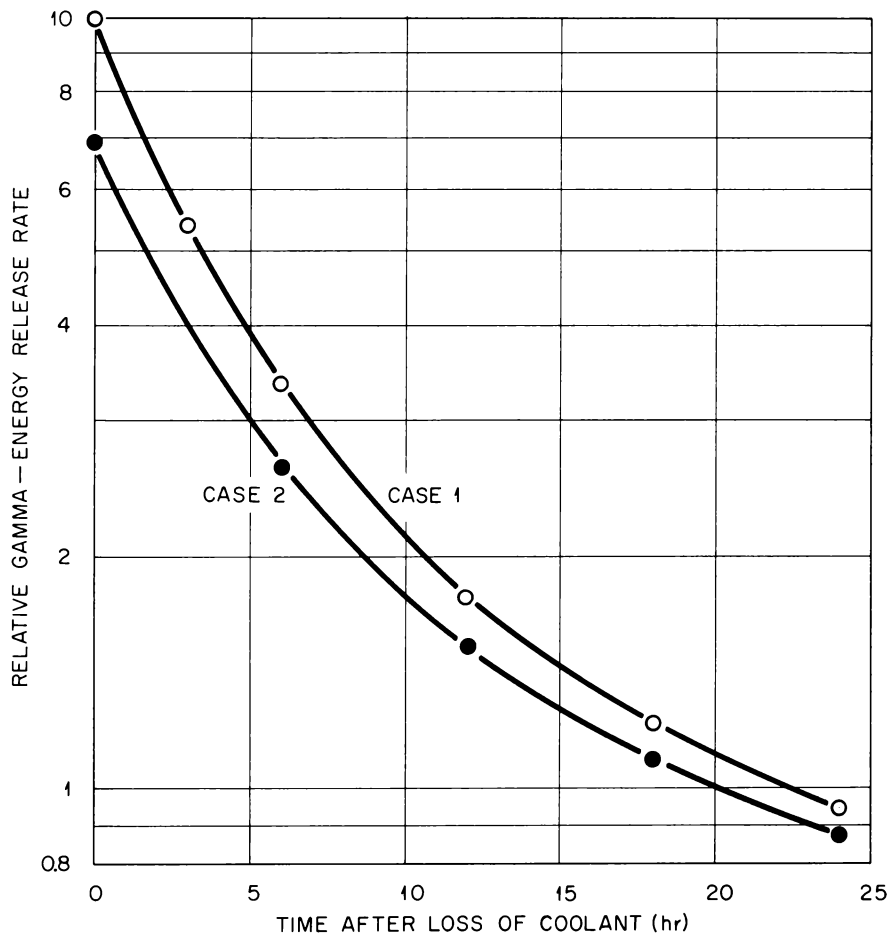
UNCLASSIFIED
ORNL-LR-DWG 77577

Fig. 2.9. Noble Gas Gamma-Energy Release Rate Relative to Initial Rate for Case 1.

Effect of Release Mechanisms on Exposures. In order to evaluate the effect of a more realistic approach to activity release on the resulting exposures, several different sets of assumptions affecting the reactor compartment ventilation, fuel failure mechanism, and fission-product decay were made. These were designated as "Modes."

1. Mode A. Continuous equilibrium release from the containment system, beginning at the time of the accident, was assumed. Considered with the power history of Case I, this Mode becomes the reference case and is typical of conventional exposure calculations made for stationary reactors.

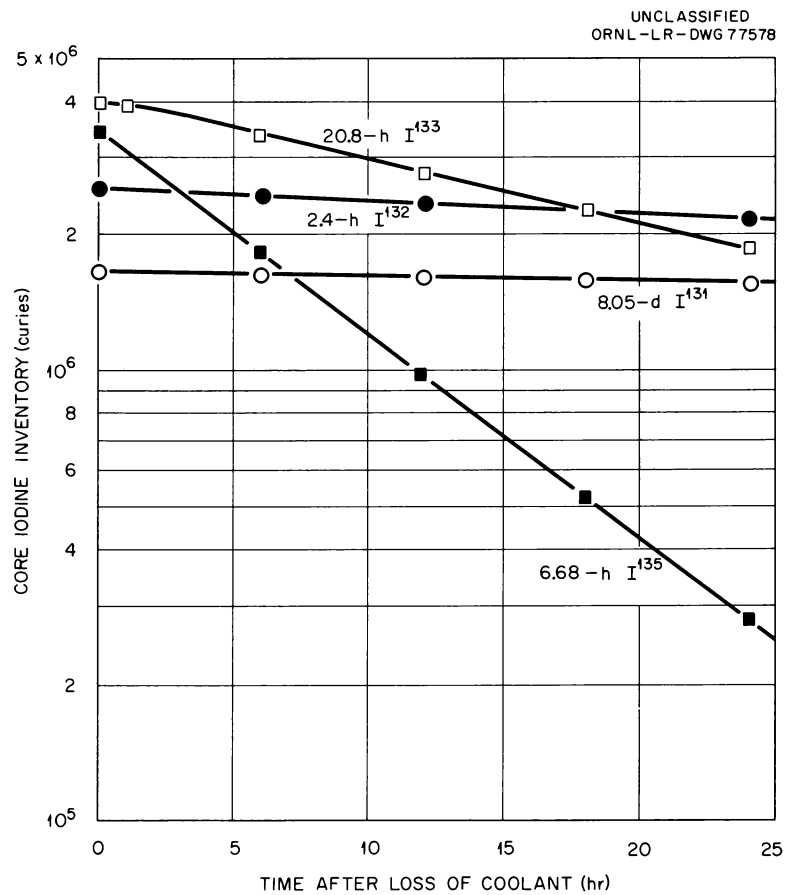


Fig. 2.10. Radioiodine Inventory in Case 1.

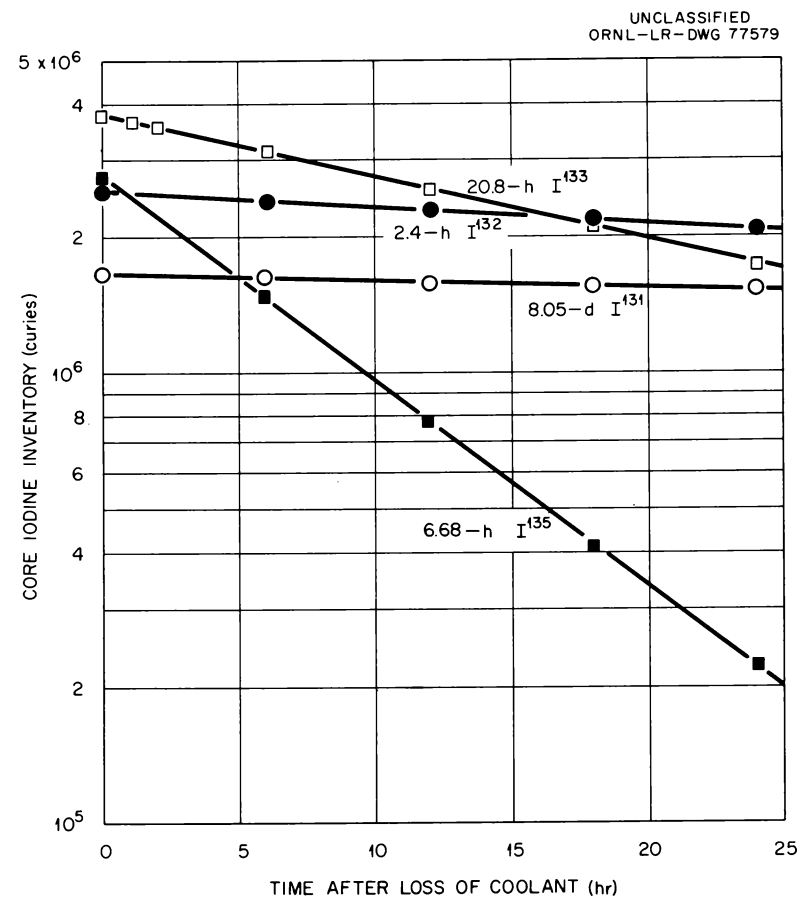


Fig. 2.11. Radioiodine Inventory in Case 2.

2. Mode B. Mode B is identical to Mode A except that the decay of fission products between the instant of the accident and the time they enter the atmosphere is included.

3. Mode C. In addition to fission-product decay as assumed in Mode B, the time required for fuel elements to fail and the holdup of the ventilation system were factored into the calculations. Of the various modes considered, Mode C is thought to be closest to real accident conditions.

The general assumptions employed in the exposure calculations are summarized in Table 2.5, and the results are shown in Figs. 2.12 through 2.18. The reference case is included for comparison. As a measure of the time available to evacuate personnel adjacent to the site, the exposure times required to receive a 25-rem whole-body dose at 500 ft can be compared for the various assumptions made. The exposure times can be obtained for submersion exposure from Fig. 2.12. If the previous power history is taken into account, as in Case 2, the time required to receive 25 rem increases from about 2 hr (the reference case) to 2.6 hr (Mode A, Case 2). If in addition, fission-product decay is considered, this time increases to 3.6 hr. Further, if the emergency ventilation system holdup time and the time needed for the cladding to fail are added, about 10 hr would elapse before the accumulated submersion dose reached 25 rem. This is a factor of 5 greater than for the reference case. Predicted reductions in submersion exposure at the tug are shown in Figs. 2.13 and 2.14.

While the reduction in thyroid exposure is smaller, it is nevertheless substantial. As a measure of the times available to evacuate the area adjacent to the site, it is of interest to compare the exposure times required to receive 300 rem to the thyroid at 500 ft. (This exposure represents a hazard comparable to a 25-rem whole-body dose.) For the reference case, these times are 0.7 and 6.6 hr for normal and emergency ventilation, respectively, as obtained from Figs. 2.15 and 2.16. Taking into account the actual power history, these times increase only slightly, as shown by the Mode A curves. This is because the operating period at reduced power (5 hr) is short compared with the half-lives of the important iodine isotopes. If decay, ventilation system holdup, and the time needed for the cladding to fail are considered, the exposure times required to receive 300 rem to the thyroid become 1.4 and 11 hr for normal

Table 2.5. Conditions Assumed for Exposure Calculations

Operating power histories considered.

Case 1, 100% power for infinite time

Case 2, 100% power for infinite time

followed by 50% power for 5 hr

Release modes considered

Mode A, no decay, holdup, or cladding
rupture delay

Mode B, decay

Mode C, decay, holdup, and cladding
rupture delay

Reactor power (100%)	69 Mw
Fission-product release from failed fuel elements	
Noble gases	100%
Halogens	50%
Halogens plated out in containment shell	50%
Containment vessel leakage rate	1.5% per day
Normal ventilation system flow	4000 cfm
Emergency ventilation system	
Flow out of compartment	200 cfm
Dilution flow	1800 cfm
Total flow	2000 cfm
Reactor compartment volume	30,000 ft ³
Iodine-removal efficiency of filter	
Normal system	90%
Emergency system	99%
Dilution factor, release point to ground	
Normal system	1000
Emergency system	100
Downwind exposure calculation	
Model	Sutton's
Point of release	Ground
Wind speed	1.64 m/sec
C _y	0.19
C _z	0.09

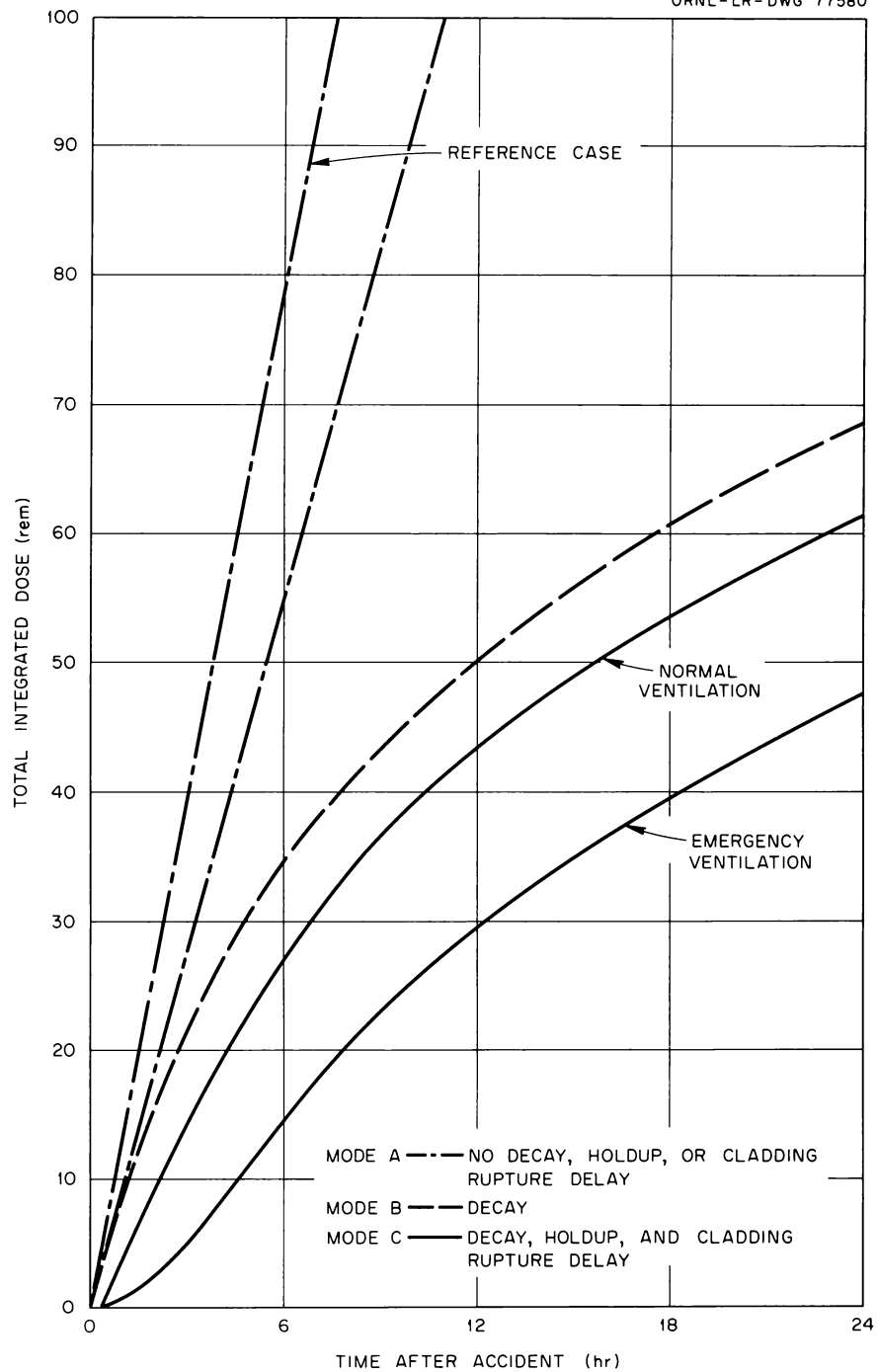
UNCLASSIFIED
ORNL-LR-DWG 77580

Fig. 2.12. Submersion Exposure at 500 ft as a Function of Time After Accident for Case 2.

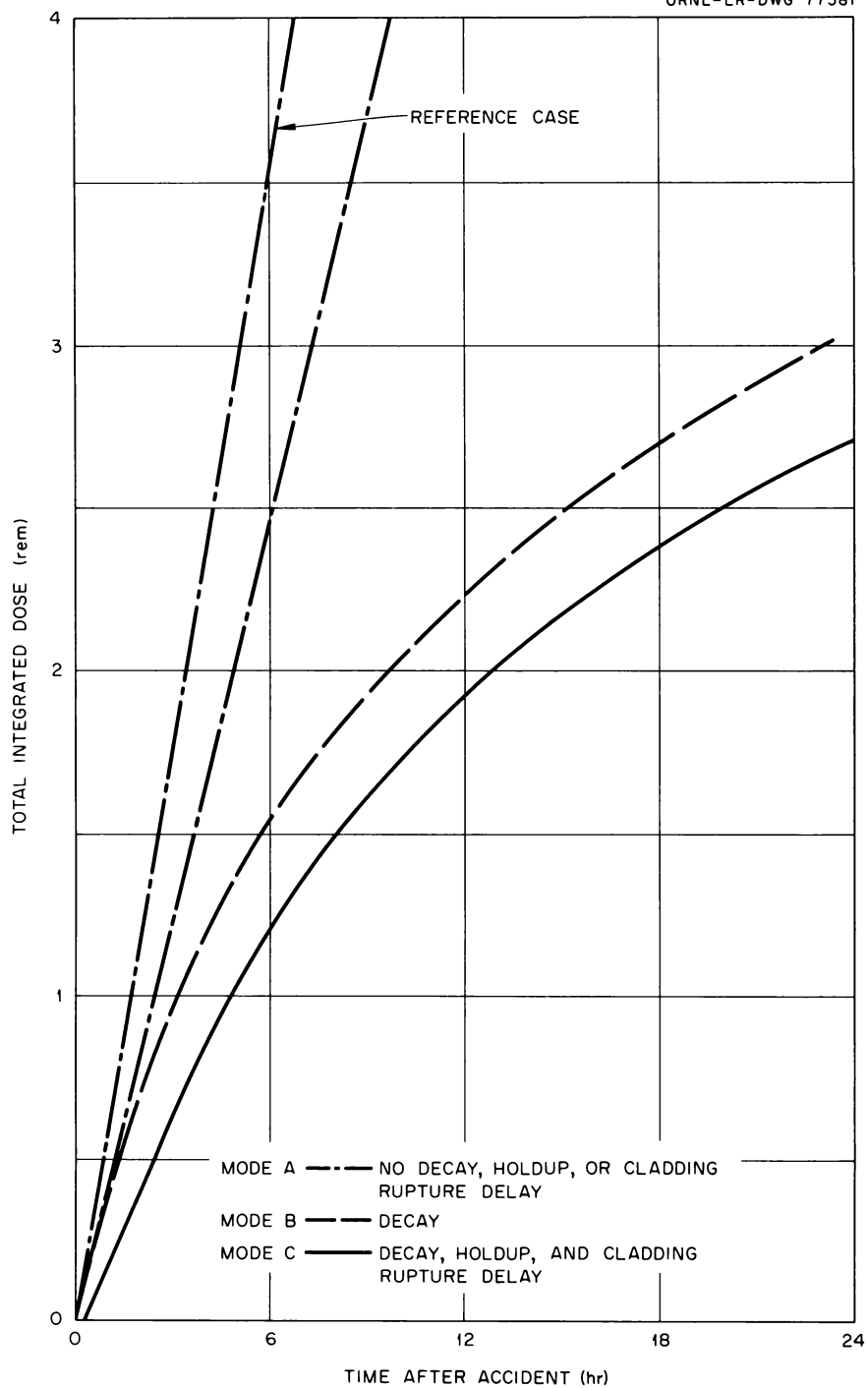
UNCLASSIFIED
ORNL-LR-DWG 77581

Fig. 2.13. Submersion Exposure at Tug as a Function of Time After Accident for Case 2 with Normal Ventilation.

UNCLASSIFIED
ORNL-LR-DWG 77582

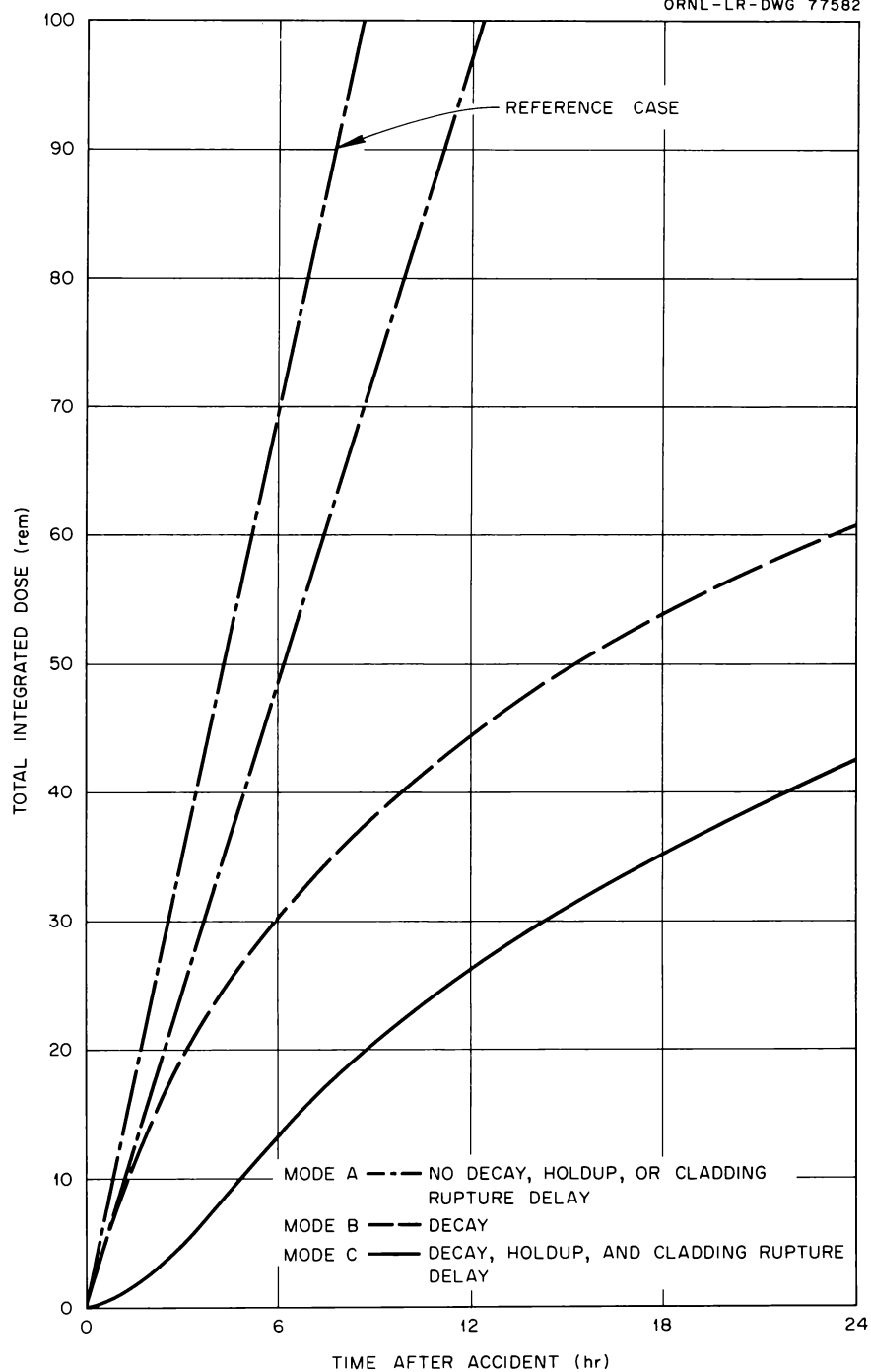


Fig. 2.14. Submersion Exposure at Tug as a Function of Time After Accident for Case 2 with Emergency Ventilation.

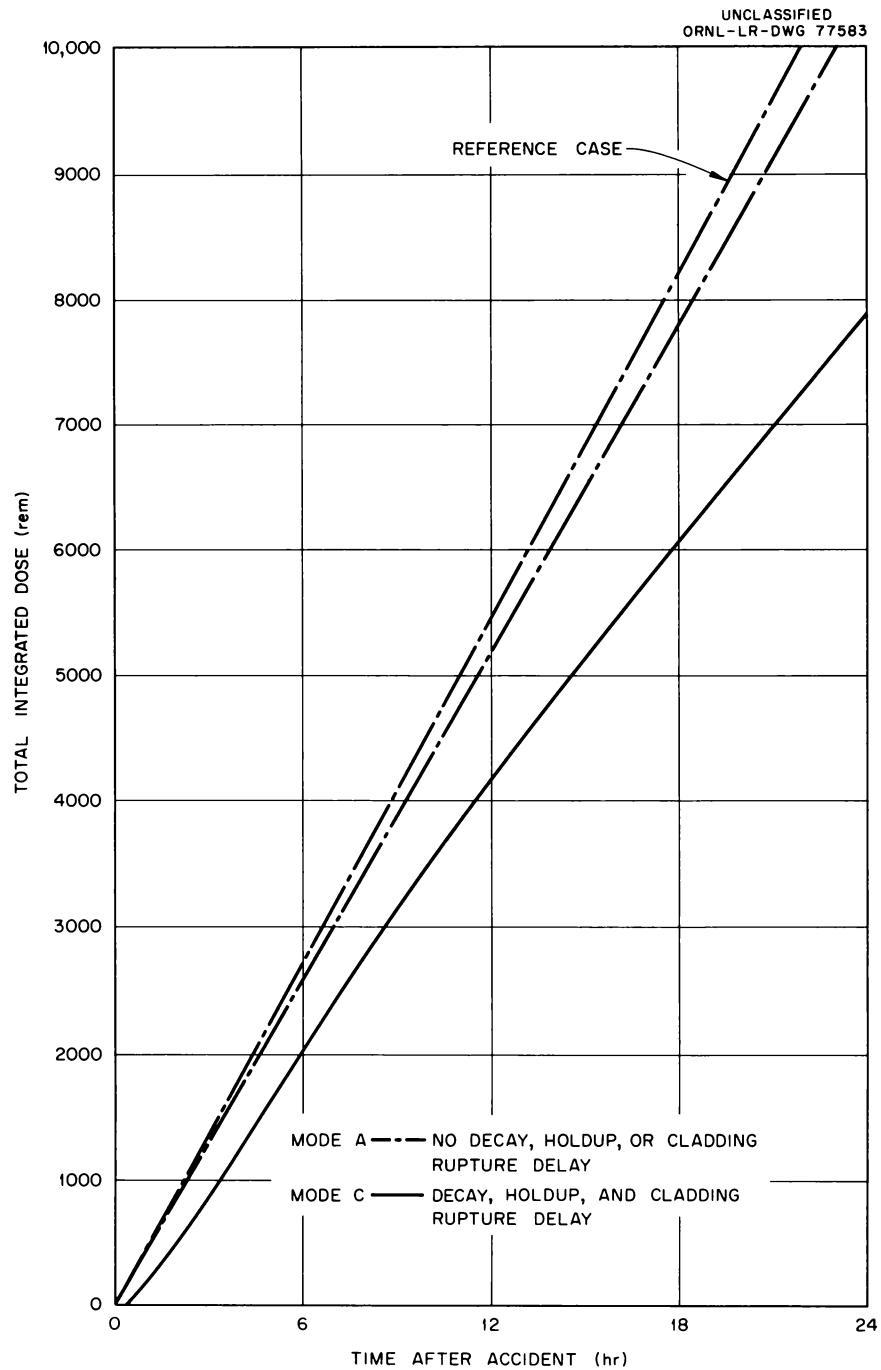


Fig. 2.15. Thyroid Exposure at 500 ft as a Function of Time After Accident for Case 2 with Normal Ventilation.

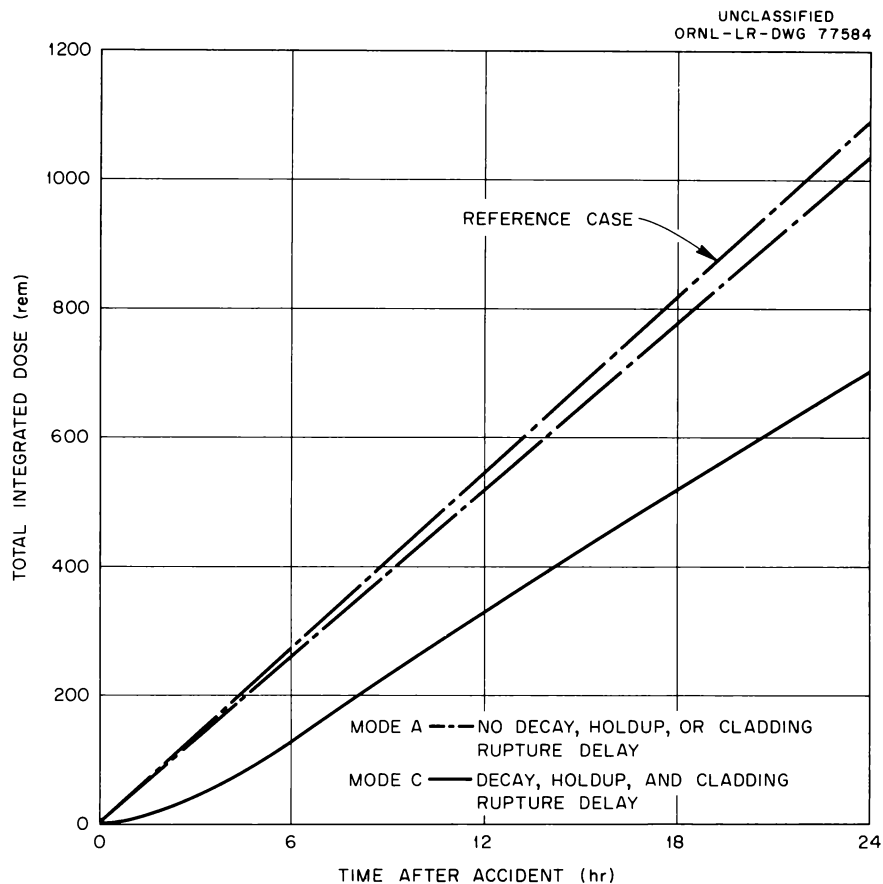


Fig. 2.16. Thyroid Exposure at 500 ft as a Function of Time After Accident for Case 2 with Emergency Ventilation.

and emergency ventilation, respectively. This is about a factor of 2 longer than for the reference case.

The integrated thyroid exposures at the tug are shown in Figs. 2.17 and 2.18. Considering again the time required to receive 300 rem to the thyroid, it was determined that Mode C increased the times by 35 and 65% over the reference case for normal and emergency ventilation, respectively.

Conclusions. It was concluded from this study that significantly smaller exposures resulted when the more realistic accident release mechanisms were assumed. In particular, estimates of exposures within the first few hours after the accident were reduced considerably, indicating that the ship could be removed from the harbor area without excessive exposure to ship or tug crews. After the accident, evacuation of passengers, visitors, and other people on or near the ship should be possible

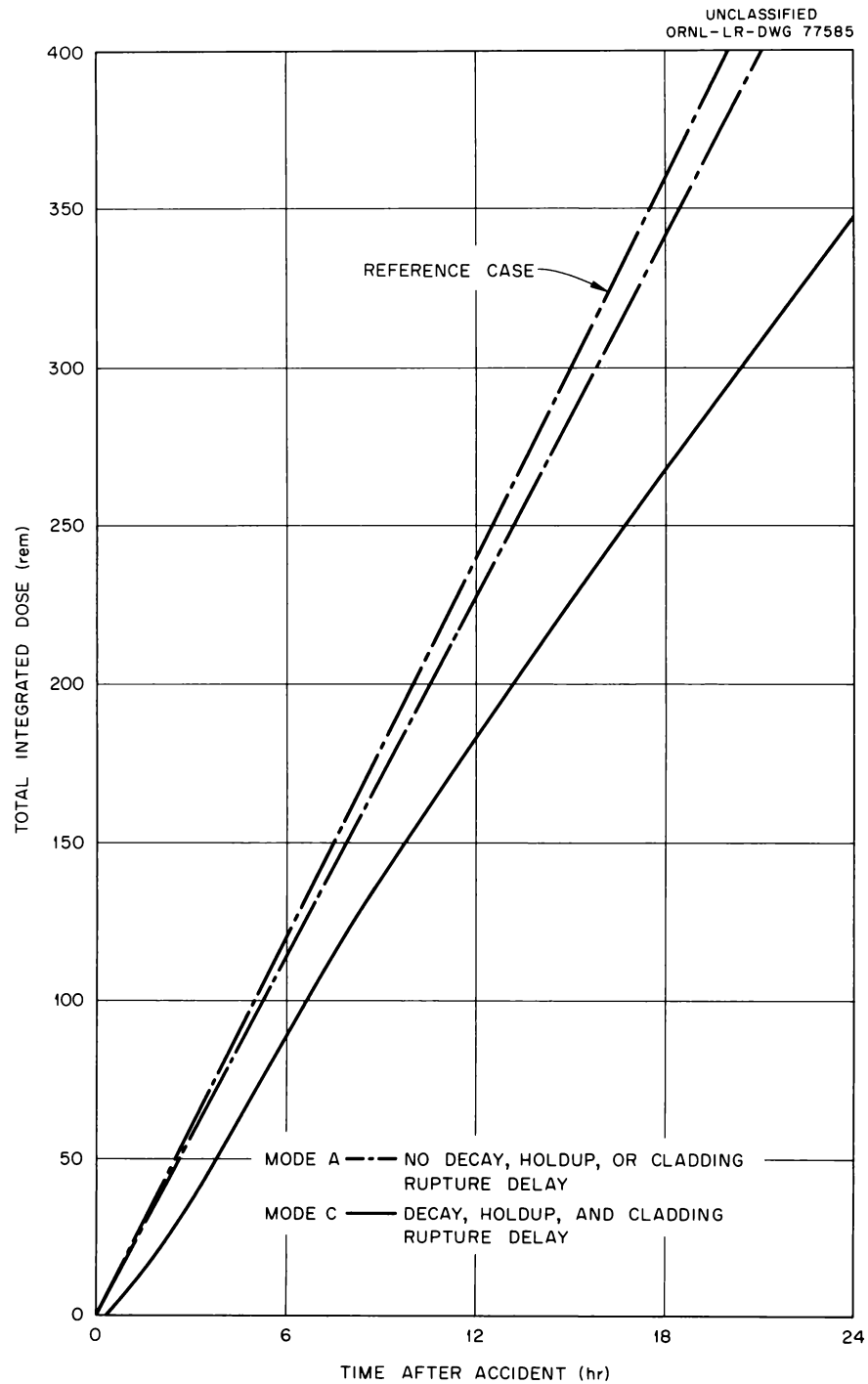


Fig. 2.17. Thyroid Exposure at Tug as a Function of Time After Accident for Case 2 with Normal Ventilation.

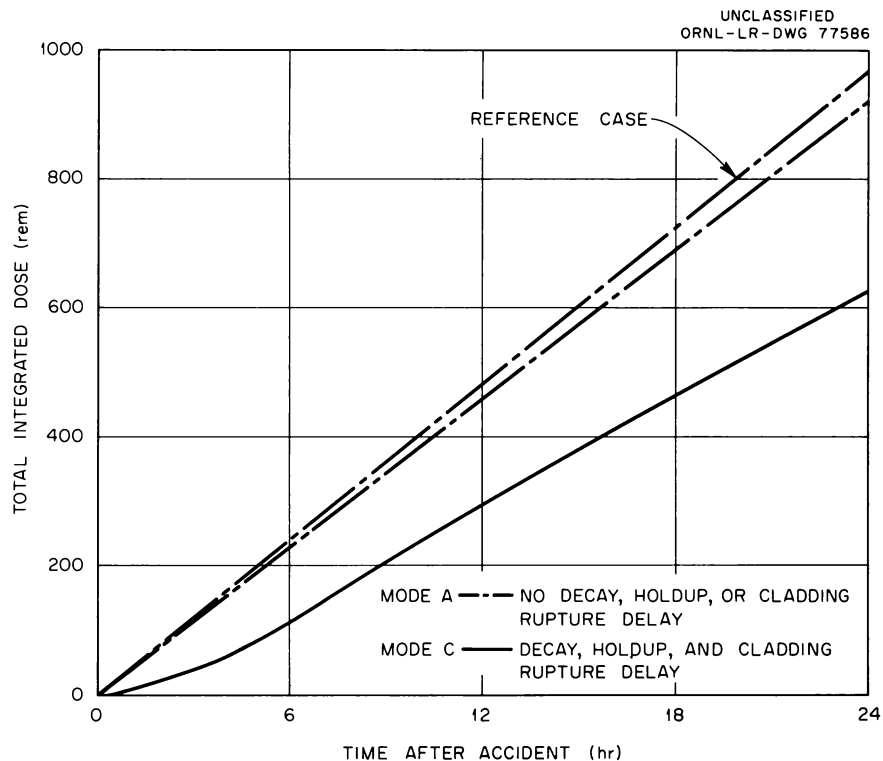


Fig. 2.18. Thyroid Exposure at Tug as a Function of Time After Accident for Case 2 with Emergency Ventilation.

before excessive exposures would be received. Estimated exposures within the first day or longer periods after the accident were also reduced significantly. Estimated submersion exposures to noble gases were decreased more than thyroid exposures to iodine. Higher iodine-removal efficiencies than those assumed here are desirable to achieve equivalent lower levels of thyroid exposures.

Port Survey Visits (S. I. Kaplan)

As prescribed for the interim operating period, the U.S. ports to be visited by the N.S. SAVANNAH have first been visited by a port survey team, which evaluated the port area from a nuclear safety standpoint and made operational arrangements for the forthcoming visit. The findings and arrangements made by the port team were incorporated in port analysis reports, which were submitted for approval of the Director of Regulation (AEC) prior to each port entry.

The port survey team has usually consisted of one or two of the ship's senior officers and a nuclear engineer from ORNL. In each port the visit has followed the same general pattern, involving all or most of the following operations:

1. visual survey of applicable berths, including inspection of dock faces and approaches from the water side aboard a pilot launch or towboat, examination of the harbor area from aerial photographs and navigational charts, and individual evaluation and measurements along the actual docks on foot and by reference to drawings;
2. meetings with local regulatory and law enforcement officials, including Coast Guard, Harbor Authority, Fire Department, Police Department, Health Departments (local, state, and U.S.), and Civil Defense, to brief them on the berth requirements and emergency precautions specified for port entry by the ship and to provide for the special action required in case of an accident alert;
3. gathering of communications information from the above authorities, as well as pilots and towboat operators, so that the ship can contact them promptly, either for normal navigational practice while maneuvering in the harbor or for alerting in case of accident;
4. arranging with local towboat operators to have adequate tug capacity within 1/2 hr call to move the ship away from the dock at any time during her visit;
5. arranging for harbor pilotage during entry, exit, and emergency situations, and consulting with a pilot regarding any local tidal conditions, etc., which might influence the choice of berth, manner of mooring, or particular time of arrival;
6. discussion with civic officials regarding welcoming ceremonies, visits to the ship of special organized groups, local transit service, etc.;
7. arranging with the local telephone company to provide service for the ship immediately upon docking;
8. arranging for the use either of off-duty policemen or of members of a private guard service as traffic control personnel aboard the ship during its stay.

During the current report period port surveys were made of Savannah, Georgia; Norfolk, Virginia; Panama Canal Zone; Seattle, Washington;

Long Beach, Los Angeles, and San Francisco, California; Honolulu, Hawaii; and Portland, Oregon.

Physics Calculations

B. W. Colston E. E. Gross
M. L. Winton

Comparison of One- and Two-Zone Core Reactivity Lifetimes

The initial core I loading for the N.S. SAVANNAH consists of 4.2 wt % U^{235} in the inner 16 fuel elements and 4.6 wt % U^{235} in the outer 16 fuel elements. This nonuniform fuel loading is important in any study of fuel reshuffling, but it was felt to be an unnecessary complication in the earlier work of comparing the virtues of Zircaloy and stainless steel as fuel-element container materials. The effect on reactivity lifetime of replacing the actual two-zone loading by a single-zone loading with the inner-zone enrichment was therefore investigated.

In the method used for generating flux-averaged microscopic cross sections, it is evident that two sets of microscopic cross sections are obtained; one for the inner-zone materials and one for the outer-zone materials. These values are listed in Table 2.6. As mentioned previously, the CANDLE code, as presently constituted, is limited to a single set of four-group cross sections for each fissionable material. The fuel was, therefore, characterized by cross sections pertinent to the inner fuel zone, since this is the most important part of the core. The effect of this approximation on reactivity lifetime should be small, since a small underestimation of cross section will produce a small overestimation of the flux, and the important product of flux and cross section should remain relatively unchanged.

With the above limitation on fuel cross sections, the reactivity lifetimes of single-zone and two-zone cores are compared in Fig. 2.19 for stainless steel fuel-element containers. The initial sharp drop in reactivity is due to the buildup of the fission-product poison Xe^{135} . Following the buildup of equilibrium samarium (~ 0.3 years), the multiplication factor as a function of time appears to be remarkably linear with the slope, $-0.036 \Delta k/\text{year}$. Evidently the two-zone core increases the reactivity

Table 2.6. Flux-Averaged Microscopic Cross Sections for
Inner and Outer Core I Fuel Zones at 508°F

Cross Section Calculated	Microscopic Cross Sections (barns)					
	U ²³⁵		U ²³⁸		E ^a	
	Inner Zone	Outer Zone	Inner Zone	Outer Zone	Inner Zone	Outer Zone
$3\sigma_{\text{trl}}$	31.43	31.78	20.31	20.54	0.4345	0.4340
σ_{al}	2.59	2.62	0.479	0.485	0.0011	0.0011
σ_{l2}	0	0	0.0047	0.0048	0.0285	0.0289
$\nu\sigma_{\text{f1}}$	5.30	5.36	0.615	0.622	0	0
$3\sigma_{\text{tr2}}$	44.38	44.63	29.48	29.64	1.1662	1.1869
σ_{a2}	29.05	29.21	1.59	1.60	0.0028	0.0027
σ_{23}	0	0	0	0	0.0806	0.0818
$\nu\sigma_{\text{f2}}$	44.67	44.92	0	0	0	0
$3\sigma_{\text{tr3}}$	75.71	75.65	26.80	26.78	1.2829	1.3146
σ_{a3}	87.55	87.48	1.34	1.34	0.0054	0.0057
σ_{34}	0	0	0	0	0.1174	0.1194
$\nu\sigma_{\text{f3}}$	154.3	154.2	0	0	0	0
$3\sigma_{\text{tr4}}$	233.2	220.7	21.33	20.19	2.4123	2.6214
σ_{a4}	326.9	309.4	1.37	1.30	0.0292	0.0333
$\nu\sigma_{\text{f4}}$	674.0	638.0	0	0	0	0

^aMaterial "E" is a fictitious element containing the information about all the structural material, channel water, followers, and control rods. Except for U²³⁵ and U²³⁸, it is the only material present in the core at the beginning of life.

lifetime of the one-zone core by only about one month. A single-zone core treatment should, therefore, be suitable for many kinds of studies.

Gross radial peak-to-average power distributions at the beginning of life calculated by CANDLE for the one- and two-zone cores are shown in Fig. 2.20. The two-zone core has a smaller peak-to-average radial power ratio ($P_{\text{max}}/P_{\text{av}} = 1.80$) than the uniformly loaded core ($P_{\text{max}}/P_{\text{av}} = 1.86$). The flatter radial-power distribution of the two-zone loading is vitiated with burnup, as shown by the power distributions at the end-of-

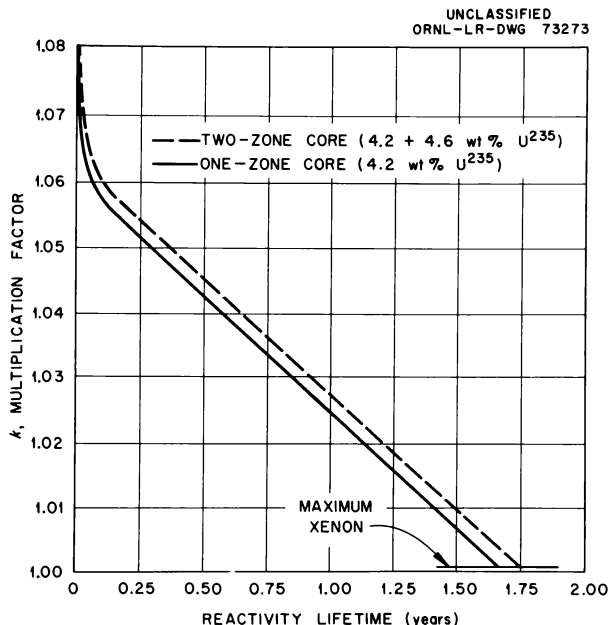


Fig. 2.19. Comparison of Reactivity Lifetimes of One and Two Fuel Zones in N.S. SAVANNAH Core I.

respectively. The burnup of U^{235} is fairly linear (Fig. 2.22), with a rate of about 25 kg per full-power year. The buildup of Pu^{239} (Fig. 2.23) occurs at a rate of about 8 kg per full-power year during the first full-power year and at the rate of about 6 kg per full-power year during the second year of full-power operation. The buildup of Pu^{241} is quadratic in nature, depending as it does on the buildup of intermediate isotopes of plutonium. These calculated plutonium inventories depend directly on the assumed resonance-absorption integral of U^{238} (20.35 barns in this study). At the end of core life (~ 1.7 full-power years) the plutonium isotopes contribute about 10% of the power production, U^{238} contributes about 9%, and U^{235} provides the remainder.

Comparison of Axial Slab-Geometry Model with Experimental Analysis

The beginning-of-life core analysis results were compared with experimental information on core reactivity and total control-rod worth and

core life, presented in Fig.

2.21. Comparison of Figs. 2.20 and 2.21 reveals the trend toward a flatter power distribution as fuel is consumed.

Of interest to the reactor operator are the core inventories of fissionable material. These materials are also of importance in fuel-cycle economic analyses.¹¹ For these reasons the calculated time dependence of U^{235} , Pu^{239} , and Pu^{241} core inventories for the two-zone prototype core are presented in Figs. 2.22, 2.23, and 2.24,

¹¹C. L. Whitmarsh, "Potential Fuel-Cycle Cost Savings Resulting from Technological Changes in the N.S. SAVANNAH Reactor," USAEC Report ORNL TM-144, Oak Ridge National Laboratory, April 6, 1962.

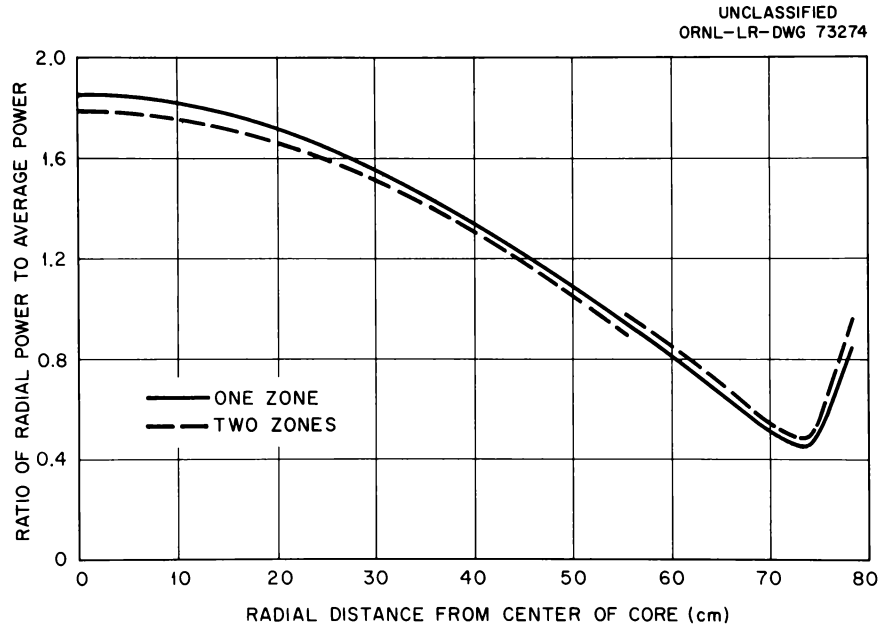


Fig. 2.20. Comparison of Radial Power Distribution for One and Two Fuel Zones in Core I at Beginning of Life.

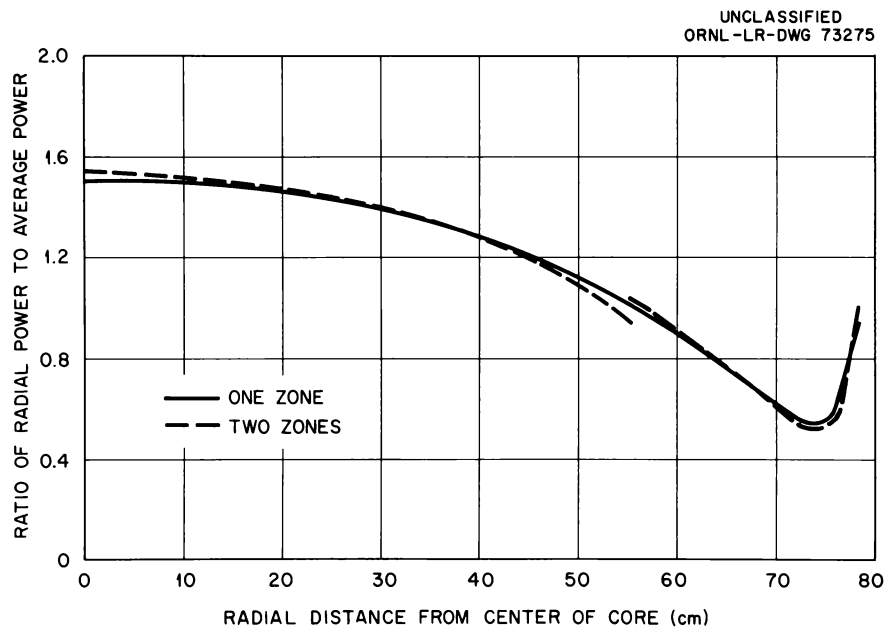


Fig. 2.21. Comparison of Radial Power Distributions for One and Two Fuel Zones in Core I at End of Life.

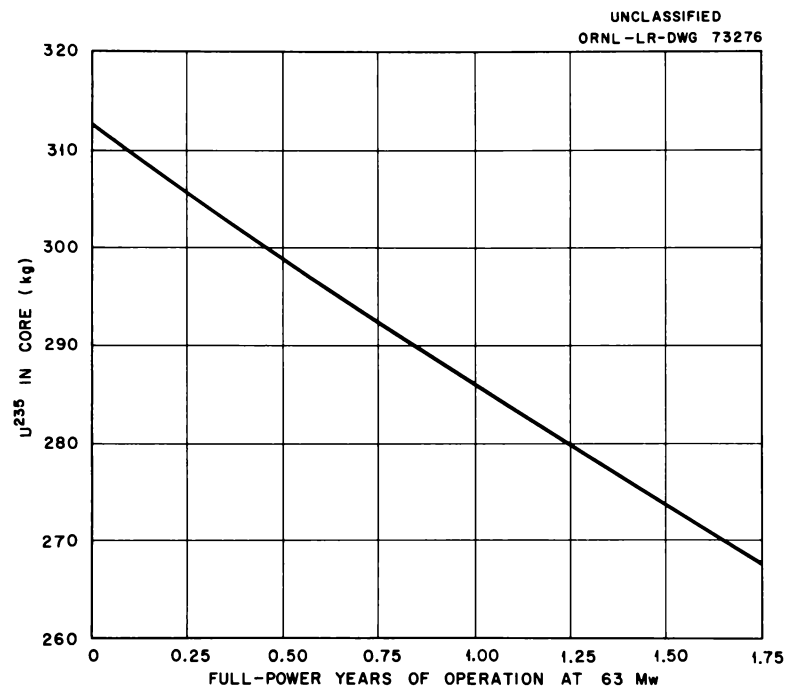


Fig. 2.22. Calculated Core I Inventory of U^{235} in Two-Zone Core I as a Function of Full-Power Years of Operation at 63 Mw.

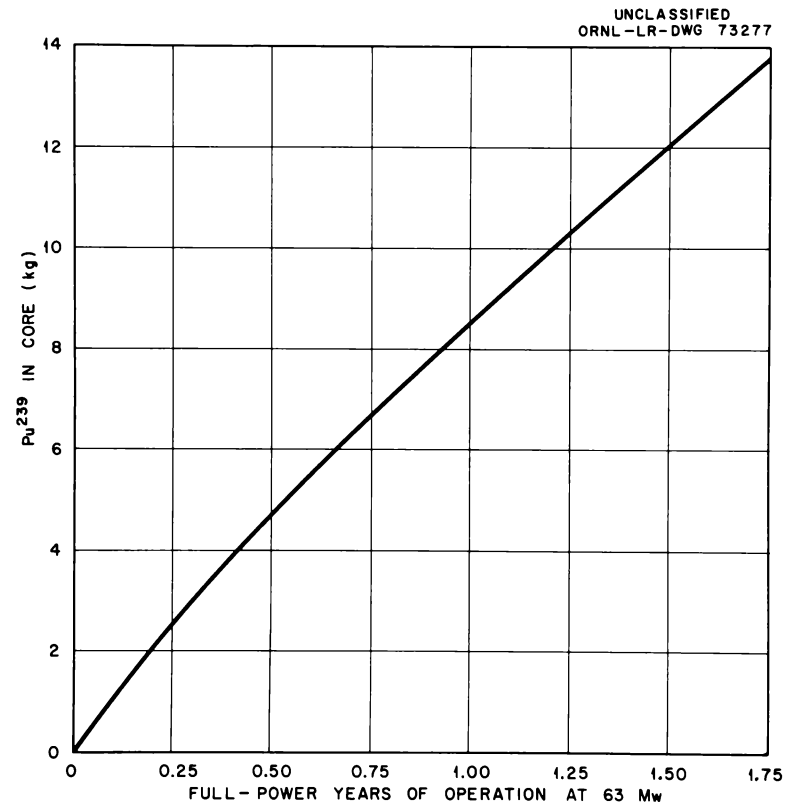


Fig. 2.23. Calculated Core I Inventory of Pu^{239} in Two-Zone Core I as a Function of Full-Power Years of Operation at 63 Mw.

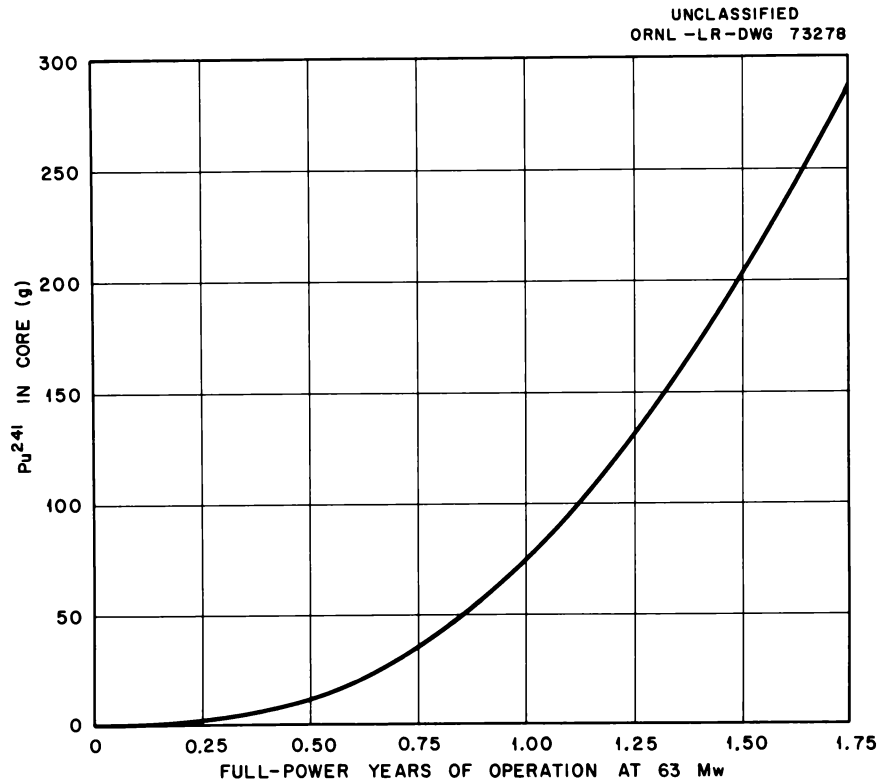


Fig. 2.24. Calculated Core Inventory of Pu^{241} in Two-Zone Core I as a Function of Full-Power Years of Operation at 63 Mw.

found to be satisfactory.¹² Additional checks on the axial slab-geometry model used in the "window-shade" burnup calculations were desired, however. One available check was the critical A control-rod bank position measured in the zero-power experiment¹³ on the prototype core. With all other control rods fully inserted, the cold, clean core was found to be critical at an A control-rod bank position of 79.0 ± 1 cm, as measured from the bottom of the active fuel region. For this same control-rod configuration, the analysis methods described here gave a multiplication factor of 1.005 at an A-bank position of 79.0 cm and $k = 1.000$ for an A-rod bank position of 69.5 cm.

¹²E. E. Gross, B. W. Colston, and M. L. Winton, "Nuclear Analyses of the N.S. SAVANNAH Reactor with Zircaloy or Stainless Steel as Fuel-Element Containers," USAEC Report ORNL-3261, Oak Ridge National Laboratory, April 24, 1962.

¹³R. W. Ball and A. L. MacKinney, "Nuclear Merchant Ship Reactor Zero Power Test, Core I," USAEC Report BAW-1202, Babcock & Wilcox Company, July 1960.

Good agreement was also obtained for the comparison of calculated and measured control-rod axial power distributions for the critical A-bank experiment. The experiment¹³ showed the power distribution to be spatially dependent; however, the calculated position for the peak power agreed with the experimental position, and the shape of the calculated axial power distribution agreed with power profiles measured near the center of the fuel elements, as may be seen in Fig. 2.25.

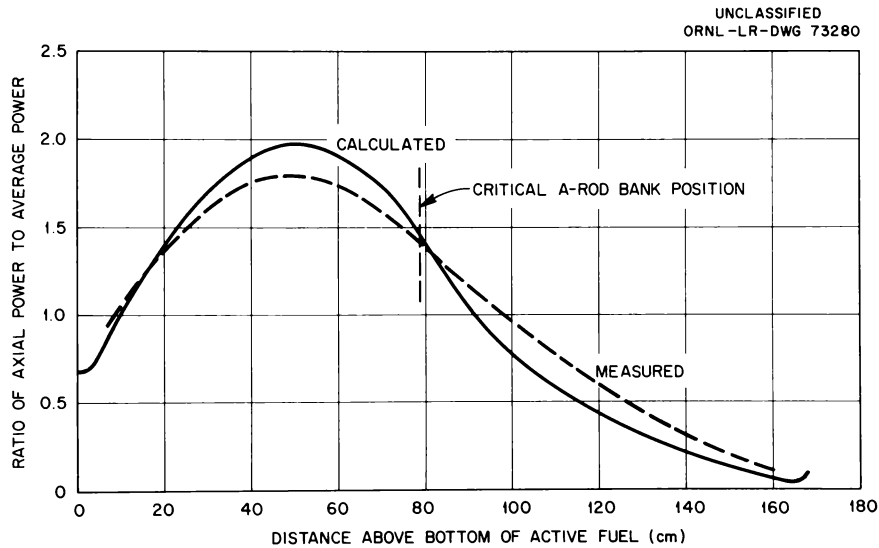


Fig. 2.25. Comparison of Calculated and Measured Axial Power Profiles for N.S. SAVANNAH Core I at 68°F with A-Rod Bank at 79 cm and all Other Rods Fully Inserted. Experimental curve is representative of conditions near the center of a fuel element.

3. PRESSURIZED-WATER IN-PILE LOOP

One of the Laboratory's early undertakings in the Maritime Reactor Program was the construction and operation of a pressurized-water in-pile loop in the Oak Ridge Research Reactor. This facility has been in continuous use since its completion in December 1959. It has been utilized principally for irradiation testing of the nonsintered bulk UO_2 fuels being considered for use in a replacement core for the N.S. SAVANNAH reactor and for water chemistry studies aimed at better understanding and control of activity transport in neutral-pH pressurized-water systems. Operation has been characterized by an absence of significant difficulties or interruptions of experimental irradiations. In July 1962, upon completion of the irradiation phase of the planned nonsintered fuel tests, the facility was transferred from the Maritime Reactor Program to the Army Reactors Program.

Loop Operation

J. A. Conlin	D. B. Trauger
J. K. Franzreb	D. E. Tidwell

The ORR pressurized-water in-pile loop operated satisfactorily in the period since the previous report.¹ Loop leakage remained low, with the result that makeup requirements were low, water purity remained high, and contamination within the equipment room and at the sample station remained low. After nearly three years of operation, all loop components continued to operate with only routine maintenance being performed. The instrumentation and automatic control equipment continued to function reliably.

Irradiation of four experimental assemblies was completed during the year. The fueled test elements consisted of both swaged and vibratory compacted UO_2 clad in type 304 stainless steel. The irradiation histories of these assemblies are presented in Table 3.1. Each of the experimental

¹J. A. Conlin, J. K. Franzreb, and D. E. Tidwell, Operation, pp. 41-43, "Maritime Reactor Program Ann. Prog. Rep. Nov. 30, 1961," USAEC Report ORNL-3238, Oak Ridge National Laboratory.

Table 3.1. Irradiation Histories of Experimental Assemblies Exposed in the ORR Pressurized-Water In-Pile Loop

Experimental Assembly	Actual Exposure Time (weeks)	Type of Fuel and Fabrication Method	Irradiation Date		Loop Position
			Starting	Ending	
5 ^a	49	UO ₂ , vibratory compacted or swaged	7-12-61	7-29-62	A-1
6	14	UO ₂ , vibratory compacted	10-21-61	2-11-62	A-2
7	14	UO ₂ , vibratory compacted	2-19-62	6-3-62	A-2
8	14	UO ₂ , vibratory compacted	6-9-62	9-23-62	A-2
9	11	UO ₂ pellets	8-4-62	10-31-62	A-1
L-1 ^b	4	ThO ₂ and UO ₂ , vibratory compacted	9-29-62	10-31-62	A-2

^aAssembly 5 contained two rods that were vibratory compacted and one rod that was cold swaged.

^bThis irradiation was performed for the Thorium Utilization Program. Two of the fuel rods of this assembly are clad with Zircaloy-2 and the third is clad with type 304 stainless steel. All three rods have a clad thickness of 0.015 in.

assemblies contained three fuel rods, and each assembly occupied one leg of the loop. Each of the assemblies was equipped with a tube containing a flux-monitor wire. The flux-monitor wires were removed for counting at the end of each reactor cycle, and new wires were inserted.

Because of the increased heat generation of experimental assembly 6 and subsequent assemblies, some of the loop operating parameters were changed slightly. Loop flow was increased from 40 to 50 gpm, and the in-pile inlet temperature was lowered from 500 to 480°F. Corresponding setpoints for control action on high in-pile inlet and outlet water temperatures and low loop flow were changed accordingly.

Design, fabrication, and installation of a small magnetite "crud" filter was completed. The filter assembly was tied into the sample station as a side stream to the loop, and samples of loop water were passed through various magnetite filters to determine their effectiveness and feasibility of operation in pressurized-water systems. This study is described in more detail in the following section. A high-temperature,

high-pressure conductivity cell to be used in conjunction with the magnetite "crud" filter was designed and is being fabricated.

The desired water purity in the loop was maintained without difficulty. The oxygen analyzer mentioned in the previous report¹ was received and installed and is presently working satisfactorily. Indications are that the present oxygen content of the loop is <10 ppb. Extensive studies are planned in which the analyzer will be used to observe changes in oxygen content as makeup water is added and when hydrogen is added to the loop.

Water Chemistry Studies

C. F. Baes, Jr. T. H. Handley

The principal objective of the water chemistry studies, aside from providing chemical and radiochemical data on water conditions pertinent to loop operation, has been to increase the basic understanding of water chemistry as an approach to more economical pressurized-water reactor operation. In particular there is a strong incentive to learn more of the mechanisms of the transport and deposition of corrosion-product "crud" and its associated radioactivity.

Results reported previously² indicated that the relatively low levels of water-borne corrosion products and radioactivity in the ORR loop were composed of two distinct fractions: (1) a particulate or "crud" fraction which, based on filtration tests and electron-microscopic and x-ray diffraction examination, was found to have a sharp lower limit in particle size of $\sim 0.5 \mu$; it was well crystallized and had a magnetite structure; and (2) a dissolved fraction which was not removed by the lowest porosity filters (0.01μ) and, based on electromigration experiments, appeared to be present as simple ions (probably the bivalent metal hydroxides of Mn, Fe, Co, and Ni) at very low concentration ($<10^{-6}$ molar). The specific activities of these two fractions, as well as that of the crud deposited

²C. F. Baes, Jr., and T. H. Handley, Water Chemistry Studies, pp. 43-50, "Maritime Reactor Program Ann. Prog. Rep. Nov. 30, 1961," USAEC Report ORNL-3238, Oak Ridge National Laboratory.

on fuel rod assemblies during operation in the in-pile section of the loop, were all comparable. This, as well as the well-crystallized appearance of the insoluble fraction, suggests that appreciable radiochemical exchange between the two fractions occurs and that this may be an important mechanism of activity transport in neutral-pH pressurized-water systems. The possibility that nonradioactive magnetite would be an effective filter and ion exchange medium for accumulating activity in neutral-pH pressurized-water systems was explored in preliminary tests.

This study of water-borne activity was continued during the past year. Samples of fuel-rod crud deposits were taken, and a high-temperature filter unit was used to study further the effectiveness of magnetite as a high-temperature filter and ion exchange medium. The results, presented here, are discussed in terms of a simple activity transport mechanism involving chemical and radiochemical exchange of dissolved ionic material in the coolant with the crud deposits on in-flux and out-of-flux surfaces.

Observed Activity Behavior

Water-Borne Activity and Crud Levels. Radiochemical analyses of loop water samples taken upstream of the ion exchangers during normal loop operation during late 1961 and early 1962 (Table 3.2) indicate a decrease in the level of water-borne activity compared with similar

Table 3.2. Results of Radiochemical Analyses of Loop Water Samples Taken Upstream of the Ion Exchanger

	Sample Taken July 27, 1961		Sample Taken November 9, 1961		Sample Taken January 8, 1962		Sample Taken March 19, 1962	
	In Filtrate	On Filter	In Filtrate	On Filter	In Filtrate	On Filter	In Filtrate	On Filter
Nuclide activity, dps per liter of sample								
Fe ⁵⁹	210		530	1600	530	120	450	115
Fe ⁵⁵	880		1900	5300	210	35	1380	203
Co ⁵⁸	130		780	580	400	45	530	70
Co ⁶⁰	220		450	530	430	83	650	45
Mn ⁵⁴	780		400		880	160	1080	150
Fraction of total activity			0.34	0.66	0.85	0.15	0.88	0.12
Nuclide activity ratio								
Fe ⁵⁵ /Fe ⁵⁹	4.2		3.6	3.3	0.4	0.3	3.1	1.8
Co ⁶⁰ /Co ⁵⁸	1.7		0.58	0.91	1.1	1.8	1.2	0.6

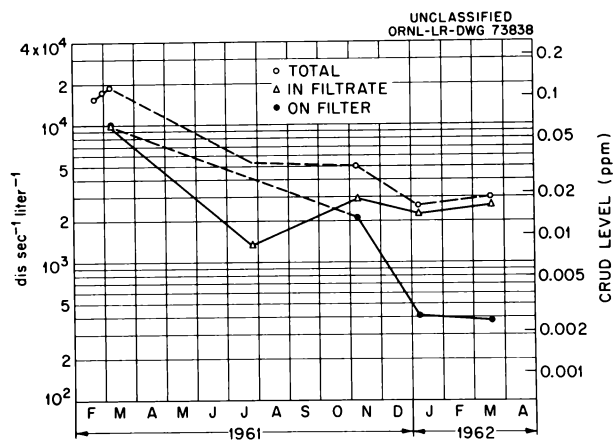


Fig. 3.1. Sum of Fe^{59} , Co^{58} , Co^{60} , Mn^{54} Activities in Loop Water.

measurements (obtained early in 1961) reported previously.² This is shown by a plot (Fig. 3.1) of the sum of Fe^{59} , Co^{58} , Co^{60} , and Mn^{54} activities for the total sample, for the fractions retained by a $0.45\text{-}\mu$ filter (filterable material), and for the fraction not retained by a $0.45\text{-}\mu$ filter (nonfilterable, presumably ionic material). In Fig. 3.1, an estimate of the weight concentra-

tion of the crud is shown that is based on the specific activity found previously for weighable samples of water-borne crud (Table 3.3). Judging from these results, the normal filterable crud level in the ORR loop since the latter part of 1961 has been 0.01 ppm or less.

Fuel Rod Crud Deposits. The history of the irradiation of fuel rod test assemblies in the loop is summarized in Table 3.4. These assemblies all consisted of 0.5-in.-OD type 304 stainless steel tubes containing UO_2 of low enrichment. They were arranged in clusters of three, one cluster being irradiated in each leg (A-1 or A-2) of the U-shaped test section. Details of these tests are given in the previous report.¹ Upon the removal of assemblies 1, 3, 4, and 6, samples of loosely deposited crud were removed from the fuel rods for radiochemical analyses. The various samples taken are listed in Table 3.3 according to the direction of water flow through the test section; that is, the water entered leg A-2 and exited from leg A-1.

There are no marked trends in the various specific activities with locations on the fuel rods, or even from one experiment to another, in spite of the differences in water-exposure time and in radiation exposure hours (Table 3.4). The variations in the Ta^{182} activities are attributable to analytical difficulties. The high Cr^{51} activities of assemblies 4 and 6 probably arose from the fact that the crud deposits were much thinner in these cases, and in scraping them off a relatively larger amount of Cr^{51} was removed from the chromium-rich underlying oxide.

Table 3.3. Radiochemical Analyses of Various Crud Samples

Date ^a	Sample ^b	Specific Activity (dps/g)							Activity Ratio	
		Fe ⁵⁹ (45.1 d)	Fe ⁵⁵ (2.94 y)	Co ⁵⁸ (72 d)	Co ⁶⁰ (5.3 y)	Ta ¹⁸² (112 d)	Cr ⁵¹ (27.8 d)	Mn ⁵⁴ (300 d)	Fe ⁵⁵ /Fe ⁵⁹	Co ⁶⁰ /Co ⁵⁸
Fuel Rod Crud Deposits										
		× 10 ⁷	× 10 ⁷	× 10 ⁷	× 10 ⁷	× 10 ⁷	× 10 ⁷	× 10 ⁷		
1-21-61	1-(A-2)	22		13	6.7		20	1.2	0.48 ± 0.05	
	1-(A-1)	19		11	4.6		13	1.0		
7-4-61	3-(A-2)-1	12	12	10	4.1	0.29	25	1.3	1.0 ± 0.1	0.39 ± 0.05
	3-(A-2)-2	19	17	14	4.9	1.6	23	2.7		
	3-(A-2)-3	21	18	19	6.4	0.31	26	2.7		
	3-(A-1)-3	11	14	10	4.1	0.84	13	1.6		
	3-(A-1)-2	11	12	11	3.9	1.4	10	1.6		
	3-(A-1)-1	9	9	7	3.5	0.88	6.5	0.9		
10-22-61	4-(A-2)-1	16	13	25	5.4	0.50	180	3.2	0.8 ± 0.2	0.27 ± 0.06
	4-(A-2)-2	18	20	23	6.3	0.29	200	4.1		
	4-(A-2)-3	17	10	18	6.9	0.43	260	3.1		
3-11-62	6-(A-2)-1	10	13	12	5.3	0.08	290	3.0	1.4 ± 0.1	0.40 ± 0.05
	6-(A-2)-2	11	14	18	7.2	0.11	180	2.8		
	6-(A-2)-3	10	15	19	6.9	0.11	290	3.0		
Water-Borne Crud										
5-17-61		7.2	17	5.4	3.2				2.5 ± 0.2	0.67 ± 0.08
		8.8	22							
		5.9	16	4.5	3.4					

^aDate fuel rod irradiation was terminated or date water sample was taken.

^bPrefix numbers refer to irradiation assembly, A-1 and A-2 refer to the legs of U-shaped test section, and the final numerals are: 1 for top, 2 for middle, and 3 for bottom of fuel rod.

Table 3.4. Irradiation History of Experimental Fuel Rod Assemblies

Experimental Assembly No.	Irradiation Dates		Location ^a in Loop	Reactor Cycles	Exposure (Mwd of reactor operation)
	Start	Finish			
1	3-26-60	5-14-60	A-1, A-2	2	2100
	10-4-60 ^b	11-20-60		1	
3	5-21-60	7-9-60	A-1, A-2	2	6000
	12-1-60 ^b	7-4-61		4	
4	7-12-61	10-22-61	A-2	2	2600
5	7-12-61	7-29-62	A-1	7	9400
6	10-31-61	2-11-62	A-2	2	2800
7	2-19-62	6-3-62	A-2	2	2600

^aLegs of U-shaped test section occupy lattice positions A-1 and A-2 in the ORR core.

^bInterrupted irradiation.

The specific activities in the samples of water-borne crud (listed in Table 3.3), while lower than those in the fuel-rod crud deposits, are not greatly different in level or in distribution of activity. Spectrochemical analyses of crud from fuel rods and from coolant samples (Table 3.5) also gave similar data.

Radiochemical Exchange. The present results provide further evidence that significant radiochemical exchange takes place between the two fractions of water-borne activity, that is, the filterable crud fraction and the nonfilterable, apparently ionic fraction. This is indicated by the similarity of the $\text{Fe}^{55}/\text{Fe}^{59}$ and the $\text{Co}^{60}/\text{Co}^{58}$ activity ratios for the two fractions (Fig. 3.2) and also by the similarity in other nuclide ratios (Table 3.2). In particular, if it is assumed that complete radiochemical exchange has occurred, the distribution ratio, $X_i = A_i^s/A_i^w$, of a given nuclide specific activity, A_i , between the filterable fraction (s) and the nonfilterable fraction (w), should be a constant. Unfortunately, such X_i ratios cannot be determined directly from the present results because concentrations in the nonfilterable fraction (in grams per liter) have been too low for direct measurement. The constancy of X_i can be tested,

Table 3.5. Spectrochemical Analysis of Various Crud Samples

Date ^a	Sample	Crud Weight (g)	Composition (wt %)			
			Fe	Ni	Mo	Cr
		Fuel Rod Crud Deposits				
7-4-61	3-(A-2)-1	0.1941	51.6	11.8		0.23
	3-(A-2)-2	0.0833	74.5	11.2		
	3-(A-2)-3	0.0165	74.2	10.1		
	3-(A-1)-3	0.0717	64.2	11.5		
	3-(A-1)-2	0.1356	51.7	12.9		
	3-(A-1)-1	0.1890	58.2	17.2	0.21	
		Water-Borne Crud				
5-17-61		0.0548	51	8.2		
		0.0074	74	11		
		0.0035	57	8.6		

^aDate fuel rod irradiation was terminated or date water sample was taken.

however, by considering the ratio of two X_1 values:

$$\frac{X_1}{X_2} = \frac{A_1^S/A_1^W}{A_2^S/A_2^W} = \frac{A_1^S/A_2^S}{A_1^W/A_2^W}.$$

It may be seen that the ratio X_1/X_2 is equivalent to a ratio of known quantities, that is, the ratio of the two different nuclide specific activities in each of the water fractions. Such ratios, listed in Table 3.6 were found to be reasonably constant in those cases for which sufficient data were available for their calculation.

Decontamination by Magnetite. As noted above, magnetite (Fe_3O_4), which is a principal constituent of crud, was tested for its effectiveness as a filter and ion exchange medium. Since this constituent of crud may both supply and exchange with the ionic material in the coolant, the introduction of a bed of nonradioactive magnetite into the system might well, by the same process which otherwise contributes to the transport of activity, accumulate the dissolved activity without otherwise disturbing the chemical or nuclear behavior of the system.

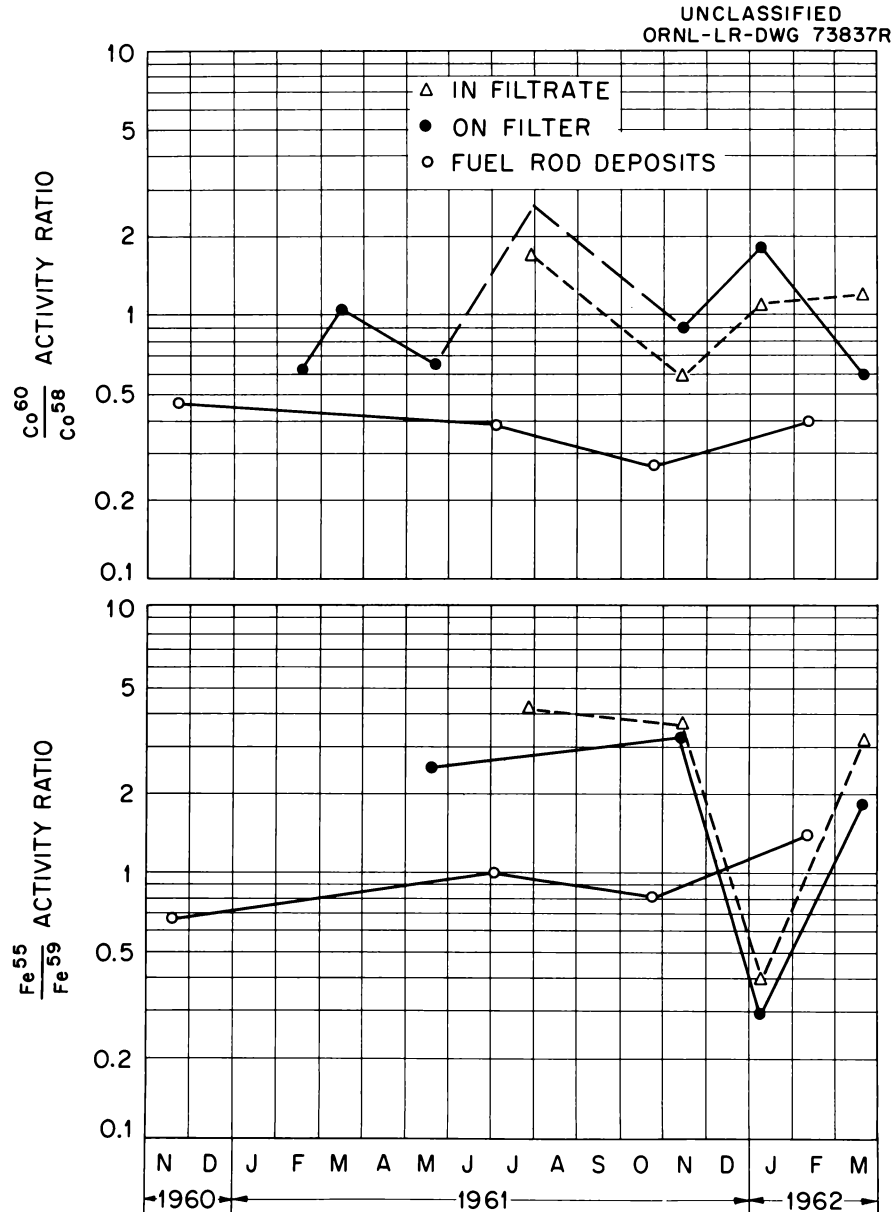


Fig. 3.2. Nuclide Activity Ratios in Loop Coolant and Fuel Rod Deposits.

A filter (Fig. 3.3) for testing the high-temperature ion-exchange and filtration properties of magnetite was installed in the ORR loop sample station. When in operation, hot loop water passes continuously through the unit (~ 70 ml/min), entering at A and leaving at B, and causes the temperature to rise to $\sim 425^\circ\text{F}$. Samples are withdrawn through filter cartridge C at outlet D. Except for the sintered nickel disks ($10\ \mu$ average pore size) that form the end closures of the cartridge, the entire unit

Table 3.6. Relative Distribution of Activities Between Filterable and Nonfilterable Water Fractions^a

Sampling Date	Activity Ratios			
	$X_{\text{Fe}55}/X_{\text{Fe}59}$	$X_{\text{Co}60}/X_{\text{Co}58}$	$X_{\text{Fe}59}/X_{\text{Co}58}$	$X_{\text{Mn}54}/X_{\text{Co}58}$
11-9-61	0.92	1.6	4.4	
1-8-62	0.72	1.7	2.0	1.6
3-19-62	0.6	0.5	1.9	1.0

^aBased on data of Table 3.2.

is made of stainless steel. Data for two kinds of magnetite (Table 3.7) show quite favorable decontamination factors for loop water activity, most of which was nonfilterable.

Activity Transport Mechanism

The small amount of particulate crud in the coolant represents only a small fraction of the coolant activity, and thus is not expected to play as great a role in the transport of activity in the system during normal operation as does the nonfilterable, presumably ionic, material. Indeed, from the present results, it appears that this dissolved material is the principal agent of activity transport in well-conditioned, neutral-pH, pressurized-water reactor systems during periods of normal, undisturbed operation. This transport process would consist of the liberation of activity from the in-flux crud deposits as ionic material, which then would exchange with crud deposits throughout the system. It would at the same time account for the well-crystallized appearance of the crud.

The simple model shown in Fig. 3.4 was developed to permit an analysis of this transport process. A system of three regions is assumed: (1) the volume V^C (cm^3) of crud deposited on in-flux surfaces, (2) the volume V^W (cm^3) of coolant water, and (3) the volume V^S (cm^3) of crud deposited on out-of-flux surfaces. The symbols N_b^C , N_b^W , and N_b^S denote the concentrations of a given nuclide, b (in atoms/ cm^3), in each region. The notations R and D refer to rate constants (in sec^{-1}) for release to and deposition from the coolant, respectively; $\sigma_a N_a^C \phi$ is the product of the parent neutron capture cross section (cm^2), parent nuclide concentration

UNCLASSIFIED
ORNL-LR-DWG 69255

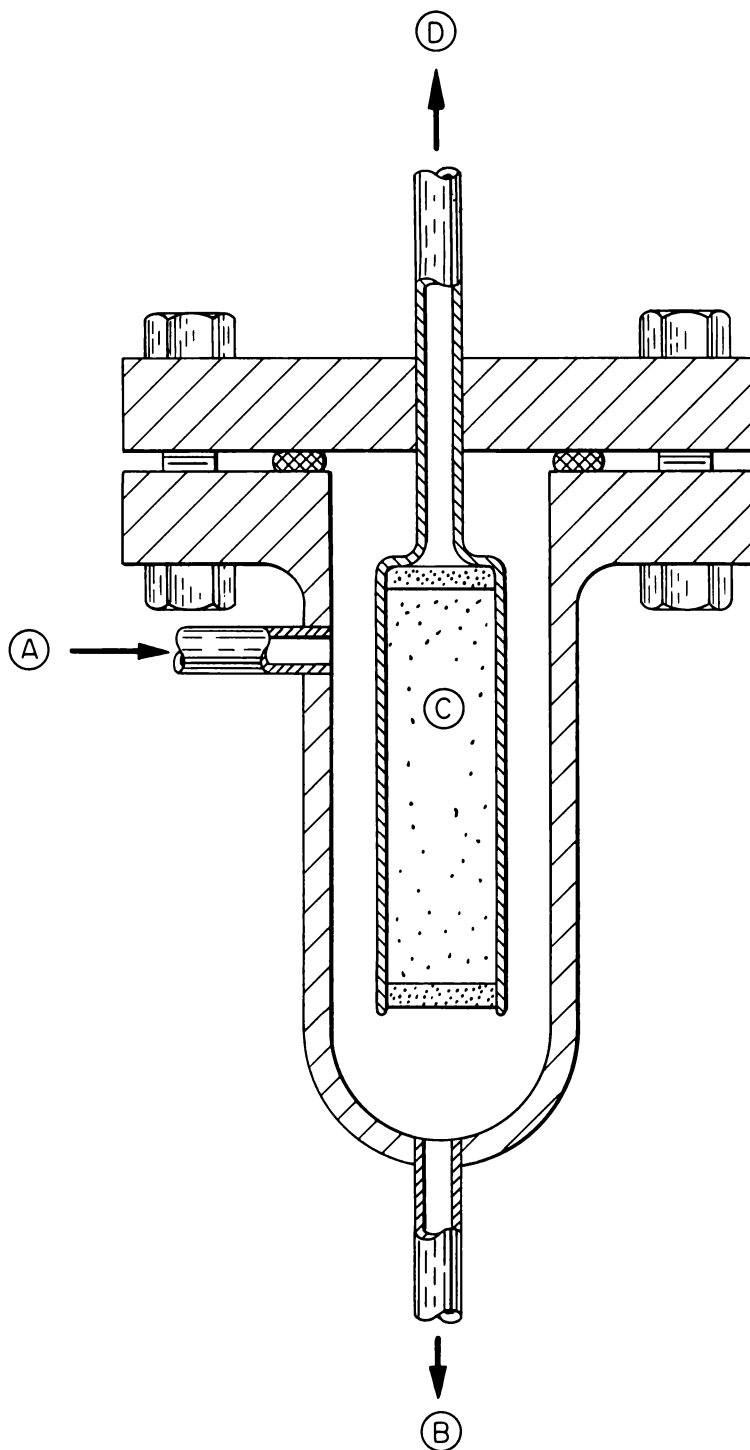


Fig. 3.3. High-Temperature Filtration Unit.

Table 3.7. Decontamination of Loop Water by Magnetite in High-Temperature (425°F) Filter Unit

Date	Magnetite	Flow Rate (ml/min)	Activity Removed (%)		
			Mn ⁵⁶	Co ⁵⁸ + Mn ⁵⁴	Co ⁶⁰ + Fe ⁵⁹
7-5-62	Prince Mfg. Co., +80 mesh	60	>99	>99	95
9-11-62	Mapico Black, sintered	80	>99	97	98

UNCLASSIFIED
ORNL-LR-DWG 73836A

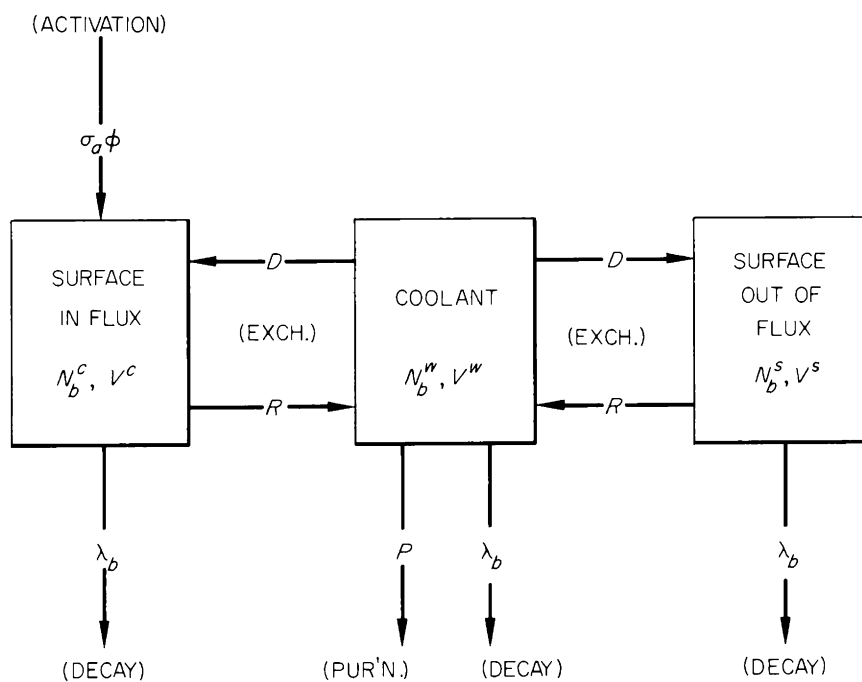


Fig. 3.4. Assumed Mechanism of Activity Transport in ORR Pressurized-Water Loop.

(atoms/cm³), and the neutron flux (neutrons/cm²·sec); λ_b is the decay constant of nuclide b (sec⁻¹); and P is the purification rate (sec⁻¹), which is the fraction of system volume that flows through the purification system per second.

The following rate processes occur, all in atoms of nuclide per second:

Gain by activation	$\sigma_a N_a^C \phi V^C$
Loss by decay	$\left\{ \begin{array}{l} \lambda_b N_b^C V^C \\ \lambda_b N_b^W V^W \\ \lambda_b N_b^S V^S \end{array} \right.$
Loss by purification (assumes absolute removal by purification system)	$PN_b^W V^W$
Release to coolant from surface	$RN_b^C V^C$ $RN_b^S V^S$
Gain to surface from coolant	$DN_b^W V^C$ $DN_b^W V^S$

The values of N_b^C and N_b^W are known from measurements. Since N_b^S is not known directly, it is taken to be equal to the corresponding quantity in the water-borne crud and to be typical of out-of-flux crud deposits. This seems reasonable, since the out-of-flux surface area is about 50 times the in-flux surface area.

Differential equations can be written describing the change with time of N_b^C , N_b^W , and N_b^S ; however, the solution of such simultaneous equations is quite involved, and the resulting expressions are complex. Culver³ has presented a complete solution for a somewhat simpler model, and Bergmann⁴ has solved a set of differential equations for a more complex model, using an analog computer.

For the present purpose, it is sufficient to examine the steady-state condition that apparently has been reached in the loop, that is, the condition wherein the concentration terms N_b^C , N_b^W , and, presumably, N_b^S are approximately constant. This permits a simple balancing of the gain and loss processes associated with each of the three regions:

³H. N. Culver, "Cooling Water and Demineralizer Activities in NMSR," USAEC Report ORNL CF 58-5-83, Oak Ridge National Laboratory, May 14, 1958.

⁴C. A. Bergmann, "SM-1 Research and Development Program: Long Lived Induced Activity Buildup in SM-1 Core I Lifetime; Task XVIII - Phase I," USAEC Report APAE No. 77, Alco Products, Inc., Nov. 30, 1960.

$$\sigma_a N_a^C \phi V^C + DV_b^C N_b^W = RV_b^C N_b^C + \lambda_b V_b^C N_b^C, \quad (1)$$

$$RV_b^C N_b^C + RV_b^S N_b^S = DV_b^C N_b^W + DV_b^S N_b^W + \lambda_b V_b^W N_b^W + PV_b^W N_b^W, \quad (2)$$

$$DV_b^S N_b^W = RV_b^S N_b^S + \lambda_b V_b^S N_b^S. \quad (3)$$

By considering first ratio N_b^S/N_b^W , the distribution of a nuclide between the coolant and the crud on out-of-flux surface, Eq. (3) can be reduced to

$$\frac{N_b^S}{N_b^W} = \frac{D}{\lambda_b + R} \sim \frac{D}{R}. \quad (4)$$

It appears that R is considerably greater than λ_b , which has a maximum value of 10^{-7} sec^{-1} for the nuclides being considered, since the data indicate that A_b^S/A_b^W and hence N_b^S/N_b^W are about the same for both long-lived and short-lived nuclides of the same element (Table 3.6). Hence N_b^S/N_b^W is not sensitive to the value of λ in the region of interest.

By considering next the ratio N_b^C/N_b^S , Eqs. (2) and (4) yield

$$\frac{N_b^C}{N_b^S} = 1 + \left(1 + \frac{V^S}{V^C}\right) \frac{\lambda_b}{R} + \frac{V^W(\lambda_b + P)(R + \lambda_b)}{DRV^C}. \quad (5)$$

Since $P \gg \lambda_b$ for the nuclides being considered, and $R > \lambda_b$, then

$$\frac{N_b^C}{N_b^S} \sim 1 + \left(1 + \frac{V^S}{V^C}\right) \frac{\lambda_b}{R} + \frac{V^W P}{V^C D}. \quad (6)$$

The ratio V^S/V^C may be taken as the ratio of the out-of-flux area to the in-flux area (~ 50). It may be seen then from Eq. (6) that if λ_b/R for shorter lived activities (Fe^{59} , Co^{58}) is greater than ~ 0.01 , the ratio of each short-lived activity in the fuel rod deposits to that in the out-of-flux surfaces will be significantly greater than for the longer lived activities (Fe^{55} , Co^{60}). As noted previously, this is indeed the case, and hence $10^{-5} > R > 10^{-7}$; however, R was estimated more closely by comparing activity ratios for each of the four nuclides Fe^{59} , Co^{58} , Fe^{55} , and Co^{60} in the two regions. The latter estimate gave $R \sim 5 \times 10^{-6}$. From the ratio $N_b^S/N_b^W \sim D/R \sim 6.3 \times 10^8$, this gives $D \sim 3100$. By considering only the long-lived Fe^{55} and Co^{60} activities, for which $N_b^C/N_b^S \sim 1$, Eq. (5) reduces to

$$\frac{N_b^C}{N_b^S} = 1 + \frac{V^W P}{V^C D} \sim 1 + \frac{0.013}{V^C}, \quad (7)$$

since $V^W = 1.1 \times 10^5$ and $P = 3.7 \times 10^{-4}$ for the ORR loop. Thus V^C is evidently considerably greater than 0.01, perhaps 0.1 cm^3 or more. Since the in-flux area of the loop is $2.5 \times 10^3 \text{ cm}^2$, it follows that the average thickness of the layer of exchangable crud is $\sim 4 \times 10^{-5} \text{ cm}$ (0.4μ) or more, which is a reasonable lower limit, in view of the observed sizes of the crud crystals.

To sum up these considerations, it can be said that the observed specific activities and nuclide ratios of in-flux deposits, of the soluble material, and of the water-borne crud are consistent with the simple model depicted in Fig. 3.4. The transport of the activity associated with dissolved material in the coolant, corresponding to total concentrations of the order of 10^{-7} molar, yields exchange-rate constants of the order of $R = 5 \times 10^{-6} \text{ sec}^{-1}$ for release, and $D = 3.1 \times 10^3 \text{ sec}^{-1}$ for deposition. With an estimated crud layer thickness of 0.4μ or more, this value of R corresponds to a dissolution rate ($R \times$ thickness of crud layer) of $2 \times 10^{-10} \text{ cm/sec}$ or more. This is about three orders of magnitude greater than the expected limiting corrosion rate for conditioned stainless steel (1 mg of stainless steel per cm^2 per month or approximately

7.5×10^{-13} cm of crud per second). It is not unreasonable, however, to expect the "crud release rates" to be much higher than the net corrosion rates.

The ratio D/R , here determined to be $\sim 6 \times 10^8$, is a constant that is expected to be applicable to other similar pressurized-water systems which use neutral pH water at the same temperature. The significance of the individual values of D and R , in units of sec^{-1} , is less clear. In general, the dissolution rate (atoms/ $\text{cm}^2 \cdot \text{sec}$, or cm/sec) should be a constant that is characteristic of a given crystalline solid at a given temperature; however, in a crud layer the effective area for dissolution could be the total area of crystallites. This might be more nearly proportional to the product of the area of the deposit times its thickness than equal to the area alone. Then the significant rate constant would not be cm/sec , but rather $\text{cm}/\text{sec} \cdot \text{cm}$ or just sec^{-1} . Thus, it is possible that R and, by the same argument, D are the significant constants at a given temperature for pressurized-water systems containing dispersed crud deposits.

Purification Requirements. As noted above, the rate at which material is released from crud deposits appears to be much greater than the rate at which the system metal corrodes. For this reason the production rate of crud and of transportable activity by corrosion has thus far been neglected. It is, nonetheless, of considerable interest to know whether over a long period of time the total amount of crud in the system will increase, decrease, or remain nearly constant at some steady-state level.

Crud is produced continuously in the system, the amount being given in cm^3/sec by considering the product of the corrosion rate constant, C (cm of crud per second), and the system area, A (cm^2). This crud is transported about the system by the ionic dissolution and deposition exchange process, as has been assumed. Since it is assumed to be lost from the system only by passage to the purification system, it follows that in order for a steady-state crud level to exist, that is, for the total amount of crud in the system to remain constant,

$$CA = PV^W/(D/R) . \quad (8)$$

Here, D/R , as before, may be assumed to represent the ratio of concentration in crud to that in the coolant. From this it is seen that a constant amount of crud will be present in the system only when

$$P = 6.3 \times 10^8 \frac{CA}{V^W} .$$

If P is greater than this, crud is removed by the purification system faster than it is produced; if P is less, crud is formed by corrosion faster than it is removed. In the case of the ORR loop, with the parameters

$$\begin{aligned} C &= 1 \text{ mg of stainless steel per dm}^2 \text{ per month} \\ &= 7.5 \times 10^{-13} \text{ cm of crud per second,} \\ A &= 1.4 \times 10^5 \text{ cm}^2, \\ V^W &= 1.1 \times 10^5 \text{ cm}^3, \end{aligned}$$

a purification rate of $>6 \times 10^{-4} \text{ sec}^{-1}$ is required to assure that crud can be removed faster than it is formed. The actual purification rate ($3.7 \times 10^{-4} \text{ sec}^{-1}$), while less, is close to this value, suggesting that an approximate steady-state crud level does exist in this system.

In the case of the N.S. SAVANNAH reactor, with

$$A = 1.7 \times 10^7 \text{ cm}^2,$$

and

$$V^W = 4.0 \times 10^7 \text{ cm}^3,$$

and assuming the same values for C and D/R , the purification rate required to balance the crud production rate is calculated from Eq. 9 to be $\sim 2 \times 10^{-4} \text{ sec}^{-1}$. Again this value is higher than the design value⁵

⁵"Nuclear Merchant Ship Reactor, Determination of the Purification Rate for Normal Operation," USAEC Report BAW-1015 (rev.), Babcock & Wilcox Company, June 1958.

of $\sim 4 \times 10^{-5} \text{ sec}^{-1}$, suggesting that crud will be produced by corrosion faster than it is removed by the purification system. These are only approximate calculations, however, since C, the long-term corrosion rate, and D/R are not accurately known. In addition the water-borne particulate crud level is neglected because it is small compared with the dissolved (ionic) crud level. This is expected to be a good approximation only for periods of undisturbed reactor operation. At other times, particulate crud levels will be comparable to or higher than the value expected from D/R, and this will result in correspondingly more rapid crud removal by the purification system. Thus, the above estimates of purification requirements are conservative ones.

Effectiveness of Magnetite Decontamination. In terms of the present assumed model of the activity transport process, the presence of a bed of natural magnetite in the system would greatly increase the value of V^S in Eq. 5. The resulting new steady state, when reached, would produce an increase in the ratio N_b^C/N_b^S . In particular, since N_b^C is also related to N_b^S by

$$N_b^C = \frac{\sigma_a N_a^C \phi}{R + \lambda_b} + N_b^S, \quad (9)$$

from a combination of Eqs. (1) and (3), then by combination with Eq. (6), N_b^S is given by

$$N_b^S = \frac{\sigma_a N_a^C \phi}{\left(1 + \frac{V^S}{V^C}\right) \lambda_b + \frac{RPV^W}{DV^C}} \sim \frac{\sigma_a N_a^C \phi V^C}{V^S \lambda_b + (R/D)PV^W}. \quad (10)$$

The activity of a given nuclide in out-of-flux deposits (dps/cm³) is thus

$$N_b^S \lambda_b \sim \frac{\sigma_a N_a^C \phi V^C}{V^S + \frac{(R/D)PV^W}{\lambda_b}}. \quad (11)$$

It is clear that the activity per unit volume of system crud, $N_b^S \lambda_b$, is decreased by increasing V^S as well as by increasing P , the relative effectiveness of the two depending on λ_b . In the present system

$$(R/D)PV^W = 6.5 \times 10^{-8} .$$

For Co^{60} ($\lambda = 4 \times 10^{-9} \text{ sec}^{-1}$), an increase in V^S of $\sim 15 \text{ cm}^3$ (as inactive exchangeable magnetite introduced into the system) would thus reduce the activity of deposited crud as effectively as would a doubled purification rate.

It might be argued that such a bed of magnetite, since it represents an increase in the amount of crud in the system, would increase water-borne crud levels and thus produce greater fouling and activity transport. Such is not expected to be the case provided the magnetite is of suitably large particle size and adequately contained. The present arguments suggest that the levels of ionic material in the coolant would remain unchanged (fixed by R/D).

Conclusions

The observations reported here support the previous conclusion that in systems of neutral pH, dissolved ionic material present at very low concentrations is responsible for appreciable chemical and radiochemical exchange that results in the recrystallization of crud and in the transport of activity from in-flux to out-of-flux crud deposits. A simplified treatment of this process, assuming steady-state conditions, permits estimates of the release and deposition rates. The treatment further allows estimation of the purification rates required to remove crud as rapidly or more rapidly than it is formed. It also indicates that magnetite could be used effectively as a high-temperature decontaminating agent in such systems, and this indication is supported by initial test results.

It should be emphasized that the assumed kinetic model is simple. The release and deposition-rate processes have been assumed to be unaffected by the reactor flux, the system has been assumed to be isothermal, and the effects of irreversible deposition of activity on system surfaces

have not been considered. The extent to which these effects can be neglected cannot be judged without further investigation; it can be said, however, that, in the present system, temperature variation is not great and the exchange rates involving the dissolved material are probably rapid compared with any irreversible deposition. In applying an analogous treatment to pressurized-water reactors, effects of varying temperature and, in particular, higher pH on release and deposition processes involving dissolved material should be examined.

4. ADVANCED CORE DEVELOPMENT

Physics Calculations

B. W. Colston E. E. Gross
M. L. Winton

Comparison of Radial and "Window-Shade" Methods for Calculating N.S. SAVANNAH Core I Burnups

Radial Burnup Results. Comparison of reactivity lifetimes for Zircaloy and stainless steel egg-crate cores containing a uniform loading of 4.2 wt % U^{235} were reported previously¹ that were based on radial burnup calculations. These calculations were for cores without control rods, control being accomplished by a uniformly distributed poison. For completeness and for contrast with the window-shade burnup calculations, these results are presented again in Fig. 4.1. Apparently, the use of the Zircaloy fuel-element container structure would double the reactivity lifetime of the 4.2 wt % U^{235} core I fuel elements relative to their reactivity lifetime in a stainless steel fuel-element container structure.

Window-Shade Burnup Results. Because of the striking effect of the Zircaloy egg crate on fuel-element reactivity lifetime, it was desirable to repeat the comparison by another, more realistic method. The one-dimensional window-shade calculation, which allows simulation of axial rod-bank control, was used. In addition to being programmed directly in terms of an actual observable position (the controlling rod-bank position), the window-shade calculation provides information on the axial power distribution and on how it changes with burnup. Since the properties for each axial zone in the window-shade calculation were obtained from two-dimensional PDQ calculations in the horizontal plane, the combination of window-shade and PDQ calculations provided some information on three-dimensional power distributions within the core.

The control-rod programming scheme simulated was based on withdrawal of rod banks from the outer regions of the core first. For the stainless

¹E. E. Gross, B. W. Colston, and M. L. Winton, "Nuclear Analyses of the N.S. SAVANNAH Reactor with Zircaloy or Stainless Steel as Fuel-Element Containers," USAEC Report ORNL-3261, Oak Ridge National Laboratory, April 24, 1962.

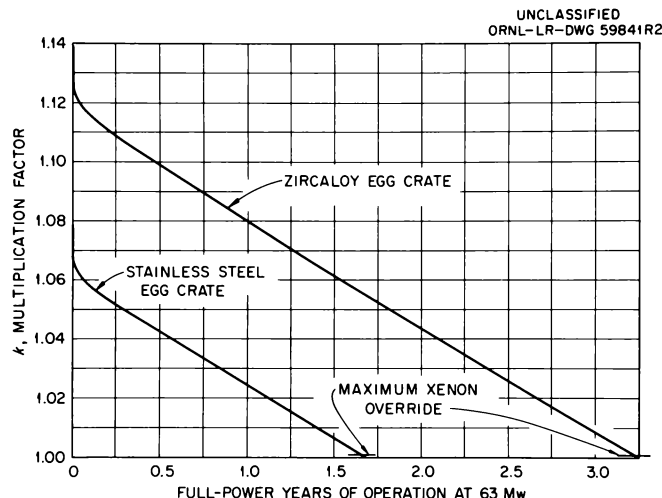


Fig. 4.1. Reactivity Lifetime of 4.2 wt % U^{235} Core I Fuel in Zircaloy and in Type 304 Stainless Steel Egg-Crates Based on Radial Burnup Calculations.

steel egg-crate core, this procedure resulted in a critical B-rod bank position of 24 in. withdrawn; X and A rods fully inserted; and the C, D, and E rods fully withdrawn. As the core burns up, the B-rod bank is withdrawn, followed by the A-rod bank, and then finally by the X rod. The calculated results for this mode of rod programming are presented in Fig. 4.2.

It is noted that this method of burnup calculation predicts a slightly greater core life than the radial burnup calculation. This was to be expected, since the rod-programming scheme employed in the window-shade calculation produces more uniform U^{235} fuel depletion than does a radial-burnup calculation with all rods out of the core. Also the rod-bank worth is slightly asymmetrical, the rod being worth slightly more in the bottom half of the core than in the top half. This is borne out by the calculated rod-bank worths as a function of bank position shown in Fig. 4.3. The rod worths shown in Fig. 4.3 are the worths within the rod configuration considered in the burnup calculation. For example, the B-rod-bank worth curve was calculated in the geometry of Fig. 4.4 for the X and A rods fully inserted and the C, D, and E rods fully withdrawn. It is believed that the presence of the full-rod region at the top of the core and its absence at the bottom produces the slightly asymmetrical rod-worth curves.

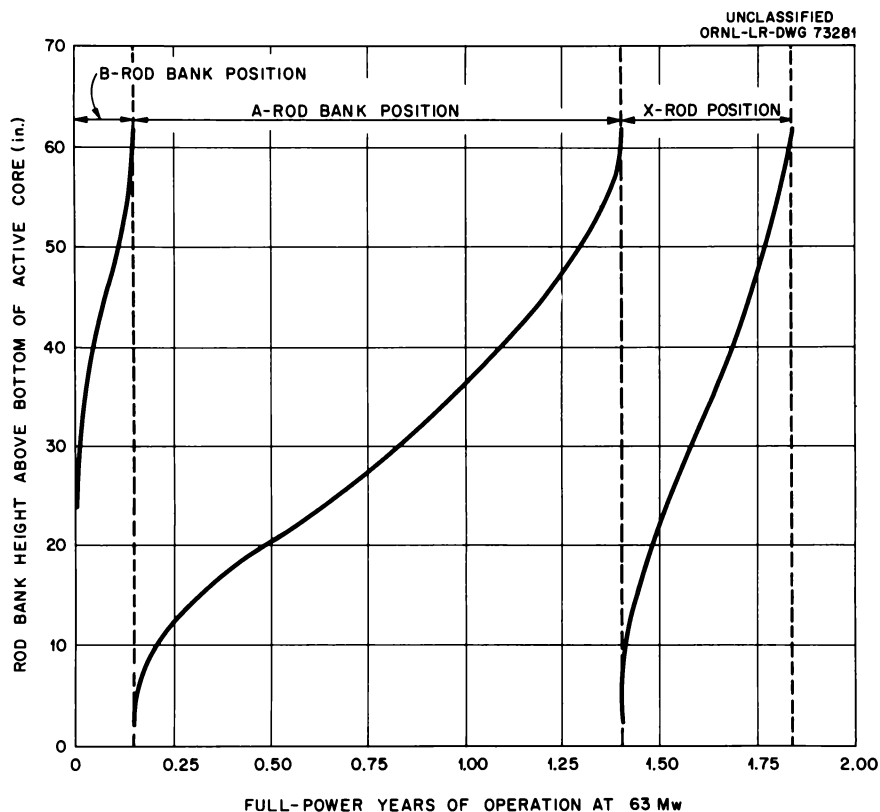


Fig. 4.2. Calculated Controlling Rod-Bank Position as a Function of Time for the Two-Zone Core I.

The rod-worth curves may be used to convert the burnup curves of Fig. 4.2 into a reactivity-lifetime curve similar to that of Fig. 4.1. If this is done, the initial multiplication factor is found to agree with the value of Fig. 4.1 to within about $\Delta k = 0.002$. The window-shade burnup results are presented in the form of Fig. 4.2 to properly contrast the results of this method with the results of the radial-burnup calculations.

Axial Power Distributions. Axial power distributions at the beginning and end of core I life obtained from the window-shade burnup calculations are shown in Fig. 4.5. Examination of the burnup results at intermediate time steps reveals that the axial power distribution at the beginning of core life is the most severe with respect to the axial peak-to-average power ratio; however, this axial peak occurs in the region of the core containing A and X rods, which have a favorable radial power distribution. Radial power peaking values at the beginning of core I life for various rod patterns are listed in Table 4.1; they were obtained

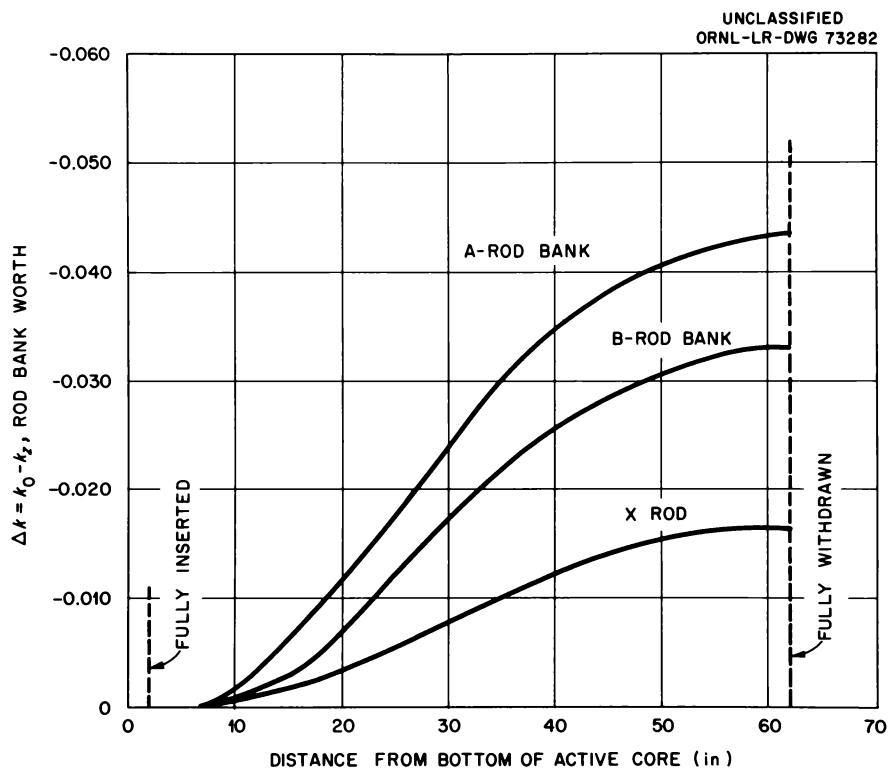


Fig. 4.3. Rod-Bank Worth as a Function of Bank Position Relative to Fully Inserted Position for Core I.

from PDQ calculations in the x-y geometry of Fig. 4.6. Combining radial and axial peaking factors, it is apparent that the most severe over-all power peaking occurs toward the end of core life when the X rod is almost fully withdrawn. At this point in core life, the over-all peak-to-average ratio obtained by simple combination of the axial window-shade results with the beginning-of-life radial peaking factor for no rods in the core is 2.9. This is considerably less than the design value² of 3.75.

The peak-to-average power peaking factor obtained in the manner described above cannot account for true three-dimensional effects. It is estimated, however, from comparison of calculations with experimental results on the A-rod bank core I critical experiment (see Fig. 2.25, Chap. 2) that the method used here gives power peaking factors that are only

²G. E. Kulynych, "Nuclear Merchant Ship Reactor, Final Safeguards Report, Description of the N.S. SAVANNAH," USAEC Report BAW-1164, Vol. I, Babcock & Wilcox Company, June 1960.

UNCLASSIFIED
ORNL-LR-DWG 73272

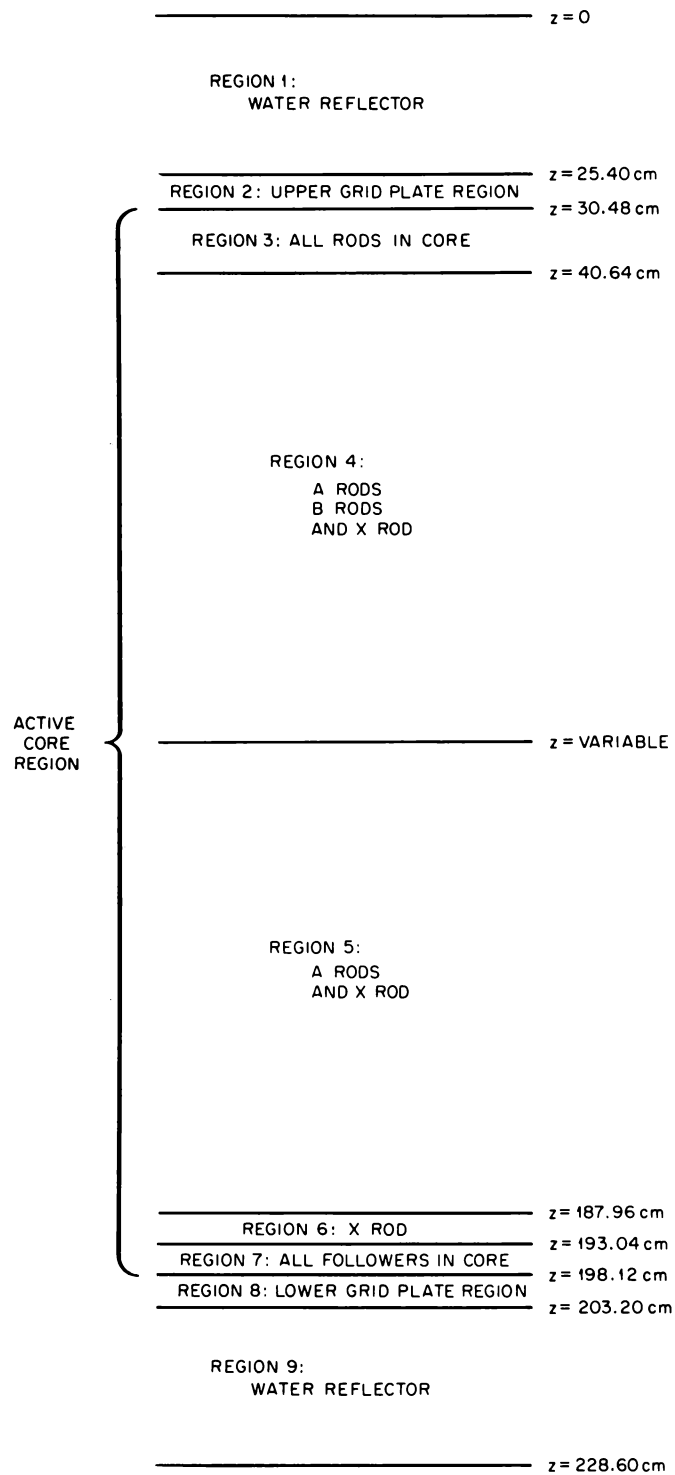


Fig. 4.4. Axial Geometry Used in Window-Shade Burnup Calculations.

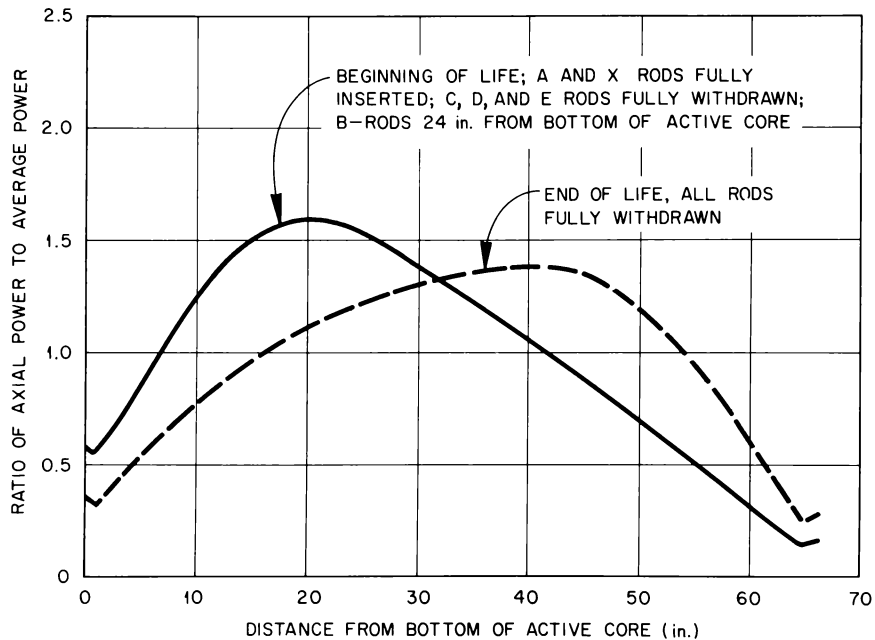
UNCLASSIFIED
ORNL-LR-DWG 73283

Fig. 4.5. Calculated Ratio of Axial Power to Average Power at Beginning and at End of Life for N.S. SAVANNAH Core I.

Table 4.1. Radial Power Peaking Factors
for Various Rod Insertions in
Core I at 508°F

Fully Inserted Rods	Radial Peak-to-Average Power Ratio	
	Two-Zone Core	One-Zone Core
No rods	1.98	2.05
X rod	1.60	1.65
A + X rods	1.44	1.48
A + B + X rods	1.49	1.48
All rods	1.44	1.70

about 10% lower than the experimental values. In addition, as shown in Figs. 2.20 and 2.21 (Chap. 2), it is expected that radial peaking factors should decrease with burnup.

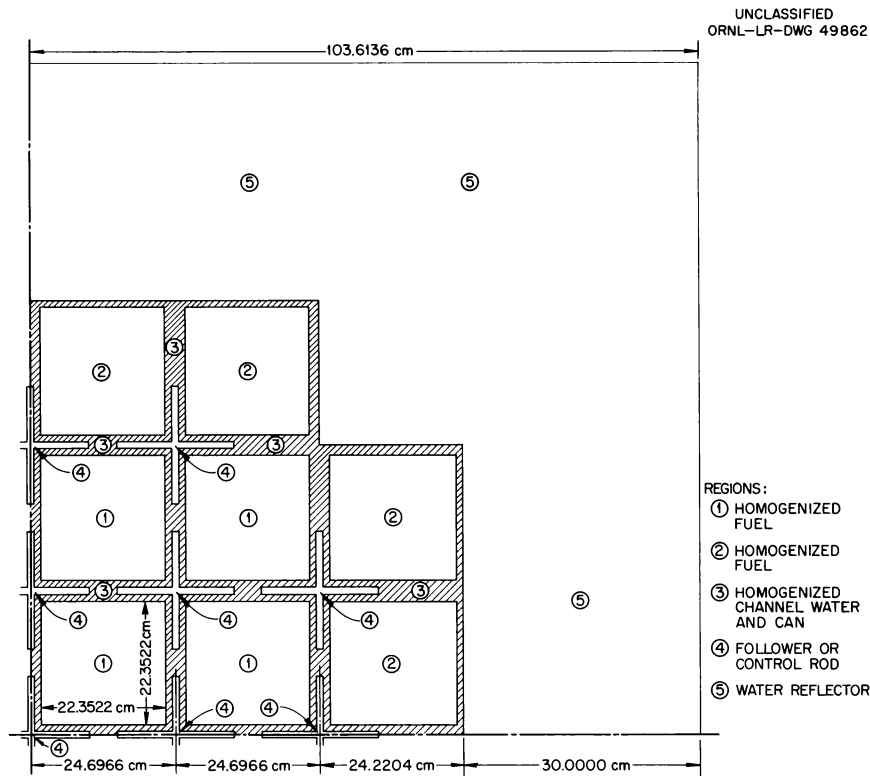


Fig. 4.6. Geometrical Model for One Quadrant of N.S. SAVANNAH Core I.

Window-Shade Burnup Results for 4.2 wt % Zircaloy Egg-Crate Core

Initial hot criticality conditions for the 4.2-wt % U^{235} Zircaloy egg-crate core require the X, A, and B rods to be fully inserted and the C, D, and E rods banked at 28 in. above the bottom of the active fuel. The rod-programming scheme followed in the window-shade burnup calculation was withdrawal of the C, D, and E rods as a unit, followed by withdrawal of B, A, and X rods in sequence, as in the stainless steel egg-crate calculations. The resulting rod-movement history is displayed in Fig. 4.7. Again the resulting core life is in good agreement with the previous radial burnup calculation (Fig. 4.1) but gives a slightly longer lifetime estimate. Comparison of Figs. 4.2 and 4.7 again predicts that the replacement of stainless steel by Zircaloy in the fuel-element container structure will essentially double the reactivity lifetime of core I fuel elements.

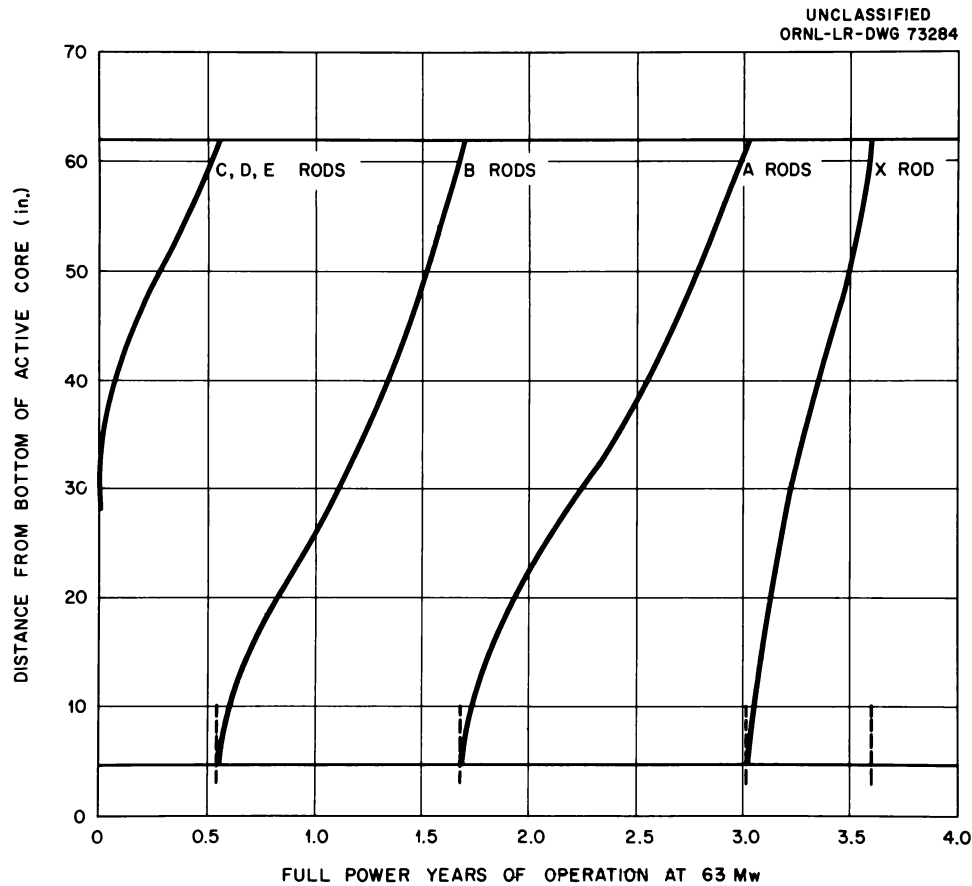


Fig. 4.7. Calculated Controlling Rod-Bank Position as a Function of Time for 4.2 wt % U^{235} Fuel in Zircaloy Egg-Crate Core.

Rod-bank worth curves for the Zircaloy egg-crate core are shown in Fig. 4.8. These curves are similar to the worth curves for a stainless steel egg-crate core shown in Fig. 4.3 and were obtained in the same manner. The clean, cold reactivity obtained by adding the worth of rods in the core is within $\Delta k = 0.002$ of the clean, cold reactivity of the core without any rods. Thus, the difference in lifetimes predicted by the radial and window-shade burnups cannot be ascribed to initial reactivity differences but is believed to be due to the more uniform fuel depletion attained in the window-shade calculation.

Beginning and end-of-life axial power distributions for the Zircaloy egg-crate core are shown in Fig. 4.9. Radial peaking factors for various rod configurations at 508°F are shown below:

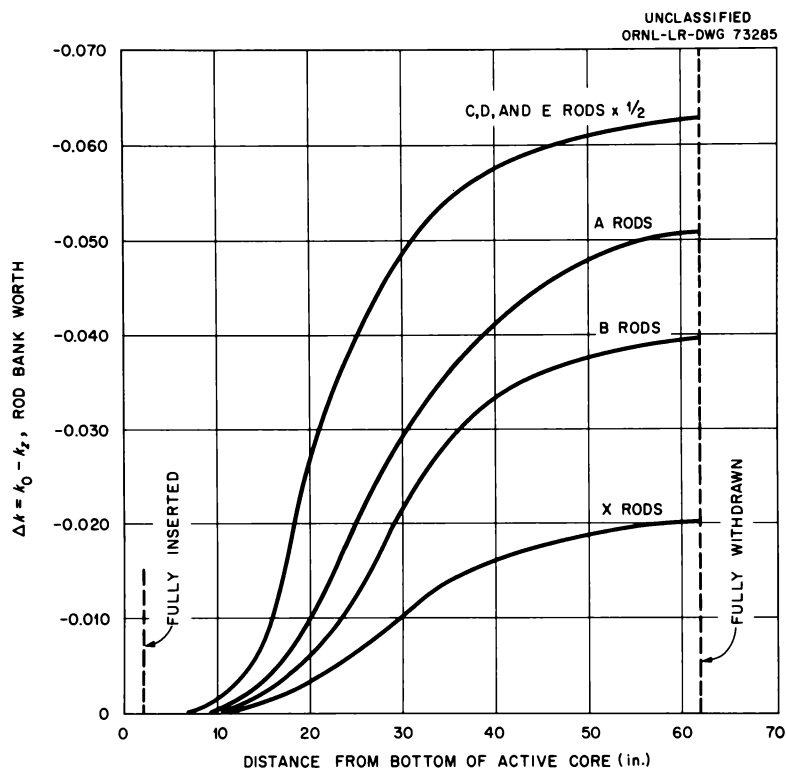


Fig. 4.8. Rod-Bank Worth as a Function of Bank Position Relative to the Fully Inserted Position for 4.2 wt % U^{235} Fuel in Zircaloy Egg-Crate Core.

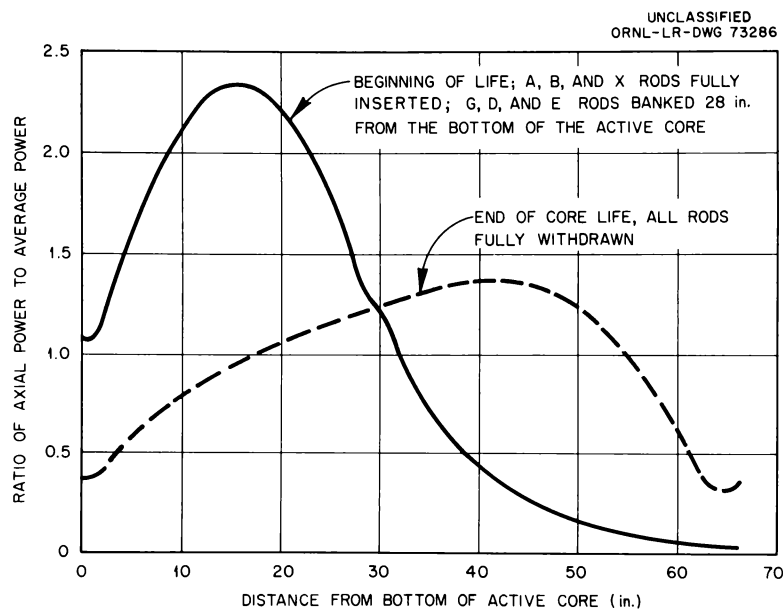


Fig. 4.9. Calculated Ratio of Axial Power to Average Power at Beginning and End of Life for 4.2 wt % U^{235} Fuel in Zircaloy Egg-Crate Core.

Fully Inserted Rods	Radial Peak-to-Average Power Ratio
No rods	2.03
X rod	1.62
A + X rods	1.46
A + B + X rods	1.53
All rods	2.15

The most severe power peaking occurs at the beginning of core life and has the value 3.55, which is lower than the design value of 3.75 but considerably higher than the maximum peaking factor of 2.9 in the stainless steel egg-crate core.

Fuel Development

W. C. Thurber

Preparation of Irradiation Test Specimens for ORR Loop (W. S. Ernst, Jr., J. W. Tackett)

As a continuation of the fuel-rod irradiation program in the ORR pressurized-water loop, additional assemblies for loop experiments 7, 8, and 9 were fabricated. Each assembly consists of three rods brazed to electroless-nickel-plated ferrule spacers, as shown in Fig. 4.10.

Assembly 7 consisted of 19-in.-long, 1/2-in.-OD, 0.035-in.-wall type 304 stainless steel-clad rods fueled with vibratory-compacted fused-and-ground UO_2 . Assembly 8 was similar, except that the fuel was sintered-and-ground oxide. In assembly 9, however, sintered UO_2 pellet fuel was utilized in combination with 0.020-in.-thick cladding tubes.

Some problems were encountered during fabrication of fuel rods for experiment 7. During the compaction process, breakup of the UO_2 occurred to the extent of about 15% degradation of both coarse and mid-fractions, and a density of approximately 85% of theoretical was the maximum obtainable. Since a higher fuel density was desired in the experiment, a quantity of previbrated UO_2 was used for each of the two larger fractions, and the fine fraction (-200 mesh) of the ternary mixture was ball milled. This scheme produced reasonable densities, as indicated in Table 4.2.

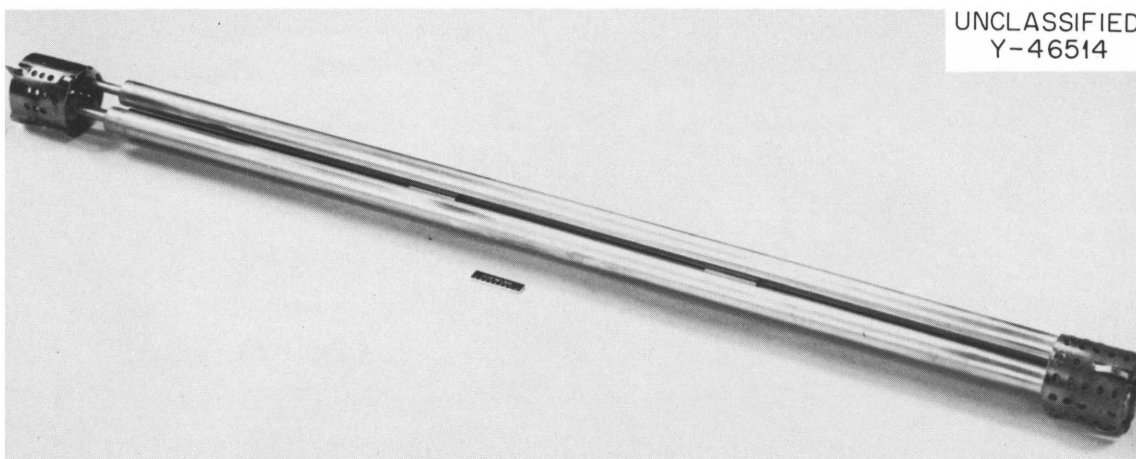


Fig. 4.10. Fuel Rod Cluster of the Type Used in ORR Pressurized-Water Loop Experiments 7, 8, and 9.

Table 4.2. Compacted Densities in Fuel Rods for Experiment 7

Tube	Relative Amount of Previbrated Oxide (%) ^a		Compacted Density ^b (%)
	-10 +16 mesh	-70 +100 mesh	
7N1	83	83	87.1
7O1	83	83	87.1
7P1	74	78	86.9
7 spare	83	83	86.8

^aParticle size distribution: 62.2 wt % -10 +16 mesh, 16 wt % -70 +100 mesh, 21.8 wt % -200 mesh.

^bVibration conditions: vibrator NAVCO BH-2 on cork suspension; time, 5 min at no load, with an additional 10 min with 1064-g load.

For experiment 8, sintered-and-crushed UO_2 (5% enriched) was vibratory compacted into four tubes of type 304 stainless steel measuring 19 in. long and 0.500 in. OD, with a 0.035-in. wall. Data on these tubes are listed in Table 4.3. It is obvious that the compacted bulk densities are slightly lower than can be attained with fused-and-crushed UO_2 vibrated under similar conditions. This difference results from the fact that the individual particles of sintered material are less dense.

The fuel rods for experiment 9 were fabricated by encapsulating 5%-enriched sintered UO_2 pellets in type 304 stainless steel cladding 0.020

Table 4.3. Vibratory-Compaction Data^a for Fuel Rods for ORR Experiment 8

Tube	UO ₂ Net Weight per Tube (g) ^b	Fueled Length of Rod (cm)	Bulk Density (% of theoretical)
8N1	365.0	41.3	85.81
8O1	367.0	41.5	85.85
8P1	364.5	41.4	85.48
8 spare	364.1	41.3	85.59

^aVibration conditions: vibrated 10 min on a NAVCO BH-2 pneumatic vibrator; a static load of 4.1 kg was placed on the free-oxide surface for approximately 8 min of the vibration cycle.

^bParticle size distribution: 60 wt % -4 +16 mesh, 15 wt % -70 +100 mesh, 25 wt % -200 mesh.

in. in wall thickness. In order to have controlled fuel-to-cladding gaps of 0.002 in. (rod 9C1), 0.007 in. (rod 9B1), and a combination of these gaps (rod 9A1), the UO₂ pellets were centerless ground to 0.447- and 0.452-in. diameters, and the stainless steel tubing was bored to an inside diameter of 0.454 in. Considerable difficulty was encountered in assembling the closely dimensioned pellets into rods 9A1 and 9C1. The centerless-ground pellets were found to be out-of-round to a considerable degree. The tubing used for rod 9A1 was expanded by heating, and a sufficient number of 0.452-in.-diam pellets were selected to complete the assembly. Some pellet breakup did occur, however. In order to assemble rod 9C1, it was necessary to rebore the cladding tube to an inside diameter of 0.458+ in.; the resulting nominal cladding wall thickness was less than 0.018 in., and the nominal fuel-to-cladding gap was approximately 0.006 in. instead of 0.002 in.

No problems were encountered in brazing the three clusters required for these experiments. Because of the tube-swelling problem encountered during the brazing step in the fabrication of the VBWR-M1 bundle, described in the next section, the UO₂ contained in the fuel rods used in experiments 8 and 9 was outgassed in vacuum immediately prior to making the final end-closure welds.

Manufacture of Test Bundles for Irradiation in the Vallecitos Boiling-Water Reactor (VBWR) (W. S. Ernst, Jr., D. O. Hobson, J. W. Tackett)

Two 16-rod fuel bundles for irradiation in the VBWR were to be manufactured in FY-1962. One bundle was to consist of rods of stainless steel-clad, rotary swaged and compacted UO_2 , and the rods of the other bundle were to consist of stainless steel-clad vibratory compacted UO_2 . The manufacturing procedures proposed for the individual fuel rods were essentially identical with those used in preparing similar test fuel rods for irradiation in the ORR. The procedures developed for brazing the fuel bundles were described previously.³

Swaged fuel rods for the 16-rod VBWR M-1 test bundle were completed, assembled into a bundle, and brazed. During brazing, however, severe swelling of the tubes occurred. The as-brazed bundle is shown in Figs. 4.11 and 4.12. This result was entirely unexpected in view of the low gas content determined for the as-received oxide ($0.061 \text{ cm}^3/\text{g}$). An investigation was therefore conducted to determine the source of the swelling and to determine the salvage value of the damaged fuel rods.

In an effort to determine the source of the swelling, the two "spare" rods (18 fuel rods were manufactured) were outgassed at temperatures up to 1000°C in a special apparatus capable of measuring the volume of gas evolved from the fuel rod. The data obtained during the first run indicated that approximately 1.6×10^{-2} moles of gas were released from the fuel rod. On the basis of the gas analysis of the as-received UO_2 ($0.061 \text{ cm}^3/\text{g}$), approximately 2.24×10^{-3} moles of gas should have been released. At the lower temperatures (0 to 300°C and 0 to 500°C), a condensate (presumably water) appeared in the Todd pressure gage as the readings were made. Prior to outgassing the other spare rod, a magnesium perchlorate dryer was installed. This run indicated that 1.2×10^{-2} moles of gas were released (7.1×10^{-3} moles of gas plus 5.1×10^{-3} moles of H_2O).

³W. S. Ernst, Jr., J. T. Lamartine, and J. W. Tackett, Test Bundles for Irradiation in the Vallecitos Boiling-Water Reactor (VBWR), pp. 92-95, "Maritime Reactor Program Ann. Prog. Rep. Nov. 30, 1961," USAEC Report ORNL-3238, Oak Ridge National Laboratory.

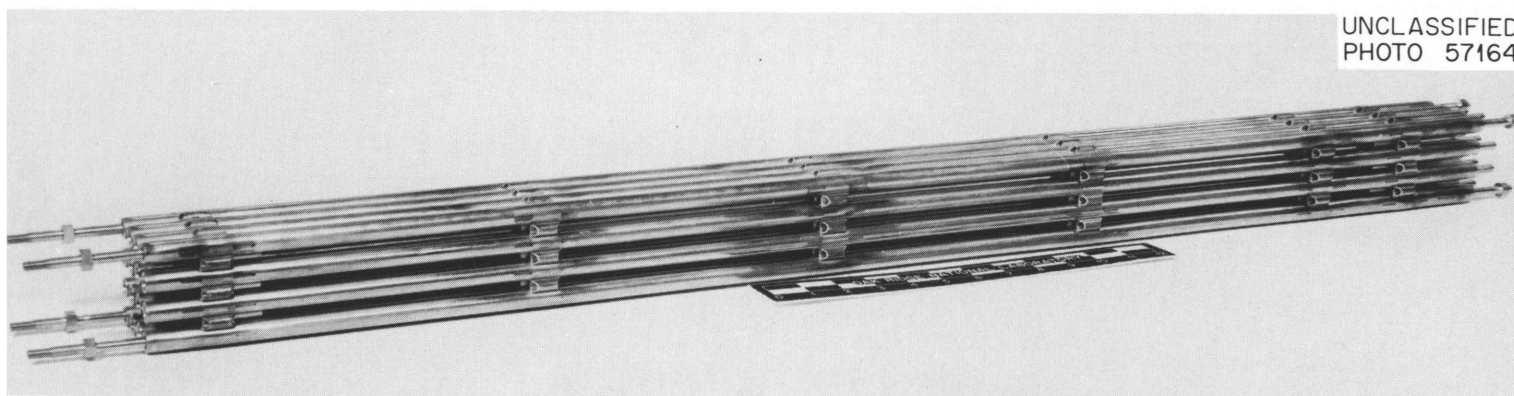


Fig. 4.11. As-Brazed VBWR-MI Irradiation Assembly.

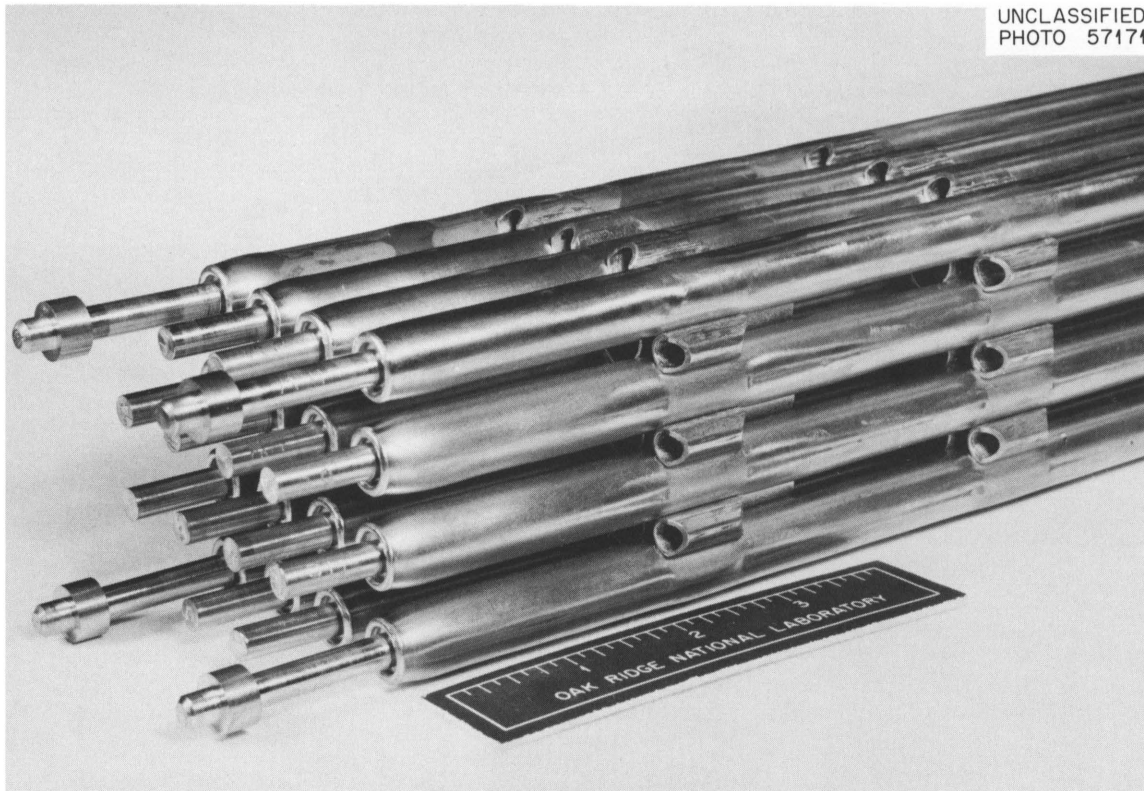


Fig. 4.12. As-Brazed Assembly Showing Swelling of Individual Fuel Tubes.

Additional UO_2 samples were then obtained from the as-received lot of UO_2 and from as-swaged scrap from the M-1 fuel rods. The results of gas analyses of these materials, as well as analyses of a spare rod, are shown in Table 4.4. The volume of gas released from the as-received lot was found to be $0.049 \text{ cm}^3/\text{g}$ of UO_2 , which compares favorably with the $0.061 \text{ cm}^3/\text{g}$ obtained almost three months earlier. In determining the gas released from the as-swaged fuel, runs were made both with and without a water dryer. Although standard analytical equipment* was used in measuring the gas evolved from the as-received and as-swaged samples, the presence of a condensate such as water is not routinely determined, and this obviously results in misleading data. From the data presented in

*This equipment was used in determining the gas release of UO_2 fuel used in all previously reported Maritime swaging and vibratory-compaction experiments.

Table 4.4. Gas Evolved by Heating UO₂ Samples

	Temperature (°C)	Gas Evolved (cm ³ /g)	Major Constituents (vol %)				
			H ₂	H ₂ O	N ₂ + CO	O ₂	CO ₂
As-received UO ₂ (2 samples) ^a	0-300 ^b	0.009	6.9	27.7	18.8		41.2
	300-500	0.013	11.7	5.5	25.9		49.8
	500-750	0.009	16.0	4.4	62.5		14.3
	750-1010	0.018	11.4	2.0	85.7		
	Total	0.049					
As-swaged UO ₂ tested without H ₂ O dryer (3 samples) ^a	0-300 ^b	0.064	15.6	46.44	5.25		31.05
	300-500 ^b	0.152	7.8	12.81	12.29		66.8
	500-750	0.046		0.91	77.33	20.09	0.69
	750-1010	0.025	20.69	1.11	72.22		5.97
	Total	0.287					
As-swaged UO ₂ tested with H ₂ O dryer (3 samples) ^a	0-300 ^c	0.145	6.1	0.6	5.2		87.4
	300-500	0.140	0.7	0.7	7.8		90.5
	500-750	0.031	7.7	1.1	66.6		23.9
	750-1010	0.023	19.9	1.6	76.5		1.5
	Subtotal	0.338					
H ₂ O removed		0.455					
	Total	0.793					
As-swaged spare rod tested with H ₂ O dryer (1 sample) ^d	0-300 ^c	0.027	52.3	0.65	22.9	3.71	13.62
	300-500	0.036		0.93	78.3	19.79	0.12
	500-750	0.108	25.77	0.21	68.0	0.41	4.32
	750-1010	0.042		0.63	79.4	18.97	0.12
	Subtotal	0.213					
H ₂ O removed		0.117					
	Total	0.330					

^aVery precise analytical equipment was used for the gas measurements.

^bCondensate (H₂O) observed in Todd pressure gage and Todd gage pressure reading did not agree with alphasatron gage reading.

^cNo condensate observed.

^dEquipment was reasonably accurate; it was constructed for this evaluation only.

Table 4.4, it is apparent that the swaged rods contained a significant amount of moisture.

The following test was then made to determine the effect of vacuum degassing an as-swaged rod. After one of the spare M-1 fuel rods had been outgassed in vacuum at 1000°C, end caps were installed and closure welds made. The rod was then placed in the brazing furnace and heated to the brazing temperature, duplicating a normal brazing cycle. Inspection of the rod following the brazing cycle indicated that no change in

the rod diameter had occurred. Thus, although the source of the moisture was not identified, outgassing techniques were devised whereby suitable rods could be produced.

Fabrication of the vibratory-compacted bundle (M-2) was then initiated. In order to preclude recurrence of the rod-swelling problem noted in bundle M-1, it was decided that the fuel should be outgassed prior to compaction. This operation was accomplished by heating the as-received oxide in a hydrogen atmosphere to 1150°C and cooling in the same environment. During handling and outgassing, the coarse UO₂ particles (-10 +16 mesh) were severely degraded into smaller particles. This change in particle size in turn limited the obtainable bulk density to about 81% of theoretical. By rescreening the degassed material to remove undesirable fractions, it was found that the vibrated bulk density could be increased to a satisfactory value; however, the yield of material in the appropriate distribution was not adequate to permit fabrication of a 16-rod bundle. Data on the nine successfully manufactured vibratory-compacted fuel rods for experiment M-2 are summarized in Table 4.5.

Since it was not possible to fabricate a 16-rod bundle and because of the problem of gas evolution in the swaged rods, it was tentatively decided that a mixed bundle containing eight cold-swaged and eight

Table 4.5. Fabrication Data on Vibratory-Compacted Rods^a for VBWR Test Bundle

Tube	UO ₂ Net Weight Per Tube (g)	Fueled Length of Rod (cm)	Bulk Density (% of theoretical)
3A	791.0	87.8	87.38
4A	792.0	88.7	86.59
18A	791.0	88.3	86.89
20A	791.0	88.7	86.50
9	801.5	90.3	86.09
24	791.5	88.3	86.94
29	792.0	88.4	86.90
30	791.0	88.7	86.50
32	793.0	88.9	86.51

^aParticle size distribution: 60 wt % -10 +16 mesh, 15 wt % -70 +100 mesh, 25 wt % -200 mesh.

vibratory-compacted rods would be fabricated. The swaged rods were to be salvaged from bundle M-1. All rods for this composite bundle were to be vacuum degassed at approximately 1000°C prior to effecting the final seal weld. To this end, bundle M-1 was disassembled and salvage operations were initiated. Each of the M-1 rods was reswaged to the correct diameter and resized to the correct length, but because of machining problems, revealed by dye-penetrant and eddy-current inspection for surface defects, it was impossible to derive a sufficient number of rods for the proposed experiment.

Each of the reworked fuel rods, when inspected with a new eddy-current instrument designed specifically for wall-thickness determinations, gave numerous indications of irregularities in the wall of the stainless steel cladding. These indications were especially prevalent in the top 5 in. of the fuel rods. In this particular portion of the fuel rods, shown in Fig. 4.12, changes in rod diameter in excess of 0.050 in. were measured prior to resizing by swaging. Some of the reswaged fuel rods were sectioned to explore further the exact nature of the tube wall irregularities and the source of dye-penetrant indications. The condition of the tube wall (3 in. from the top end) of the fuel rod previously located in the No. 1 position of the bundle is shown in Fig. 4.13. Extensive cracking in the tube wall occurred, probably as a result of the swelling phenomenon. This type of cracking is typical of specimens subjected to creep deformation. Completion of the VBWR test bundle awaits procurement of additional UO_2 .

Vibratory-Compaction Development (W. S. Ernst, Jr.)

Vibratory-compaction studies with depleted, fused UO_2 were performed in direct support of the irradiation program. Results from these studies and from others for the fuel cycle program indicate that it is reasonable to expect bulk densities of 90% of theoretical in a reactor core loading. Based on experience with several small-sized lots and a large lot of fused UO_2 from Spencer Chemical Company, it appears that the product of large fusions, subsequently sized by the fabricator, shows a marked improvement in the quality of the starting materials used for vibratory compaction.

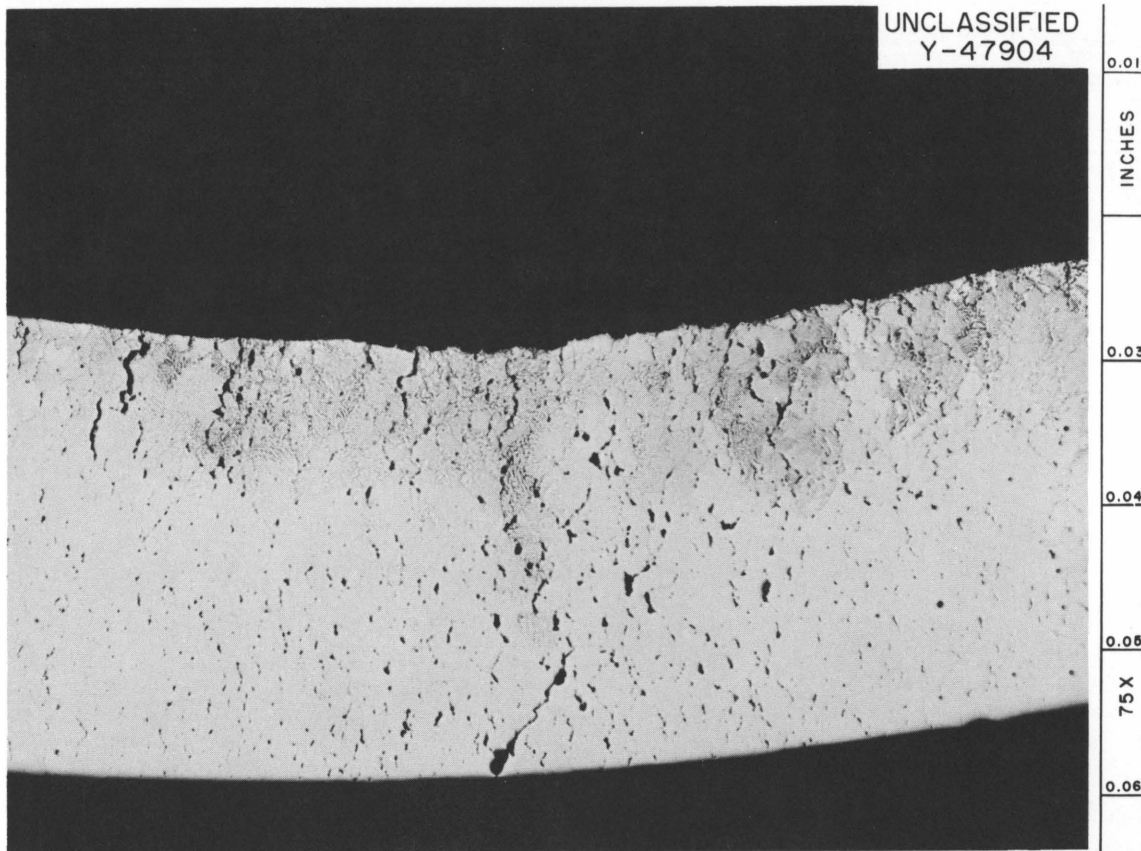


Fig. 4.13. Extensive Cracking Typical of that Observed in the Tube Wall of Fuel Rod No. 1.

The effect of differing particle-size distributions within the fine fraction (-200 mesh) on the vibrated bulk density was studied. An apparent correlation was found between the bulk density and an apparent Stokes diameter, d_{mw} , for which 50% by weight of the material is smaller than a given value. Since this experiment was conducted in support of the VBWR fuel-rod fabrication, depleted, fused UO_2 with a particle-size distribution of 60 wt % -10 +16 mesh, 15 wt % -70 +100 mesh, and 25 wt % -200 mesh material was chosen. The coarse- and medium-size fractions were generated by a semicontinuous ball-milling procedure. Seven different fine (-200 mesh) fractions were generated, and the size distributions were determined by a sedimentation technique. The values of d_{mw} were determined from these analyses. The vibrated bulk densities were measured for UO_2 in type 304 stainless steel tubes 45 in. long and 0.500 in. OD, with a 0.039-in. wall; the compaction was performed with a NAVCO

BH-3 pneumatic vibrator. The dependence of the vibrated bulk density on the d_{mw} values of the fine fractions is indicated in Table 4.6.

Table 4.6. Effect of Size Distribution in the Fine (-200 mesh) Fraction on Bulk Density of Vibration-Compacted Rods^a Containing Fused UO₂

Fine Fraction Designation	Apparent Stokes Diameter, d_{mw} (μ)	Bulk Density (% of theoretical)
A	29	87.5 \pm 0.2
C	24	89.2 \pm 0.1
B	23	88.5 \pm 0.1
G	20	88.8 \pm 0.2
D	17	88.7 \pm 0.3
E	15	89.5 \pm 0.3
F	11	89.3 \pm 0.1

^aParticle-size distribution: 60 wt % -10 +16 mesh, 15 wt % -70 +100 mesh, 25 wt % -200 mesh.

With the exception of the results obtained for fractions C and D, the densities of the compacts seem to increase with decreasing particle size to a d_{mw} value of approximately 15 μ . If the size is less than this, the density appears to decrease. An explanation for the reversal of the density for fractions C and D may be found in the particle-size distribution within the fine fraction. It should be noted that each bulk density listed in Table 4.6 represents the average of four determinations.

The trends indicated in Table 4.6 were applied in fabricating experimental fuel rods for irradiation in the VBWR, as discussed in a preceding section. The fine fraction found after outgassing the enriched, fused UO₂ exhibited a d_{mw} of 27 μ , and the mixture yielded a bulk density of only 84% of theoretical. By changing the d_{mw} to 16 μ by ball milling, a bulk density of 87% of theoretical was obtained.

In addition to the effect of particle-size distribution within the fraction, screen analyses of the depleted UO₂ mixtures after the compaction process showed that only 2 1/2 to 7 1/2% of the coarse fraction was degraded during the compaction process. This is to be compared with a

degradation of 15% or greater in the enriched material. It should be noted that the enriched material represented small fusions, whereas the depleted material was from a larger fusion.

Although high bulk densities can be obtained with the ternary particle-size distributions mentioned above, binary distributions appear to be equally acceptable. By changing the vibration characteristics and the coarse particle size, bulk densities of 90% of theoretical are readily obtainable, as shown in Table 4.7. These data were obtained from tests in tubes 45 in. long and 1/2 in. OD, with a 0.035-in. wall. The tubes were vibrated a total of 8 min on the pneumatic-powered Branford Vibrator. The coarse material was screened from the large batch of crude, depleted UO_2 mentioned previously. It is thought that the high densities were obtained because degradation of coarse material formed a suitable midfraction. Experiments with sol-gel ThO_2 -3 wt % UO_2 , which does not degrade as readily, support this postulate. Thus it appears that the binary mixture transforms in situ into various size particles that compact well.

Table 4.7. Bulk Densities of Fused UO_2 Obtained Using Binary Particle-Size Distributions and a Branford Variable Impact Vibrator

Particle-Size Distribution (wt %)		Bulk Density (% of theoretical)
-4 +16 mesh	-200 mesh	
80	20	90.3
75	25	90.3
70	30	89.6
65	35	87.9

Fuel Irradiation Tests

V. O. Haynes W. C. Thurber

Irradiation tests of nonpelletized UO_2 fuel were conducted in the ORR pressurized-water loop to aid in the determination of the suitability of such fuel for use in a replacement core for the N.S. SAVANNAH. The test specimens were 0.5-in.-OD rods consisting of UO_2 clad with type 304

stainless steel of 0.035-in. wall thickness. The fabrication techniques used were described in previous reports⁴⁻⁶ and in the previous section of this report.

Twenty-seven nonpelletized fuel rods have been irradiated in clusters of three in the pressurized-water loop, with high-purity water at 1750 psi and about 500°F flowing past the specimens at a rate of approximately 10 fps. Typical irradiation specimens are shown in Fig. 4.14, which is a preirradiation photograph of the specimen assemblies for experiments 4 and 6. Eighteen of the specimens (experiments 1, 3, 4, and 6) have been examined destructively at the General Electric Company's Vallecitos Atomic Laboratory. Nine of the specimens (experiments 5, 7, and 8) are presently awaiting destructive examinations at ORNL. The general characteristics of the specimens and the status of the experiments are summarized in Table 4.8.

Another experimental assembly (No. 9) was fabricated as an initial step in an investigation of pelletized fuel with reduced cladding thickness. As with previous specimens, this was a three-rod cluster. The cladding was 0.494-in.-OD type 304 stainless steel, with a nominal wall thickness of 0.020 in. Pellets were chosen to give either 0.002 or 0.007 in. diametral clearance. This experiment was intended to involve a long-term (~1 yr) irradiation; however, the specimens were scratched during an examination necessitated by fission-product activity in the loop coolant caused by another experiment. Because of the scratches it was felt that further irradiation might confound rather than benefit the experiment. The irradiation was therefore terminated after about 2 months, and the specimens were placed in storage.

⁴R. J. Beaver, J. T. Lamartine, and W. C. Thurber, Rotary Swaging of Stainless Steel-Clad UO₂ Fuel Rods, pp. 50-52, "Maritime Reactor Project Ann. Prog. Rep. Nov. 30, 1960," USAEC Report ORNL-3046, Oak Ridge National Laboratory.

⁵J. T. Lamartine, Fuel-Rod Swaging Studies, pp. 79-80, "Maritime Reactor Program Ann. Prog. Rep. Nov. 30, 1961," USAEC Report ORNL-3238, Oak Ridge National Laboratory.

⁶W. S. Ernst, Jr., Fabrication Studies on Vibratory Compaction of Fuel, pp. 89-92, "Maritime Reactor Program Ann. Prog. Rep. Nov. 30, 1961," USAEC Report ORNL-3238, Oak Ridge National Laboratory.

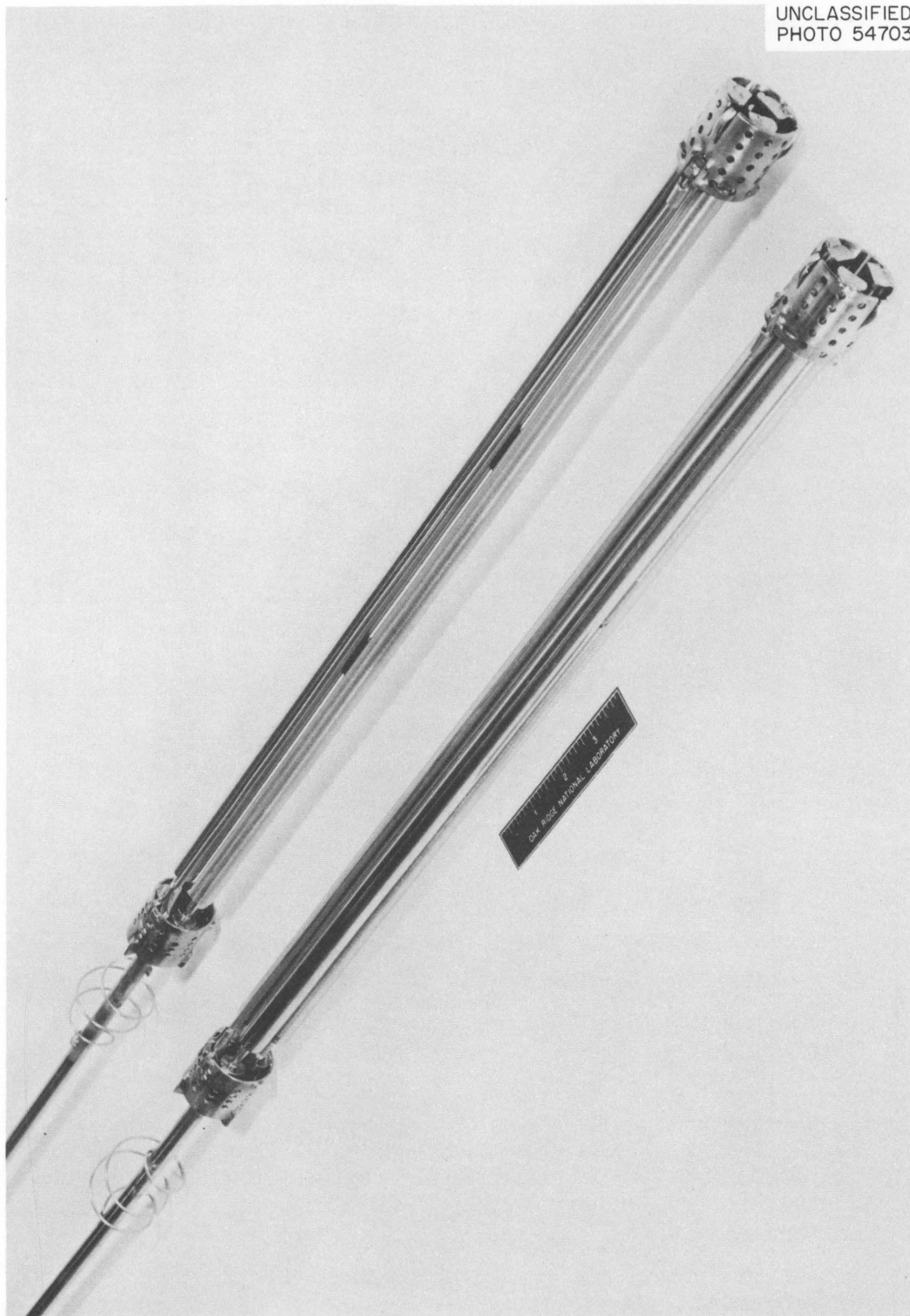


Fig. 4.14. Irradiation Test Assemblies for Experiments 4 and 6 Prior to Irradiation.

Table 4.8. Description of Nonsintered UO₂ Fuel Specimens Irradiated in the ORR Pressurized-Water Loop

Experiment No.	Specimen No.	UO ₂ Specimen Characteristics ^a					Fabrication Method	Fueled Length of Rod (in.)	Status
		U235 Content (wt %)	Particle Size (mesh)	Density (% of theoretical) ^b	Surface Area (m ² /g)	Oxygen-to-Uranium Ratio			
1	1A1	2.03	-20 +35	90	0.27	2.027	Cold swaged	16 3/8	Experiment completed and postirradiation results reported in a GE-VAL topical report
	1B1	2.03	-20 +35	90	0.27	2.026	Cold swaged	16 3/8	
	1C1	2.04	-170 +325	87	0.46	2.017	Cold swaged	16 3/8	
	1N1	0.80	-170 +325	89		2.021	Cold swaged	16 3/8	
	1O1	0.83	-20	90	0.17	2.026	Hot swaged	16 3/8	
	1P1	0.83	-20	90	0.14	2.024	Hot swaged	16 3/8	
3	3A1	2.03	-20 +35	90	0.27	2.019	Cold swaged	16 3/8	Experiment completed and postirradiation results reported in GE-VAL informal monthly reports
	3B1	2.03	-20 +35	90	0.33	2.025	Cold swaged	16 3/8	
	3C1	2.04	-170 +325	87	0.41	2.021	Cold swaged	16 3/8	
	3N1	0.80	-170 +325	89	0.36		Cold swaged	16 3/8	
	3O1	0.83	-20	90	0.18	2.030	Hot swaged	16 3/8	
	3P1	0.83	-20	90	0.19	2.024	Hot swaged	16 3/8	
4	4N1	1.87	-20 +35	90.5	0.03	<2.001	Cold swaged	16 1/4	Experiment completed and postirradiation results reported in GE-VAL informal monthly reports
	4O1	1.87	(c)	87.2	0.05	<2.001	Vibratory compacted	16 1/4	
	4P1	1.12	(c)	88.1	0.08	2.002	Vibratory compacted	16 1/4	
5	5A1	3.78	(c)	88.2	0.07	2.002	Vibratory compacted	16 1/4	Irradiation completed; specimens to be examined at ORNL
	5B1	4.22	(c)	88.0	0.12	2.002	Vibratory compacted	16 1/4	
	5C1	4.22	-20 +35	91.0	0.02	<2.002	Cold swaged	16 1/4	
6	6N1	2.85	(c)	88.0	0.07	2.004	Vibratory compacted	16 1/4	Experiment completed and postirradiation results reported in GE-VAL informal monthly reports
	6O1	2.85	(c)	87.9	0.07	2.004	Vibratory compacted	16 1/4	
	6P1	2.85	(c)	87.5	0.07	2.004	Vibratory compacted	16 1/4	
7	7N1	5.09	(d)	87.1		2.002	Vibratory compacted	16 1/4	Irradiation completed; specimens to be examined at ORNL
	7O1	5.09	(d)	87.1		2.002	Vibratory compacted	16 1/4	
	7P1	5.09	(d)	86.9		2.002	Vibratory compacted	16 1/4	
8	8N1	5.09	(e)	85.8	0.13	2.003	Vibratory compacted	16 1/4	Irradiation completed
	8O1	5.09	(e)	85.8	0.13	2.003	Vibratory compacted	16 1/4	
	8P1	5.09	(e)	85.5	0.13	2.003	Vibratory compacted	16 1/4	

^aAll specimens contained fused and ground UO₂ prepared by Spencer Chemical Co., except the specimens for experiment 8 which contained sintered and crushed UO₂.

^bTheoretical density taken to be 10.97 g/cm³.

^c60 ± 1 wt % -10 +16 mesh, 15 ± 1 wt % -70 +100 mesh, 25 ± 1 wt % -200 mesh.

^d62.2 wt % -10 +16 mesh, 16 wt % -70 +100 mesh, 21.8 wt % -200 mesh.

^e60 wt % -4 +16 mesh, 15 wt % -70 +100 mesh, 25% -200 mesh.

The postirradiation examinations performed at the Vallecitos Atomic Laboratory (GE-VAL) on the specimens of experiments 1, 3, 4, and 6 included gamma scans of each rod, dimensional measurements, analyses of crud adhering to the rods, burnup analyses based on Cs^{137} and Ce^{144} , fission-gas-release analyses, metallographic studies, and determination of plutonium content, uranium isotopic abundance, and the oxygen-to-uranium ratio.

The gamma scan indicated a peak-to-average burnup of about 1.18 and showed numerous axial discontinuities that represented transverse cracks in the fuel body. For further investigation of these cracks, two 4.25-in.-long sections were selected from rods A and C of experiment 3 and sectioned longitudinally. Macrographs of the 3A1 section revealed many narrow longitudinal and transverse cracks, while the 3C1 section had fewer but wider cracks. The photomacrographs were compared with the gamma scans, and the results are shown in Figs. 4.15 and 4.16.

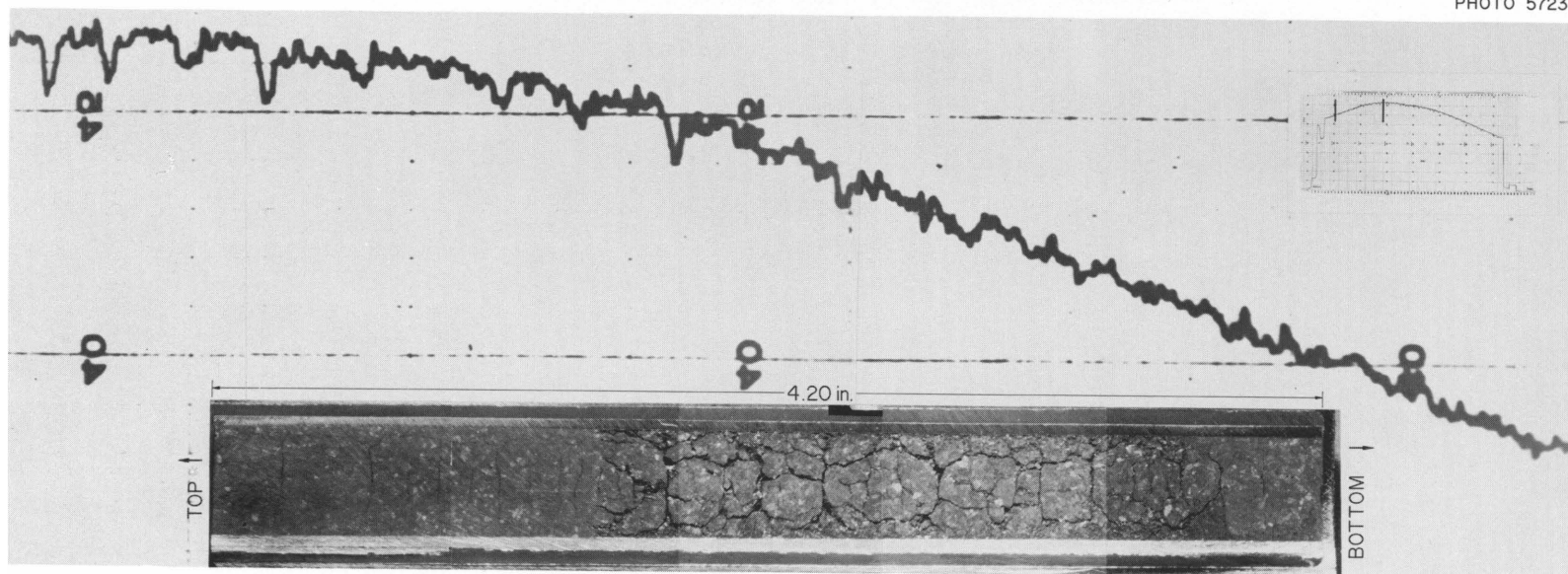
Postirradiation measurements of the diameters of some of the rods of experiment 3 do not agree very well with the preirradiation data, as indicated below:

<u>Rod Designation</u>	<u>Diametral Change</u>
3A1	No significant change
3B1	Generally 7 to 10 mils smaller
3C1	No significant change, except 5 to 10 mils increase at top end and 1 to 2 mils increase over bottom half
3N1	No significant change, except 1 to 3 mils increase at top 2 in. and bottom 4 in.
3O1	No significant change
3P1	Top 8 in. generally 0 to 8 mils larger; lower 10 in. 0 to 5 mils smaller

The specimens of experiments 4 and 6 showed no significant changes in diameter.

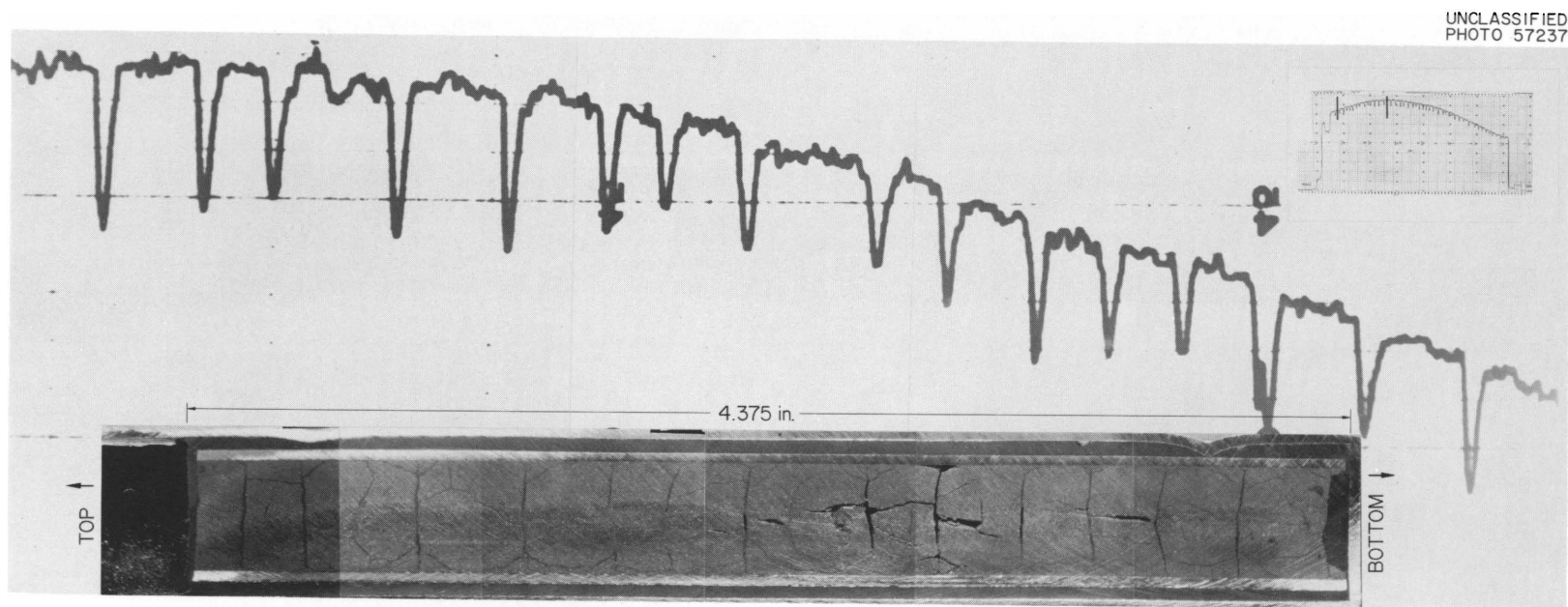
The character of the crud found on the specimens of experiments 4 and 6 was considerably different from the loose, black crud found on the specimens of experiments 1 and 3. Experiment 6 specimens had a reddish-brown adherent layer, portions of which had a darker color that gave a

UNCLASSIFIED
PHOTO 57236



Rod 3-A-1 Cold Swaged (-20 +35 Mesh UO_2)

Fig. 4.15. Correlation of Fuel Cracks with Gamma-Scan Profile for Rod 3A1.



Rod 3-C-1 Cold Swaged (-170 +325 Mesh UO_2)

Fig. 4.16. Correlation of Fuel Cracks with Gamma-Scan Profiles for Rod 3C1.

mottled appearance. A 2-in.-long band of electroless nickel had been applied near the middle of rod 6Pl because it had been observed that the experiment 3 specimens had a shiny appearance on the fuel rod surfaces adjacent to some of the brazed ferrules. There was little or no crud deposited on the banded area of rod 6Pl. The surfaces of experiment 4 specimens tended more to the black color, with some areas being dull and some shiny.

Analyses were made of the Cs^{137} -to-uranium and Ce^{144} -to-uranium ratios of peak burnup fuel sections to obtain burnup data. Release of the fission gas Kr^{85} was also measured, and the percentage release was computed based on the burnup values. The peak burnup values and Kr^{85} release, as computed at GE-VAL, are given in Table 4.9. These numbers are subject to refinement, but no significant changes are expected. Experiment 5, 7, and 8 specimens have not been examined; however, the estimates of heat ratings and burnup are expected to be reasonably accurate and are included for completeness. The highest Kr^{85} release (23.43%) occurred in a specimen that developed a central void and extensive structural changes in the fuel body.

Metallographic examinations were made of selected sections of each specimen. The detailed observations are discussed in the following section. There was slight evidence of sintering in three of the experiment 3 specimens; no sintering was detected in the other three. Two of the experiment 4 specimens sintered from the mid-radius inward, but the third did not have evidence of sintering. Experiment 6 specimens were operated at the highest heat rating and to the highest burnup of any specimens in the group examined so far. The fuel structure changed in all these specimens and, although melting was not evidenced, one specimen had a 9-in.-long central void with a maximum diameter of 0.040 in.

Plutonium and uranium analyses were performed on a few selected samples. The samples were complete sections taken between 6 and 7 in. from the bottom end of the fuel rods. The results are summarized in Table 4.10.

A few oxygen-to-uranium ratio determinations were made, and the results are compared with the preirradiation control data in Table 4.11. The postirradiation ratio was slightly lower in all the samples examined.

Table 4.9. Burnup and Fission-Gas-Release Data from Experiments 1, 3, 4, and 6

Experiment No.	Specimen No.	Peak Heat Rating (w/cm)	Peak Burnup ^a (Mwd/MT of U)	Kr ⁸⁵ Release ^b (%)
1	1A1	95	940	0.72
	1B1	115	1,120	4.98
	1C1	115	1,280	6.05
	1N1	120	1,040	6.02
	1O1	120	1,070	2.53
	1P1	145	1,300	3.44
3	3A1	90	2,480	3.7
	3B1	110	3,030	3.4
	3C1	105	3,320	7.6
	3N1	120	2,950	3.3
	3O1	115	2,900	3.1
	3P1	150	3,820	3.2
4	4N1	300	3,120	4.12
	4O1	265	2,870	2.19
	4P1	205	2,240	2.93
6	6N1	330	3,750	4.74
	6O1 ^c	360	4,150	10.51
	6P1 ^c	400	4,660	23.43
5	5A1	200	8,150	
	5B1	280	11,650	
	6C1	275	10,070	
7	7N1	450	5,470	
	7O1	455	5,550	
	7P1	540	6,750	
8	8N1	440	5,670	
	8O1	445	5,830	
	8P1	535	7,080	

^aBased on fission product Ce¹⁴⁴ analysis and 205 Mev/fission.

^bCalculated with reference to burnup based on cerium.

^cData for specimens 6O1 and 6P1 are given in exchanged order from that reported by GE-VAL; the order given here is believed to be correct.

Table 4.10. Results of Plutonium and Uranium Analyses of Experiment 3, 4, and 6 Specimens

Specimen No.	Isotopic Constituents (at. %)								Plutonium-to-Uranium Ratio (mg/g)
	U ²³⁸	U ²³⁵	U ²³⁶	U ²³⁴	Pu ²³⁹	Pu ²⁴⁰	Pu ²⁴¹	Pu ²⁴²	
3C1	98.25	1.67	0.08		90.50	8.3	1.1		1.74
3P1	99.47	0.47	0.06		79.60	15.7	4.2	0.47	3.52
4N1	98.30	1.64	0.06	0.01	92.87	6.34	0.77	0.02	1.65
4O1	98.31	1.62	0.06	0.01					
4P1	98.94	1.01	0.05	0.01	90.91	7.87	1.16	0.05	1.87
6N1 ^a	97.44	2.46	0.08	0.02	92.80	6.41	0.79		1.34
6P1 ^a	97.52	2.36	0.10	0.02					
6O1 ^a	97.46	2.44	0.09	0.02	92.63	6.47	0.87	0.03	1.58

^aData for specimens 6O1 and 6P1 are given in exchanged order from that reported by GE-VAL. The order given here is believed to be correct.

Table 4.11. Oxygen-to-Uranium Ratio of Experiment 1 and 3 Specimens

Specimen	Oxygen-to-Uranium Ratio	
	Preirradiation	Postirradiation
1A1	2.027	2.0095
1P1	2.024	2.0148
3A1	2.019	2.0137
3P1	2.024	2.0219

Postirradiation Metallographic Examination of Fuel Specimens Irradiated in ORR Loop

E. L. Long, Jr.

Metallographic examination of experiment 3, 4, and 6 specimens was completed, and the results were compared with those of examinations of unirradiated control samples. Postirradiation metallographic examination of experiment 1 specimens was reported previously.⁷

At least one metallographic specimen was selected from each rod near the point of maximum burnup determined by gamma scans. Additional

⁷E. L. Long, Jr., Postirradiation Metallographic Examination of Experimental Assembly No. 1, pp. 106-112, "Maritime Reactor Program Ann. Prog. Rep. Nov. 30, 1961," USAEC Report ORNL-3238, Oak Ridge National Laboratory.

metallographic specimens were selected to determine the integrity of the end-plug welds and the ferrule-to-spacer brazed joints.

Fuel Cladding

The metallographic examination of transverse sections from the fuel rods of assemblies 3, 4, and 6 showed no evidence of corrosion at the outer surfaces of the type 304 stainless steel cladding. A difference was noted, however, at the inner surfaces. All the cladding of the rods from assembly 3, both as-fabricated and irradiated, contained a lamellar precipitate that extended from the inner surface to a maximum depth of 0.005 in. A lamellar precipitate was also noted in the inner surface regions of two of the three rods from assembly 4. There was no evidence of this type of precipitate in any of the cladding of rods from assembly 6. Examination of the unirradiated control specimens showed that the UO_2 used in experiment 1 and 3 specimens contained a globular second-phase material, which was identified by x-ray as uranium nitride. The unirradiated fuel used in experiment 4 and 6 specimens also contained a second-phase material, but it had an acicular structure and was identified as U_4O_9 both metallographically and by x-ray diffraction.

Although nitrogen analyses were not run on the UO_2 in each fuel rod in the three assemblies, those that were run showed an increase in the amount of lamellar precipitate with an increase in nitrogen content. This is illustrated in Fig. 4.17. There was a range in the nitrogen impurity level in the UO_2 in the three assemblies from 590 ppm in rod 3A1 to 80 ppm in rod 6Pl. It has been shown that a lamellar precipitate can be formed in type 304 stainless steel if it is exposed to nitrogen under certain conditions.⁸ It is therefore postulated that the lamellar precipitate found in the cladding of experiment 1 and 3 specimens is a result of the nitrogen content of the UO_2 .

None of the end-cap welds examined showed any deleterious effects of irradiation. The brazed joints examined were similar in appearance to those of experiment 1 specimens, as shown in the previous report.⁷

⁸H. E. McCoy et al., "Effect of Environment on the Mechanical Properties of Metals," pp. 166-167 in 1961 Proceedings of the Institute of Environmental Sciences National Meeting, April 5-7, Washington, D.C.

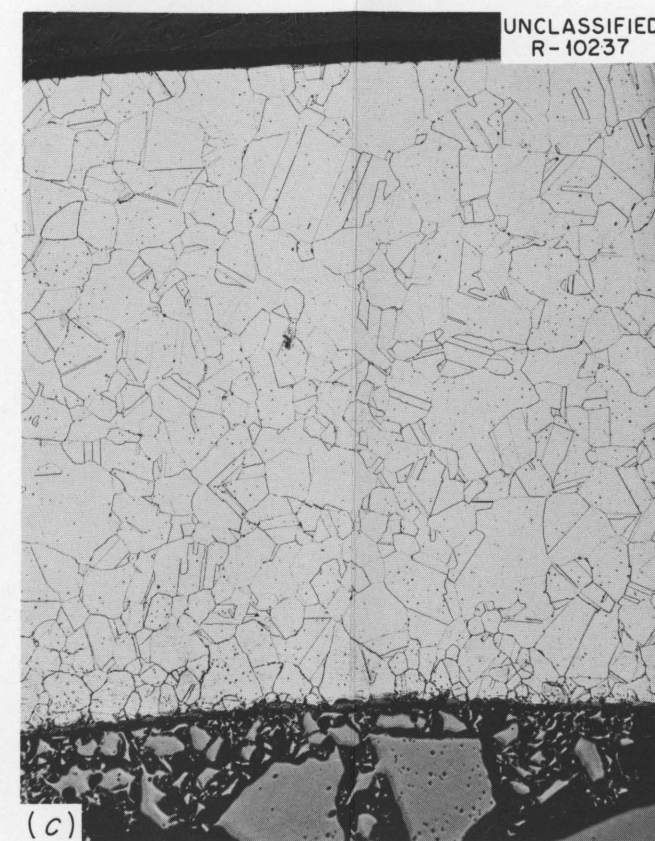
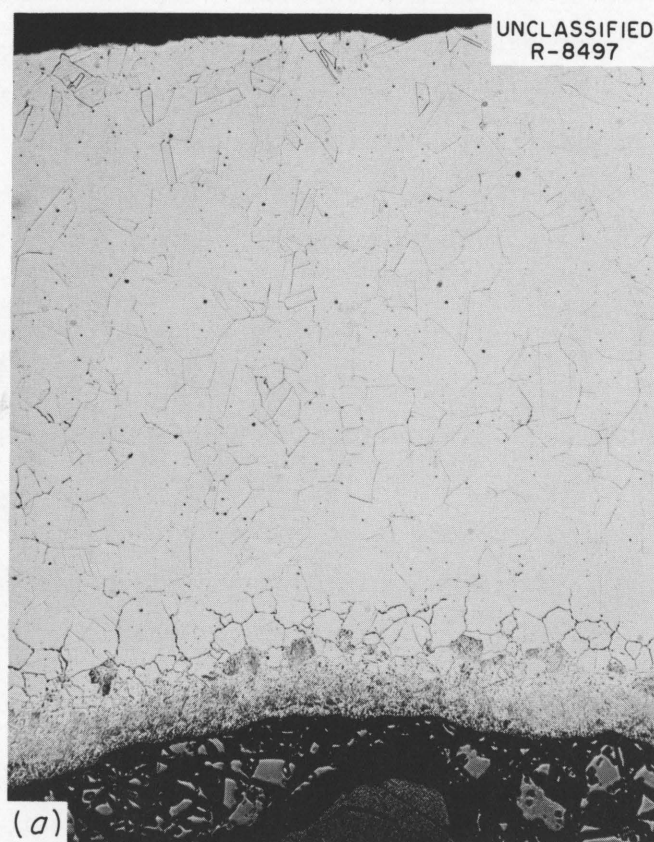


Fig. 4.17. Microstructural Effects of Nitride Compounds in UO_2 on Type 304 Stainless Steel Cladding from Experimental Assemblies 3, 4, and 6. (a) Transverse section from fuel rod 3A1; nitrogen impurity level in the UO_2 was 590 ppm. (b) Transverse section from fuel rod 4N1; nitrogen impurity level in the UO_2 was 210 ppm. (c) Transverse section from fuel rod 6P1; nitrogen impurity level in the UO_2 was 80 ppm. Note decreasing depth of lamellar and grain boundary precipitate with decreasing nitrogen impurity level in the UO_2 . Etched. 100X.

Fuel Columns

A transverse specimen taken from the maximum flux region of fuel rod 3Pl was the only specimen from the six rods of assembly 3 that showed definite evidence of sintering. Areas from the unirradiated control and the center of irradiated fuel rod 3Pl are shown in Fig. 4.18; there was evidence of sintering from the center to the mid-radius of the fuel column. The white globular phase in the unirradiated fuel was identified as primarily UN_2 . Upon irradiation, the nitride phase apparently dissolved in the central region of the fuel column and precipitated along slip lines in the form of an acicular phase, as shown in Fig. 4.19. The acicular nitride phase was identified by x-ray diffraction as a hexagonal form of U_2N_3 .

A second-phase material was present in all unirradiated fuel used in experiment 4 and 6 specimens and was identified as U_4O_9 , both metallographically and by x-ray diffraction. A typical area from the unirradiated control for rod 401 is shown in Fig. 4.20. In contrast to assembly 3 rods, all but one rod (rod 401) from assemblies 4 and 6 showed evidence of sintering. The other five fuel rods showed microstructural changes that ranged from the formation of new grains in rod 4N1 to central void formation in rod 6Pl.* Typical areas from the central regions of the fuel columns of experiment 4 and 6 specimens are shown in Fig. 4.21.

Sintering to the mid-radius was seen in fuel rods 3Pl, 4N1, 4Pl, and 601.* Sintering occurred to about two-thirds of the radius in rod 6N1 and extended past two-thirds of the radius in rod 6Pl* but not to the outer-surface regions of the fuel column. The exact location of the termination of sintering was difficult to determine because of the differences in size of the UO_2 particles. Another transverse section taken approximately 4 1/2 in. from the top of rod 6Pl* did not contain a central void, although the UO_2 showed signs of sintering past the mid-radius of the fuel column.

*Data for rods 601 and 6Pl are discussed in exchanged order from that in the original postirradiation examination reports. The identification given here is believed to be correct.

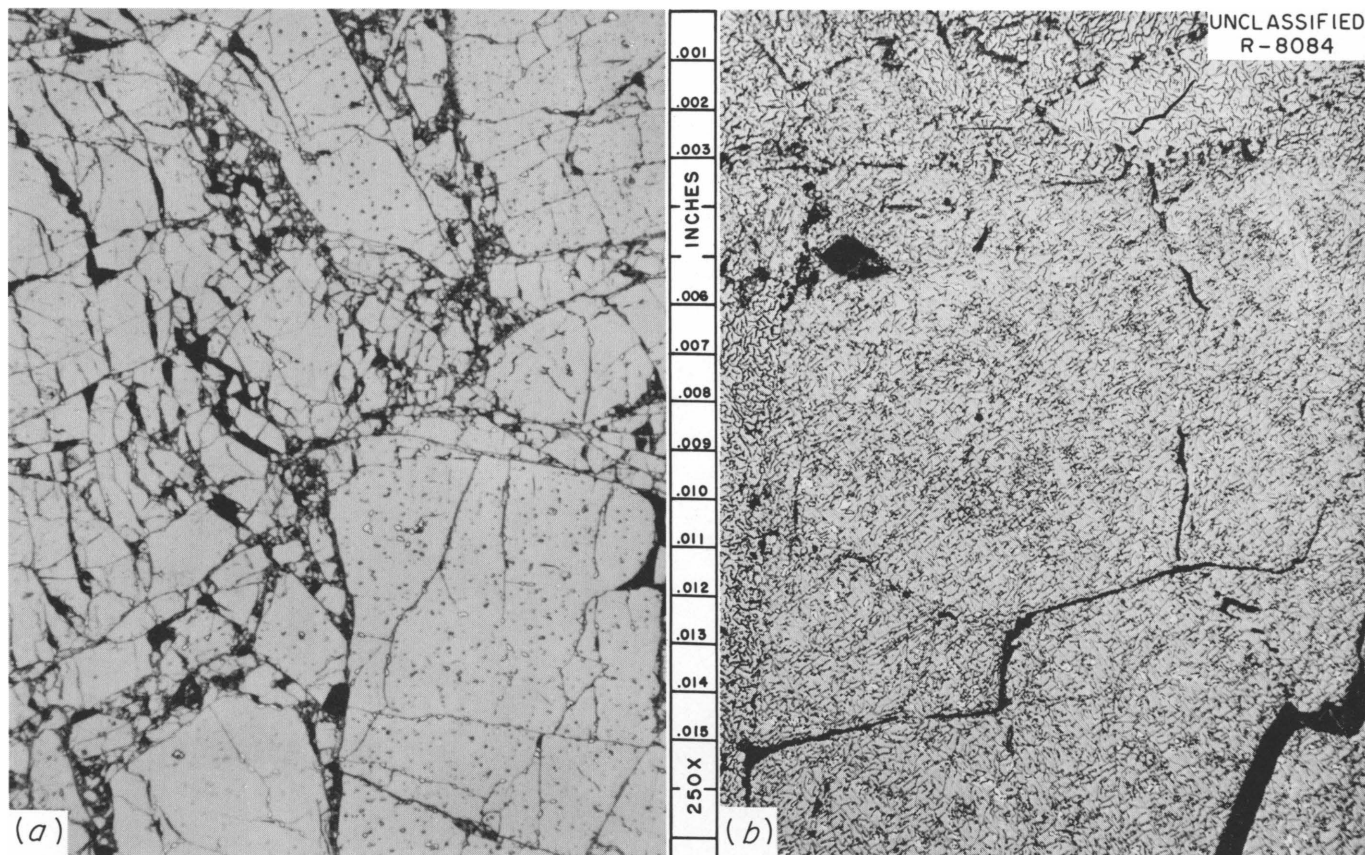


Fig. 4.18. Areas from (a) the Unirradiated Control Specimen and (b) the Center of Irradiated Fuel Rod 3Pl from Experimental Assembly 3. Etched. 250X.

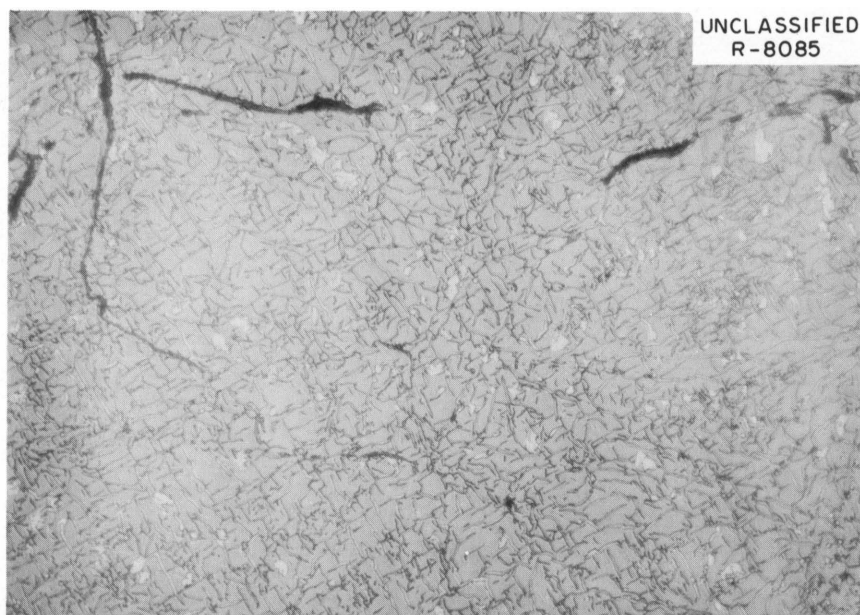


Fig. 4.19. Area from Near the Center of Fuel Rod 3Pl. The acicular phase was identified as U_2N_3 (hexagonal). Etched. 500 X.

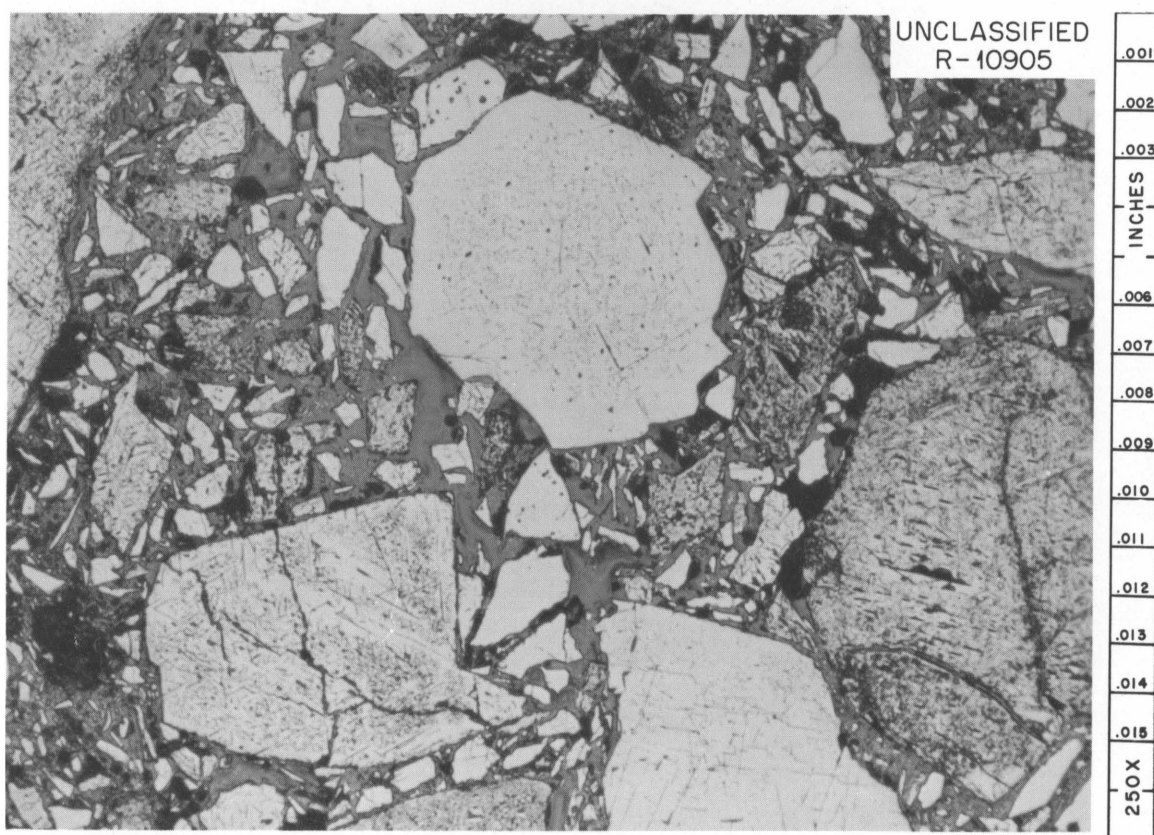
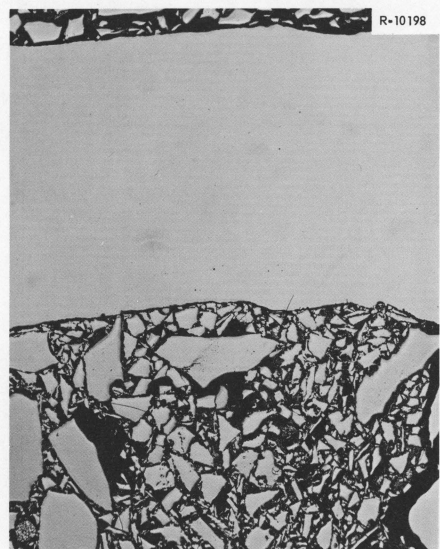


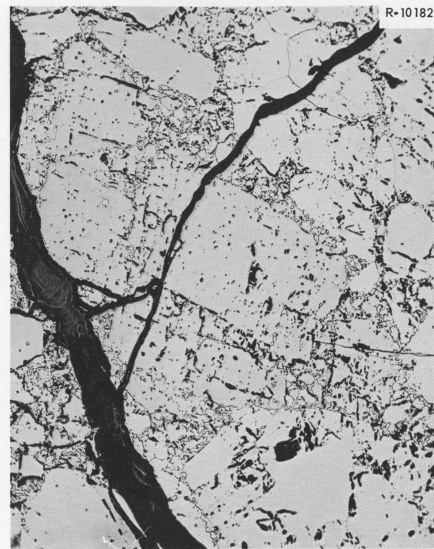
Fig. 4.20. Typical Area from the Unirradiated UO_2 for Fuel Rod 401 of Experimental Assembly No. 4. The precipitate in the UO_2 was identified as U_4O_9 . Etched. 250X.



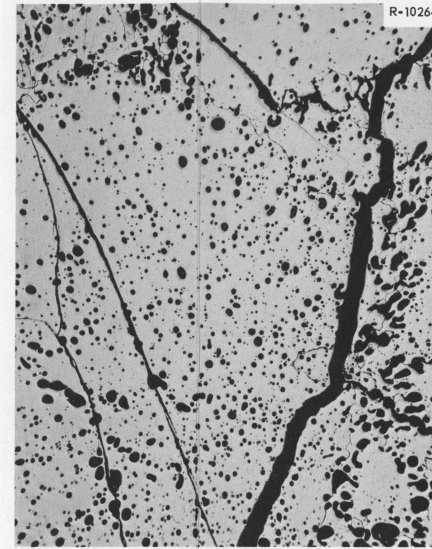
ROD 401



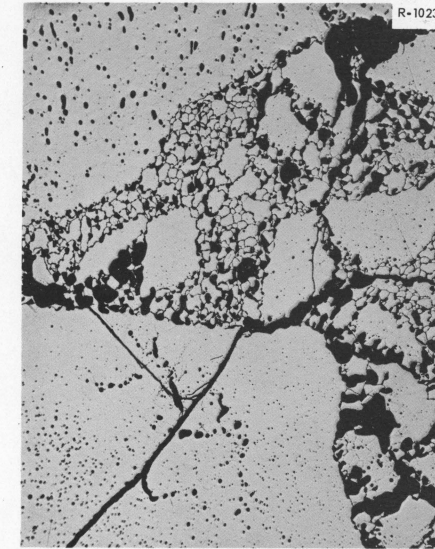
ROD 4P1



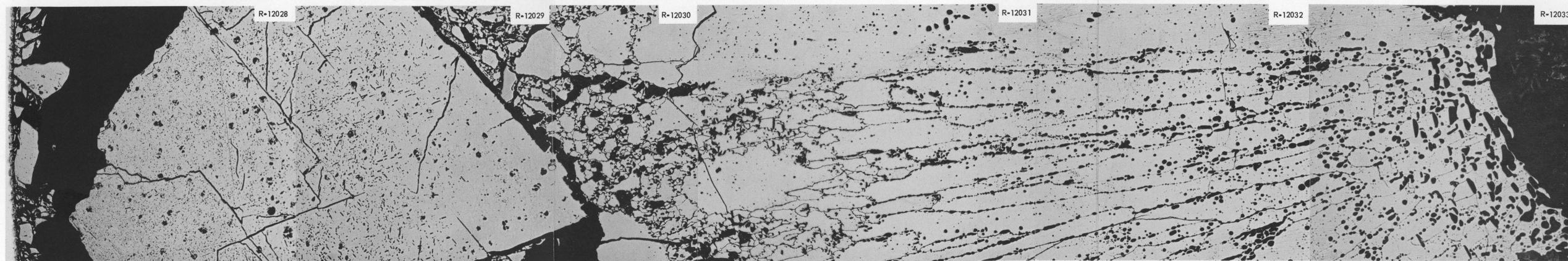
ROD 4N1



ROD 601



ROD 6N1



ROD 6P1

Fig. 4.21. Typical Areas from the Central Region of the Fuel Rods from Experimental Assemblies 4 and 6. The panorama is from a transverse section of fuel rod 6P1 and shows an area from the central void to the cladding. Etched. 100X. Original reduced 5%.

Conclusions

The appearance of the lamellar and intergranular precipitates observed in the inner surface regions of the type 304 stainless steel cladding was apparently dependent upon the nitrogen impurity level in the UO_2 ; no precipitation was observed with a nitrogen impurity level below 80 ppm. Furthermore, the lamellar and intergranular precipitates were formed during the brazing cycle in the fabrication of the fuel rod clusters. Although no deleterious effects of the precipitates were found, none of the fuel rods that contained UO_2 with an appreciable nitrogen level was held at a high enough heat rating to produce extensive sintering or central void formation.

In experimental assembly 3, only one fuel rod showed evidence of sintering (rod 3Pl). In assemblies 4 and 6, all fuel rods except one, rod 401, showed evidence of sintering, and one fuel rod (rod 6Pl*) contained a central void approximately 0.040 in. in diameter. There was no evidence of sintering near the cladding or of central melting of the UO_2 in any of the fuel rods.

Evaluation of Nonsintered UO_2 Fuel for an N.S. SAVANNAH Core

T. D. Anderson V. O. Haynes
W. C. Thurber

A significant part of the N.S. SAVANNAH fuel-cycle cost is associated with core fabrication. One possible way to reduce the cost of a replacement core is to eliminate the need for fabricating a large number of UO_2 pellets. This can be done by the use of either the swaging or the vibratory-compaction fabrication processes. Both of these processes have been investigated at ORNL and at other places, and the fabrication techniques have been developed to the point where satisfactory full-sized core loadings can be made. In conjunction with the ORNL fuel fabrication work, an irradiation program was carried out with the objective of evaluating the performance of nonsintered UO_2 fuels for future N.S. SAVANNAH cores. In addition experimental data on nonsintered UO_2 fuel are being obtained by several other organizations.

Based on the information available on nonsintered UO_2 fuel from ORNL and other programs, an over-all evaluation was made⁹ to assess nonsintered fuel for application to the N.S. SAVANNAH reactor; this evaluation is summarized here. The areas considered were fuel performance characteristics and fuel-cycle economics.

Thermal Performance

An analysis of the expected thermal performance characteristics of a SAVANNAH core using swaged UO_2 fuel was made based on the results of several tests at Chalk River^{10,11} in which swaged UO_2 fuel specimens were irradiated at high heat ratings. Essentially, the analysis consisted of adjusting the experimental results to account for the N.S. SAVANNAH core I fuel surface temperature and the power distribution within a fuel rod. The results of the analysis are shown in Figs. 4.22 and 4.23, which give the radial extent of a physical change (i.e., melting, grain growth, or sintering) in the UO_2 as a function of the linear heat rate of a core I type of fuel rod. Figure 4.22 is based on short-term, hydraulic-rabbit data and is, therefore, considered to be applicable to short-term operation. Figure 4.23 is based on longer term data from an in-pile loop specimen, and therefore the information given in Fig. 4.23 is applicable to long-term operation. It is to be noted that Fig. 4.23 does not give information on UO_2 melting, because the loop specimen did not melt.

The linear heat rates associated with the N.S. SAVANNAH core are:

	Linear Heat Rate (w/cm)
Peak at overpower scram level of 89.7 Mw	409
Average at overpower scram level	102
Peak at design power level of 69 Mw	314
Average at design power	78

⁹T. D. Anderson, V. O. Haynes, and W. C. Thurber, "An Evaluation of Nonsintered UO_2 Fuel for an N.S. SAVANNAH Core," USAEC Report ORNL TM-421, Oak Ridge National Laboratory (to be published).

¹⁰G. H. Chalder et al., "Swaged UO_2 Fuel Elements," unpublished AECL work, April 1961.

¹¹A. S. Bain et al., "Postirradiation Examination of Miscellaneous Uranium Oxide Specimens of the X-2-n Loop Test," Canadian Report EXP-NRX-204, June 7, 1960.

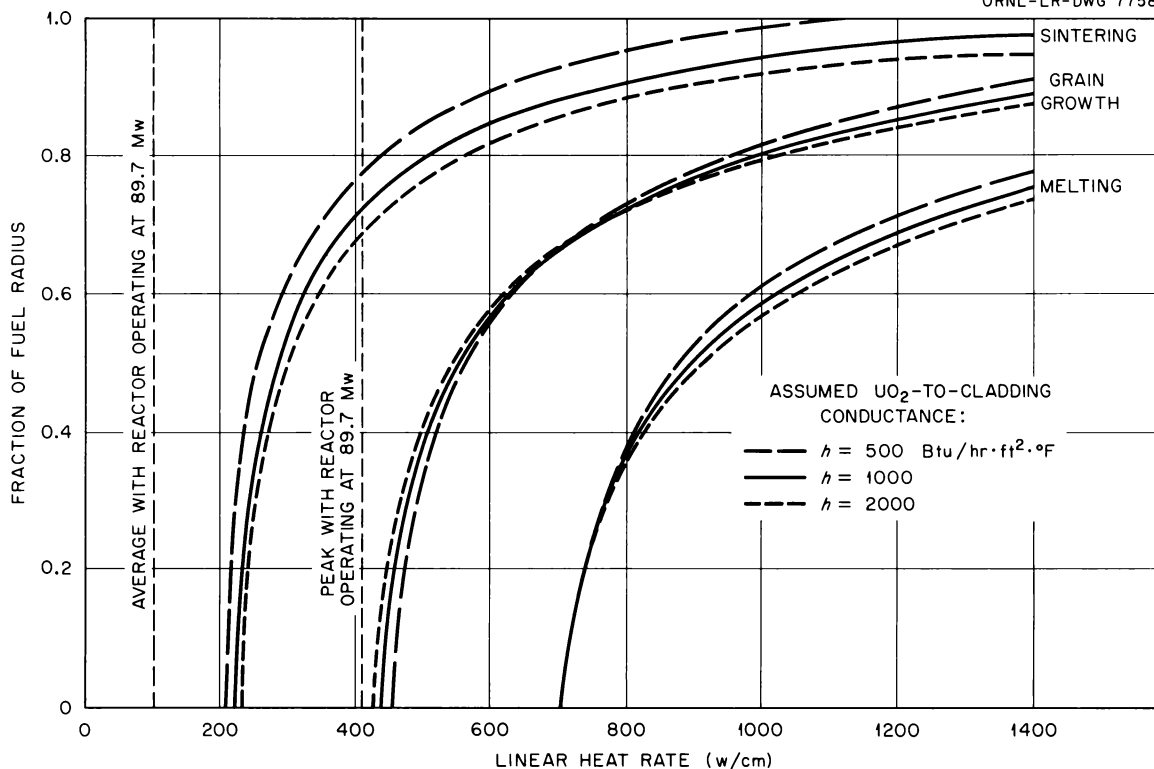


Fig. 4.22. Radial Extent of Physical Change in Swaged UO_2 Versus Linear Heat Rate for Short-Term Operation of N.S. SAVANNAH Core.

It is clear from Fig. 4.22 that even the highest rated element would not experience melting or grain growth if the core should go to its maximum permissible power (89.7 Mw) early in core lifetime. Figure 4.23 shows that, for long-term operation, both sintering and grain growth would be more extensive because of the time dependence of these changes. For long-term operation at the design power of 69 Mw, the highest rated element would experience grain growth over about 30% of the fuel radius and sintering would occur over about 90% of the fuel radius. The average fuel at design power would show no grain growth and little, if any, sintering. Although no information is given in Fig. 4.23 concerning melting, it is felt that the short-term melting information (Fig. 4.22) is valid for longer periods, because the more extensive grain growth and sintering produced by time-at-temperature would, if anything, improve the conductivity.

Although these results are specifically applicable to swaged fuel rods, there appears to be little reason to believe that the conductivity

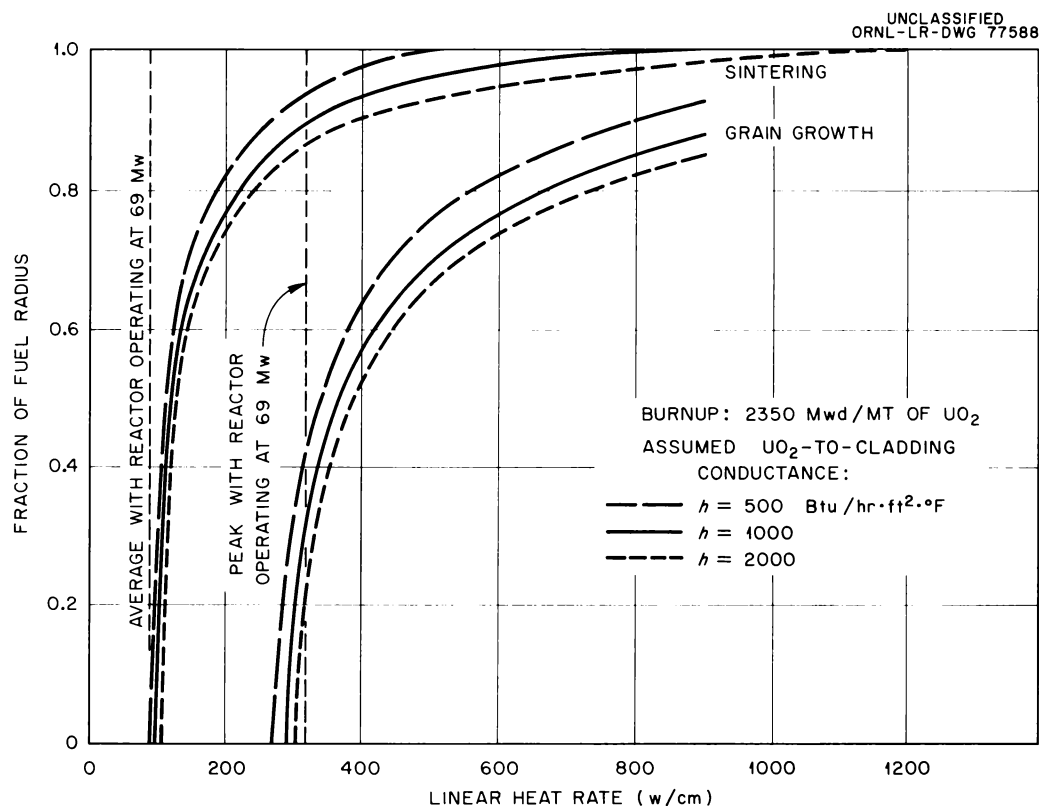


Fig. 4.23. Radial Extent of Physical Change in Swaged UO₂ Versus Linear Heat Rate for Long-Term Operation of N.S. SAVANNAH Core.

of vibratory-compacted fuel would be significantly different from that for swaged fuel at comparable densities. It therefore seems evident that nonsintered UO₂ fuel would be acceptable for the N.S. SAVANNAH core from the thermal performance standpoint.

Waterlogging

A possible failure mechanism of metal-clad, bulk-oxide fuel rods operating in water-cooled reactors is waterlogging. In this process it is envisioned that the cooling water enters the fuel rod through a cladding defect, probably when the reactor is shut down. Upon subsequent reactor startup, the water rapidly transforms to steam; and, since the steam cannot escape from the fuel rod with sufficient rapidity, a large internal pressure is generated that causes rupture of the rod. Fission products and particulate oxide fuel are then released to the coolant.

Such a sequence of events presupposes two conditions. First, a defect must be present. Although extensive quality control is exercised to manufacture defect-free rods, absolute assurance of integrity cannot be given. Further, the possibility of defects developing in-pile cannot be discounted. Such defects could form by corrosion, fuel ratcheting, or internal pressure in the fuel rods. Sound design and quality control can, of course, reduce these possibilities to a minimum, but not to zero. The second condition is that the steam might not be able to rapidly escape through the same defect by which the water entered. This could result if the defect became plugged with fuel or if the path length for steam escape was long relative to the rate at which the steam was generated. Such a situation potentially exists to a greater extent in fuel rods fabricated by vibratory compaction or rotary swaging than for pelletized fuel rods. In rods with nonsintered fuel, the tightly packed but permeable oxide fuel column presents a tortuous path for egress of steam. The probability of a defect in a nonsintered fuel rod becoming plugged by loose particulate matter is also greater than in a rod fueled with sintered pellets. A further concern is that in the event of a cladding failure the release of oxide particles would probably be greater from nonsintered fuel rods.

In an attempt to ascertain whether these speculations are valid, an appraisal of the literature was made, and a few cursory experiments were conducted at ORNL.¹² It was hoped that such an approach would provide sufficient background information to confidently recommend nonsintered UO₂ fuel in stainless steel cladding for a future core of the N.S. SAVANNAH. The results of the assessment, as will be seen, indicate that a potential waterlogging problem does exist with this type of fuel.

Previous Experience with Pellet Fuels. An extensive experimental program for testing the waterlogging hypothesis was conducted by the Bettis Atomic Power Laboratory as part of the development of blanket fuel rods for the initial loading of the Shippingport reactor. The type of

¹²J. C. Griess and W. C. Thurber, Defective Fuel Rod Testing, pp. 80-82, "Maritime Reactor Program Ann. Prog. Rep. Nov. 30, 1961," USAEC Report ORNL-3238, Oak Ridge National Laboratory.

fuel pin evaluated was, in nearly all cases, a 0.413-in.-diam, 10.25-in.-long, Zircaloy-2 tube containing pressed-and-sintered UO_2 pellets. Twenty-four tests were run in high-temperature water on specimens containing 0.005-in.-diam defects.¹³ In this group of experiments, the heat fluxes ranged from 223,000 to 682,000 Btu/hr.ft² and the burnups varied from 800 to >5500 Mwd/T. In only one instance was a waterlogging failure noted (sample 1 of experiment X-1-b). This specimen, which contained pellets of only 80% theoretical density, bulged and ruptured during testing. A diameter increase of 0.080 in. was reported. The failure was attributed to the low pellet density, coupled with significant carbon contamination of the UO_2 from a hot-pressing operation. The uranium carbide contaminant was believed to have reacted with the water to have helped to precipitate failure. Subsequent tests were conducted with relatively high-density oxide pellets (>90% theoretical density) prepared, in general, by the cold pressing-and-sintering technique. The maximum diametral increase was 0.012 in., and changes in dimension were usually not detectable. One experiment (25-2) was particularly noteworthy. The defective sample used in this test was thermally cycled 533 times during its in-pile tenure, and no change in diameter was observed.

In addition to the Bettis work cited above, several defective fuel rod tests have been conducted by other organizations. It has generally been concluded that waterlogging is not a problem in fuel rods containing high-density UO_2 pellets. This conclusion is based on the experiments described above and the successful operating experience with large power reactors. A note of caution should be added, however. Most of the available information was obtained for relatively short fuel rods (less than 3 ft long). It is conceivable that the propensity for waterlogging failures could be a function of fuel-rod length. Thus the possibility of such a failure in some of the presently operating power reactors may be greater than the available data indicates.

Experience with Nonsintered Fuels. The most extensive experimental program for studying the behavior of defective nonsintered fuel rods has

¹³J. D. Eichenberg et al., "Effects of Irradiation on Bulk UO_2 ," USAEC Report WAPD-183, Westinghouse Electric Company, October 1957.

been conducted by the Hanford Laboratories, and it is primarily in this work that waterlogging failures have been noted.^{14,15} A series of five tests on defective nonsintered fuel rods was conducted with 80°F water at 92 psi in the GEH-4 loop, a facility located in the MTR. The specimens were clad with 0.56-in.-diam, 0.026- to 0.030-in.-wall Zircaloy. Four samples were compacted by swaging, and the fifth was vibratory compacted. A summary of the test conditions is given in Table 4.12. The duration of each test was 1 to 2 hr.

Failure by waterlogging was noted in the one vibratory-compacted fuel rod (designated GEH-4-54). This 24-in.-long rod was made up by butt welding a 12-in. length of Zircaloy-2 to a similar piece of Zircaloy-4. The defect was located at the junction of the two materials. The fuel in this test specimen was sintered-and-ground UO_2 . Postirradiation examination revealed that the Zircaloy-4 had split in a brittle manner, but no evidence of hydrides was noted. This rupture was a sufficient restriction to flow that the Zircaloy-2 portion of the specimen downstream was damaged by heat-transfer burnout.

No damage to the four swaged rods was noted under similar conditions. It has been suggested by the Hanford workers that the failure may have been associated with the relatively low density in the vibratory-compacted rod (80.6% of theoretical) as compared with its swaged counterparts (82.4 to 85.5% of theoretical). The lower density would permit more water intake through the defect and possibly present a more difficult path for the escape of steam. However, it is difficult to perceive how the density change from 80.6 to 82.4% would preclude a waterlogging failure.

The five specimens received various amounts of thermal cycling during their brief in-pile tenure. This cycling resulted from the rapid changes in reactor power which often occur when starting up the MTR. No

¹⁴M. K. Millhollen, G. R. Horn, and J. L. Bates, "Hydriding in Purposely Defected Zircaloy-Clad Fuel Rods," USAEC Report HW-65465, Hanford Atomic Products Operation, August 1961.

¹⁵"Quarterly Progress Report, Fuels Development Operation, July, August, September 1960," pp. 5.31-5.39, USAEC Report HW-69085, Hanford Atomic Products Operation, Oct. 15, 1960.

Table 4.12. Parameters for Tests of Defective Fuel Rods in GEH-4 Facility

Test No.	1	2	3	4	5
Specimen designation	GEH-4-39	GEH-4-45	GEH-4-52	GEH-4-53	GEH-4-54
Maximum linear heat rate, w/cm	702	930	905	1060	920
Maximum surface heat flux, Btu/hr.ft ²	~500,000	~660,000	~640,000	~760,000	~700,000
Defect diameter, in.	0.005-0.006	0.005	0.006	0.006	0.006-0.007
UO ₂ density, % of theoretical	84.9	83.1	82.4	85.5	80.6
Coolant pressure, psig	92	92	92	92	92
Coolant inlet temperature, °F	83	73	83	87	82
Method of fabrication	Swaged	Swaged	Swaged	Swaged	Vibratory compacted
Cladding material	Zircaloy-2	Zircaloy-2	Zircaloy-4	Zircaloy-4	Zircaloy-2 and -4

obvious correlations can be drawn between heating rate or number of thermal cycles and fuel-rod behavior.

Another waterlogging failure occurred in a test of cold-swaged fuel rods (GEH-12-20).¹⁴⁻¹⁶ In this experiment, a seven-rod cluster was irradiated in the ETR in 500°F, 2000-psi water, flowing at 13 ft/sec. The 32-in.-long specimens were clad with 0.030-in.-wall, 0.565-in.-diam tubes of either Zircaloy-2 or Zircaloy-4. Four of the seven rods contained a 0.006-in. defect through the cladding. Each rod was fueled with fused-and-ground UO₂ swaged to 85% theoretical density. The cluster operated at a peak surface heat flux of 300,000 Btu/hr·ft² (linear heat rate of 560 w/cm), with a peak-to-average factor of about 1.5.

Failure occurred shortly after reactor startup and before the loop had reached its rated temperature. The test continued for 17.8 effective full-power days after failure was indicated by activity in the loop water. The failure was an axial split of a Zircaloy-4 sheath along its entire length. The split occurred on the side opposite the intentionally introduced defect. Nearly all the UO₂ was removed from the entire 32-in. fuel column. Apparently the failure did not catalyze further disintegration of the cluster, since both the defective and nondefective rods adjacent to the failed rod were unaltered.

A test of nonsintered UO₂ fuel in which there were no intentional defects was also noteworthy.¹⁷ A prototype element containing 19 fuel rods (GEH-12-4) fabricated by swaging was irradiated in the ETR for 24 effective full-power days. The 34-in.-long fuel rods were clad with 0.563-in.-OD, 0.030-in.-wall Zircaloy-2 and contained UO₂ compacted to 88% theoretical density. The cluster operated at a peak heat flux of ~600,000 Btu/hr·ft² in pressurized water at 2000 psi and 400°F. As a result of scrams, the fuel received at least nine thermal cycles during the irradiation.

¹⁶"Quarterly Progress Report, Fuels Development Operation - October, November, December 1960," pp. 5.18-5.19, USAEC Report HW-70355, Hanford Atomic Products Operation, Jan. 13, 1961.

¹⁷M. K. Millhollen et al., "Erosion Resistance of Swaged UO₂ Following an In-Reactor Fuel Rod Cladding Failure," USAEC Report HW-70315, Hanford Atomic Products Operation, June 1961.

Fission-gas release in the coolant water indicated the presence of a defect. After the failure was detected, the test was continued for an additional 15 hr at a reduced coolant temperature before the test element was discharged at a burnup of approximately 1000 Mwd per ton of UO_2 . Postirradiation examination revealed that one rod had ruptured. The rupture was an elliptical exfoliation about 1 1/2 in. long. It was observed that a maximum of 10% of the UO_2 in the failure region was washed out. This may be contrasted with the GEH-12-20 test, in which nearly all the fuel was removed. Metallographic examination of the flaw revealed that the cladding had retained significant ductility. A 22% reduction in thickness was measured at the point of fracture.

The Savannah River Laboratory has not conducted any tests on intentionally defective fuel rods; however, in one test conducted on a presumably sound fuel tube, a probable failure by waterlogging was reported.^{18,19} One stainless steel fuel tube in an assembly of five ruptured during in-pile operation. The tube was 2.14 in. OD, 1.46 in. ID, and 3 ft long; it contained swaged UO_2 . The failure was a 9-in.-long axial crack in the cladding. Little or no UO_2 was observed to have escaped. Examination of the end closures indicated that a defect through which water could enter the tube existed in one of the welds.

A group of Phillips Petroleum Company personnel conducted a series of transient experiments at SPERT on cold-swaged fuel rods originally manufactured by The Babcock & Wilcox Company for N.S. SAVANNAH critical experiments.²⁰ The type 304 stainless steel-clad rods were 6 ft long and 0.500 in. OD, with 0.028-in. walls; they contained high-fired UO_2 at a compacted theoretical density of approximately 87%. A waterlogging

¹⁸R. R. Hood and L. Isakoff, "Heavy Water Moderated Power Reactors Prog. Rep., May 1960," p. 38, USAEC Report DP-505, E. I. DuPont de Nemours & Co.

¹⁹R. R. Hood and L. Isakoff, "Heavy Water Moderated Power Reactors Prog. Rep., July 1960," pp. 16-17, USAEC Report DP-525, E. I. DuPont de Nemours & Co.

²⁰J. E. Houghtaling et al., "Calculation and Measurement of the Transient Temperature in a Low-Enrichment UO_2 Fuel Rod During Large Power Excursions," IDO-16773, Phillips Petroleum Company, May 18, 1962.

failure occurred in a single-rod test in the SPERT I facility after eight excursions with periods varying from 1.1 sec down to 7.5 msec. During the first seven transients, no problems were encountered. Following the seventh transient the rod remained in the reactor water for two days prior to the 7.5-msec test, during which the failure occurred.

Previously, eleven holes, each 0.013 in. in diameter, had been drilled through the rod at 1-in. intervals near mid-length and parallel to the longitudinal axis. These holes, which were for thermocouple installation, were sealed with an epoxy resin. It is believed that these seals broke during previous power excursions and allowed water to enter the rod. Steam pressure then built up sufficiently to rupture the cladding.

The failure was an axial split approximately 12 in. long at mid-length. The rupture may have started at one of the holes in the cladding and followed approximately in line with the series of holes previously drilled for the thermocouples. About 44% of the UO_2 in the rod (700 g) was removed during the incident.

In order to validate the waterlogging hypothesis, another pin with no defects in the cladding was tested through the same series of excursions. As expected, no problems were encountered in this test.

Other Performance Considerations

Experimental evidence indicates that fission-gas release from non-sintered UO_2 is considerably greater than from pelletized fuel at comparable heat ratings. Based on the N.S. SAVANNAH core I design, however, there should be no difficulty in accommodating the fission-gas release. Tests of swaged UO_2 stainless steel-clad fuel of core I geometry in the ORR pressurized-water loop indicated no serious dimensional stability problems, at least up to moderate burnups.

Fuel redistribution by relocation to an end or production of a central void have been observed only for low-density powder or very high heat ratings. Neither of these conditions apply to the use of nonsintered fuel in the N.S. SAVANNAH core. Cracking of the fuel body might occur, but no serious problems would be anticipated.

Economics

Estimates of both the N.S. SAVANNAH core I fuel-cycle costs and the fuel-cycle cost reduction that would result from the use of nonsintered fuel were made by Whitmarsh.²¹ The results of the cost analyses are summarized in the following paragraphs.

Core I Fuel-Cycle Cost. Estimated fuel-cycle cost for the N.S. SAVANNAH core I are listed in Table 4.13. It is to be noted that the core procurement cost, which is of primary interest in the evaluation of nonsintered fuel, represents about 39% of the total fuel-cycle cost.

Although the most important single expense associated with procuring a core is the fabrication cost, a number of other important costs are involved. Table 4.14 gives a detailed breakdown of the various costs associated with core procurement.

Cost Reduction Resulting from Use of Nonsintered Fuel. The use of nonsintered UO_2 fuel was considered to affect the following core procurement cost components:

1. UF_6 to UO_2 Conversion. The cost of fused-and-ground oxide needed for swaged or vibratory-compacted fuel is greater than the cost of the ceramic-grade oxide used in pelletized fuel. Sintered-and-ground oxide was not considered, since it was felt that the fused-and-ground material would be required to achieve a satisfactory bulk density.

2. Process Losses. Process losses would be less for nonsintered fuel than for sintered fuel.

3. Fabrication. Fabrication cost would be reduced by elimination of the pelletizing process.

The core-procurement cost reductions resulting from the use of nonsintered fuel are listed in Table 4.15. The factor of 2 between the minimum and maximum estimated cost reductions indicates the large uncertainties in the cost analyses.

In addition to the reduction in core procurement cost, there would be a slight reduction in the cost of working capital; however, this

²¹C. L. Whitmarsh, "Potential Fuel-Cycle Cost Savings Resulting from Technological Changes in the N.S. SAVANNAH Reactor," USAEC Report ORNL-TM-144, Oak Ridge National Laboratory, April 6, 1962.

Table 4.13. Estimated Core I Fuel-Cycle Cost

	Dollars per Core	Dollars per Year ^a	Unit Cost (mills/shp-hr)
Core procurement	\$ 959,000	\$ 394,700	3.4
Net fuel burnup	387,000	159,300	1.4
Reprocessing	582,800	239,800	2.0
Use charge	368,900	151,800	1.3
Working capital	186,400	76,700	0.7
Total	\$2,484,000	\$1,022,000	8.8

^aBased on core lifetime of 1.63 full-power years and load factor of 0.67.

Table 4.14. Breakdown of Core-Procurement Costs for N.S. SAVANNAH Core I

	Dollars per kg of Uranium	Dollars per Core
Withdrawal charge	\$ 1.12	\$ 9,000
UF ₆ to UO ₂ conversion	20.16	161,000
Loss during conversion	3.88	31,000
Use charge during conversion	3.84	30,700
Core fabrication	64.00	511,300
Loss during fabrication	5.77	46,100
Use charge during fabrication	11.42	91,200
Shipment	3.00	24,000
Use charge during storage	6.85	54,700
Total	\$120.04	\$959,000

reduction is small compared with the various uncertainties and was therefore not considered. Core I fuel-cycle cost reductions corresponding to the core-procurement cost reductions shown in Table 4.17 are: minimum, 4.5%; maximum, 8.9%; and average, 6.7%.

Conclusions

Using "no fuel melting" as the thermal design criterion, nonsintered UO₂ fuel appears to be adequate for N.S. SAVANNAH operating conditions.

Table 4.15. Core-Procurement Cost
Reductions Resulting from Use
of Nonsintered UO_2

	Savings (\$/core)	Cost Reduction (%)
Minimum	\$111,000	11.6
Maximum	\$220,000	22.9
Average	\$166,000	17.3

This conclusion presupposes the use of high-density UO_2 (near 90% of theoretical) with an oxygen-to-uranium ratio near 2.0.

Waterlogging failures have been noted in rods containing sintered-and-ground and fused-and-ground UO_2 . These failures have occurred in both swaged and vibratory-compacted rods with lengths varying from 24 to 70 in. Two rather tentative conclusions are that, relative to pelletized fuel, the nonsintered fuel is more susceptible to waterlogging and that, should a failure occur, more fuel would be transferred to the coolant from a nonsintered UO_2 fuel rod.

Fission-gas release appears to be greater for nonsintered UO_2 than for pelletized UO_2 ; however, it should not be difficult to design nonsintered fuel rods to accommodate the gas release. Fuel redistribution and dimensional stability do not seem to present any problems.

Any conclusions concerning the economic incentive for using nonsintered fuel must be made with the realization that economic analyses involve a number of uncertainties. With this in mind, it appears that the use of nonsintered UO_2 would reduce the N.S. SAVANNAH fuel-cycle cost by about 5 to 9% (\$46,000 to \$91,000 per year). Although significant, this reduction is not as large as was presupposed.

The applicability of any new technology to the N.S. SAVANNAH reactor must be judged in light of the unique operating conditions of merchant ships. In particular, the requirement of accessibility to the vessel by the public and the necessity for close approach to highly populated areas specifies a degree of reliability and safety beyond that necessary for

land-based plants. It is felt on the basis of present knowledge that nonsintered UO_2 fuel could be used in the N.S. SAVANNAH core with confidence in all aspects of performance, with one important exception. The susceptibility of this fuel to waterlogging failures and the consequences of such failures are uncertain. It appears therefore that more experience is necessary before the use of nonsintered UO_2 in the N.S. SAVANNAH reactor can be recommended with confidence.

Previous reports in this series are:

ORNL-2657	Maritime Reactor Project Ann. Prog. Rep. Nov. 30, 1958
ORNL-2865	Maritime Reactor Project Ann. Prog. Rep. Nov. 30, 1959
ORNL-3046	Maritime Reactor Project Ann. Prog. Rep. Nov. 30, 1960
ORNL-3238	Maritime Reactor Program Ann. Prog. Rep. Nov. 30, 1961

ORNL-3416

UC-80 - Reactor Technology
TID-4500 (19th ed.)Internal Distribution

- | | |
|--------------------------|-------------------------|
| 1. R. E. Adams | 42. W. R. Grimes |
| 2. T. D. Anderson | 43. E. E. Gross |
| 3. V. E. Anderson (K-25) | 44. T. H. Handley |
| 4. C. F. Baes, Jr. | 45. V. O. Haynes |
| 5. S. E. Beall | 46. M. R. Hill |
| 6. R. J. Beaver | 47. D. O. Hobson |
| 7. M. Bender | 48. H. W. Hoffman |
| 8. R. G. Berggren | 49. W. H. Jordan |
| 9. D. S. Billington | 50. S. I. Kaplan |
| 10. R. E. Blanco | 51. P. R. Kasten |
| 11. E. P. Blizard | 52. G. W. Keilholtz |
| 12. T. V. Blosser | 53. O. H. Klepper |
| 13. A. L. Boch | 54. R. B. Korsmeyer |
| 14. C. J. Borkowski | 55. J. A. Lane |
| 15. G. E. Boyd | 56. C. E. Larson (K-25) |
| 16. R. B. Briggs | 57. E. L. Long, Jr. |
| 17. W. E. Browning, Jr. | 58. R. N. Lyon |
| 18. F. R. Bruce | 59. H. G. MacPherson |
| 19. J. Buchanan | 60. W. D. Manly |
| 20. D. W. Cardwell | 61. E. R. Mann |
| 21. F. L. Carlsen, Jr. | 62. H. C. McCurdy |
| 22. T. E. Cole | 63. H. F. McDuffie |
| 23. J. A. Conlin | 64. A. J. Miller |
| 24. W. B. Cottrell | 65. E. C. Miller |
| 25. J. A. Cox | 66. K. Z. Morgan |
| 26. F. L. Culler | 67. F. H. Neill |
| 27. J. E. Cunningham | 68. M. L. Nelson |
| 28. I. T. Dudley | 69. P. Patriarca |
| 29. E. P. Epler | 70. A. M. Perry |
| 30. W. K. Ergen | 71. M. E. Ramsey |
| 31. W. S. Ernst, Jr. | 72. M. W. Rosenthal |
| 32. B. R. Fish | 73. G. W. Royster, Jr. |
| 33. M. Fontana | 74. A. F. Rupp |
| 34. A. P. Fraas | 75. G. Samuels |
| 35. J. K. Franzreb | 76. H. W. Savage |
| 36. R. M. Freestone, Jr. | 77. A. W. Savolainen |
| 37. J. H. Frye, Jr. | 78. L. D. Schaffer |
| 38. W. R. Gall | 79. J. L. Scott |
| 39. R. G. Gilliland | 80. O. Sisman |
| 40. B. L. Greenstreet | 81. M. J. Skinner |
| 41. J. C. Griess | 82. G. M. Slaughter |

- | | |
|------------------------|--|
| 83. A. H. Snell | 93. M. S. Wechsler |
| 84. I. Spiewak | 94. A. M. Weinberg |
| 85. P. E. Stein (Y-12) | 95. G. D. Whitman |
| 86. J. A. Swartout | 96. M. L. Winton |
| 87. J. W. Tackett | 97-99. Central Research Library |
| 88. W. C. Thurber | 100-102. ORNL-Y-12 Technical Library |
| 89. D. E. Tidwell | Document Reference Section |
| 90. D. F. Toner | 103-128. Laboratory Records Department |
| 91. D. B. Trauger | 129. Laboratory Records, ORNL RC |
| 92. G. M. Watson | |

External Distribution

- 130. Ira Adler, New York Operations Office, AEC
- 131-132. Col. R. B. Burlin, Division of Reactor Development (Army Reactors), AEC, Washington
- 133. J. J. Catalano, New York Operations Office, AEC
- 134. B. W. Colston, Atomics International, Canoga Park, Calif.
- 135-136. D. F. Cope, Reactor Division, AEC, ORO
- 137. K. H. Dufrane, Martin Company, Nuclear Division
- 138. Capt. J. P. Franklin, Nuclear Power Field Office, Ft. Belvoir, Virginia
- 139. M. J. Letich, American Bureau of Shipping, New York, N.Y.
- 140. Zel Levine, Martin Company, Nuclear Division
- 141-144. W. F. Long, Babcock & Wilcox Company, Atomic Energy Division
- 145. J. H. MacMillan, Babcock & Wilcox Company, Atomic Energy Division
- 146-147. D. C. McMillan, George G. Sharp, Inc., New York
- 148. R. W. McNamee, Manager, Research Administration, UCC
- 149-153. R. O. Mehann, States Marine Lines, Inc.
- 154. L. J. Misenheimer, Nuclear Power Field Office, Ft. Belvoir, Virginia
- 155-158. J. F. O'Brien, Martin Company, Nuclear Division
- 159-168. J. E. Robb, Division of Reactor Development (Maritime Reactors), AEC, Washington
- 169. W. C. Stamm, Ebasco Services, Inc., New York
- 170-172. B. W. Winchell, Todd Shipyard Corporation, Nuclear Division
- 173-174. Commandant (MMT) U. S. Coast Guard, Washington, D.C.
- 175. Research and Development Division, AEC, ORO
- 176-781. Given distribution as shown in TID-4500 (19th ed.) under Reactor Technology category (75 copies - OTS)

